

A GEOPHYSICAL STUDY OF THE  
STEAMBOAT SPRINGS, COLORADO  
GEOTHERMAL SYSTEMS

by

Karen Rae Christopherson

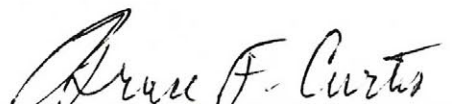
B.A., University of Colorado, 1977

A thesis submitted to the Faculty of the Graduate  
School of the University of Colorado in partial  
fulfillment of the requirements for the degree of  
Master of Science

Department of Geological Sciences

1979

This Thesis for the Master of Science Degree by  
Karen Rae Christopherson  
has been approved for the  
Department of  
Geological Sciences  
by

  
Bruce F. Curtis

  
J. Chris Harrison

Date April 17, 1979



Christopherson, Karen Rae (M.S., Geology)

A Geophysical Study of the Steamboat Springs, Colorado

Geothermal Systems

Thesis directed by Professor Bruce F. Curtis

During the summer of 1978, a geophysical study was done of the Steamboat Springs, Colorado, area to determine the structural and hydrological features involved with geothermal activity. By mapping electrical structure and density contrasts, a better understanding was gained of the geothermal systems, their recharge, areal extent, and physical parameters. This was accomplished by compiling previous work in geology and geothermometry with four geophysical techniques: gravity, audio-magnetotellurics, telluric profiling, and self-potential mapping.

The area's two main zones of hot springs, one in Steamboat Springs and the other seven kilometers north at Routt Hot Springs, lie on or near normal and transverse faults associated with the up-thrust of the Park Range. Near Steamboat Springs, Precambrian crystalline rocks (mainly gneiss and metavolcanics) are faulted into contact with Cenozoic and Mesozoic sedimentary rocks.

The gravity map delineated geologic contrasts, especially the crystalline-sedimentary rock contact, and showed an upfaulted basement block south of Steamboat Springs (not apparent from surface geology). The audio-magnetotellurics determined resistivity values for local rocks and showed the geothermal activity to be non-shallow in origin.

The telluric profiles reflected geologic structure and denoted a 500 to 750 meter wide zone of lower resistivity centered over Routt Hot Springs. The self-potential survey also defined a low (about -20 millivolt in magnitude) near the Routt spring area.

The geothermometry estimates for subsurface temperatures (by silica, Na-K-Ca, Na-K, and Mixing model) are between 125°C and 175°C for both Steamboat and Routt springs. Since there are no recent volcanics in the region, it is assumed that the geothermal activity is the result of meteoric waters (runoff from the Park Range) circulating along the many faults zones near the mountain front in an area of above normal heat flow. By circulating to a depth of four to five kilometers, the waters could reach desired temperatures. Subsurface flow could be possible along subhorizontal faults (connected with the major reverse fault) in fractures kept open by tensional activity (as evidenced by the above average microseismic activity near Steamboat Springs).

This abstract is approved as to form and content.

Signed

A. F. Curtis  
Faculty member in charge of thesis

#### ACKNOWLEDGEMENTS

The author wishes to acknowledge the following: the U.S. Geological Survey, Branch of Electromagnetism and Geomagnetism for providing financial support, equipment, and field assistants; the Colorado Geological Survey for financial support; Carl Long, Vicky Bankey, Bob Jones, Bill Heran, Janis Christopherson, Chinook, and Pumpkin for helping with field work; Danny Dansereau for aiding with computer gravity reductions; Don Hoover of the U.S. Geological Survey for encouragement and advising; Professors Bruce F. Curtis, J. Chris Harrison, and William C. Bradley for advising and reviewing; and the Tugboat Saloon in Steamboat Springs for providing a relaxing atmosphere for the reviewing of each field day's results.

## TABLE OF CONTENTS

	PAGE
ACKNOWLEDGMENTS . . . . .	v
LIST OF FIGURES . . . . .	vii
INTRODUCTION . . . . .	1
GEOLOGY . . . . .	9
GEO THERMOMETRY . . . . .	18
Routt Hot Springs . . . . .	18
Steamboat Springs . . . . .	19
GRAVITY . . . . .	21
AUDIO-MAGNETOTELLURICS . . . . .	26
TELLURICS . . . . .	78
SELF-POTENTIAL . . . . .	85
CONCLUSION . . . . .	91
BIBLIOGRAPHY . . . . .	95
APPENDIX	
A. GRAVITY DATA . . . . .	98
B. AUDIO-MAGNETOTELLURIC DATA SHEETS . . . . .	

# LIST OF ILLUSTRATIONS

FIGURE	PAGE
1. Location of the four-quadrangle study area . . . . .	2
2. Cow Creek, Colorado 7½' quadrangle . . . . .	3
3. Mad Creek, Colorado 7½' quadrangle . . . . .	4
4. Rocky Peak, Colorado 7½' quadrangle . . . . .	5
5. Steamboat Springs, Colorado 7½' quadrangle . . . . .	6
6. Major springs location map . . . . .	7
7. Geologic map of the Cow Creek quadrangle . . . . .	10
8. Geologic map of the Mad Creek quadrangle . . . . .	11
9. Geologic map of the Rocky Peak quadrangle . . . . .	12
10. Geologic map of the Steamboat Springs quadrangle . . . . .	13
11. Audio-magnetotelluric station location map . . . . .	27
12. AMT apparent resistivity map at 7.5 hertz . . . . .	30
13. AMT apparent resistivity map at 27 hertz, E-line N-S . . . . .	31
14. AMT apparent resistivity map at 27 hertz, E-line E-W . . . . .	32
15. AMT sounding curve, station 1NS . . . . .	33
16. AMT sounding curve, station 1EW . . . . .	34
17. AMT sounding curve, station 2NS . . . . .	35
18. AMT sounding curve, station 2EW . . . . .	36
19. AMT sounding curve, station 3NS . . . . .	37
20. AMT sounding curve, station 3EW . . . . .	38
21. AMT sounding curve, station 4NS . . . . .	39
22. AMT sounding curve, station 4EW . . . . .	40
23. AMT sounding curve, station 5NS . . . . .	41



FIGURE	PAGE
24. AMT sounding curve, station 5EW . . . . .	42
25. AMT sounding curve, station 6NS . . . . .	43
26. AMT sounding curve, station 6EW . . . . .	44
27. AMT sounding curve, station 7NS . . . . .	45
28. AMT sounding curve, station 7EW . . . . .	46
29. AMT sounding curve, station 8NS . . . . .	47
30. AMT sounding curve, station 8EW . . . . .	48
31. AMT sounding curve, station 9NS . . . . .	49
32. AMT sounding curve, station 9EW . . . . .	50
33. AMT sounding curve, station 10NS . . . . .	51
34. AMT sounding curve, station 10EW . . . . .	52
35. AMT sounding curve, station 11NS . . . . .	53
36. AMT sounding curve, station 12NS . . . . .	54
37. AMT sounding curve, station 12EW . . . . .	55
38. AMT sounding curve, station 13NS . . . . .	56
39. AMT sounding curve, station 13EW . . . . .	57
40. AMT depth versus resistivity plot, Bostick inversion, station 1 . . . . .	58
41. AMT depth versus resistivity plot, computer inversion, station 1 . . . . .	59
42. AMT depth versus resistivity plot, Bostick inversion, station 2 . . . . .	60
43. AMT depth versus resistivity plot, computer inversion, station 2 . . . . .	61
44. AMT depth versus resistivity plot, Bostick inversion, station 3 . . . . .	62
45. AMT depth versus resistivity plot, computer inversion, station 3 . . . . .	63

FIGURE	PAGE
46. AMT depth versus resistivity plot, computer inversion, station 4 . . . . .	64
47. AMT depth versus resistivity plot, Bostick inversion, station 4 . . . . .	65
48. AMT depth versus resistivity plot, Bostick inversion, station 5 . . . . .	66
49. AMT depth versus resistivity plot, Bostick inversion, station 6 . . . . .	67
50. AMT depth versus resistivity plot, Bostick inversion, station 7 . . . . .	68
51. AMT depth versus resistivity plot, Bostick inversion, station 8 . . . . .	69
52. AMT depth versus resistivity plot, Bostick and computer inversions, station 9 . . . . .	70
53. AMT depth versus resistivity plot, Bostick inversion, station 10 . . . . .	71
54. AMT depth versus resistivity plot, Bostick inversion, station 11 . . . . .	72
55. AMT depth versus resistivity plot, Bostick inversion, station 12 . . . . .	73
56. AMT depth versus resistivity plot, Bostick inversion, station 13 . . . . .	74
57. Telluric profile and self-potential survey location map . . . . .	79
58. Telluric profiles location map . . . . .	80
59. Telluric profile 1 . . . . .	82
60. Telluric profile 2 . . . . .	83
61. Self-potential station location map . . . . .	87
62. Self-potential profiles . . . . .	88
63. Complete Bouguer Gravity Map . . . . .	in pocket

## INTRODUCTION

During the summer of 1978, a geophysical study was done of the Steamboat Springs, Colorado area to determine the structural and hydrological features involved with geothermal activity. By mapping electrical structure and density contrasts, a better understanding was gained of the geothermal systems, their recharge, areal extent, and physical parameters. This was accomplished by compiling previous work in geology and geothermometry with four geophysical techniques: gravity, audio-magnetotellurics, telluric profiling, and self-potential mapping.

The study area centered around Steamboat Springs in Routt County of northwest Colorado and covered four  $7\frac{1}{2}'$  topographic quadrangles: Cow Creek, Mad Creek, Rocky Peak, and Steamboat Springs. Most of the work was done within a 50 square kilometer area from  $40^{\circ}28'$  to  $40^{\circ}35'$  north latitude and  $106^{\circ}49'$  to  $106^{\circ}53'$  west longitude.

Steamboat Springs lies on the west flank of the Park Range, on which lies the Continental Divide. From the range, two major drainages, the Elk and Yampa Rivers, flow through the area. Elevations range from over 3000 meters (near the divide) to 2000 meters (near Steamboat Springs). The major features and quadrangle outlines are located in figure 1. The four quadrangles were reduced to a scale of 1:62,500 for convenience and are shown in figures 2 through 5.

There are two major zones of hot springs near Steamboat Springs: one in the town itself and one about seven kilometers north at Routt Hot Springs. There are reportedly 150 mineral springs in all and most are located near the main springs shown in figure 6. The geology of the area has been mapped in detail by Snyder (1977), who shows that the



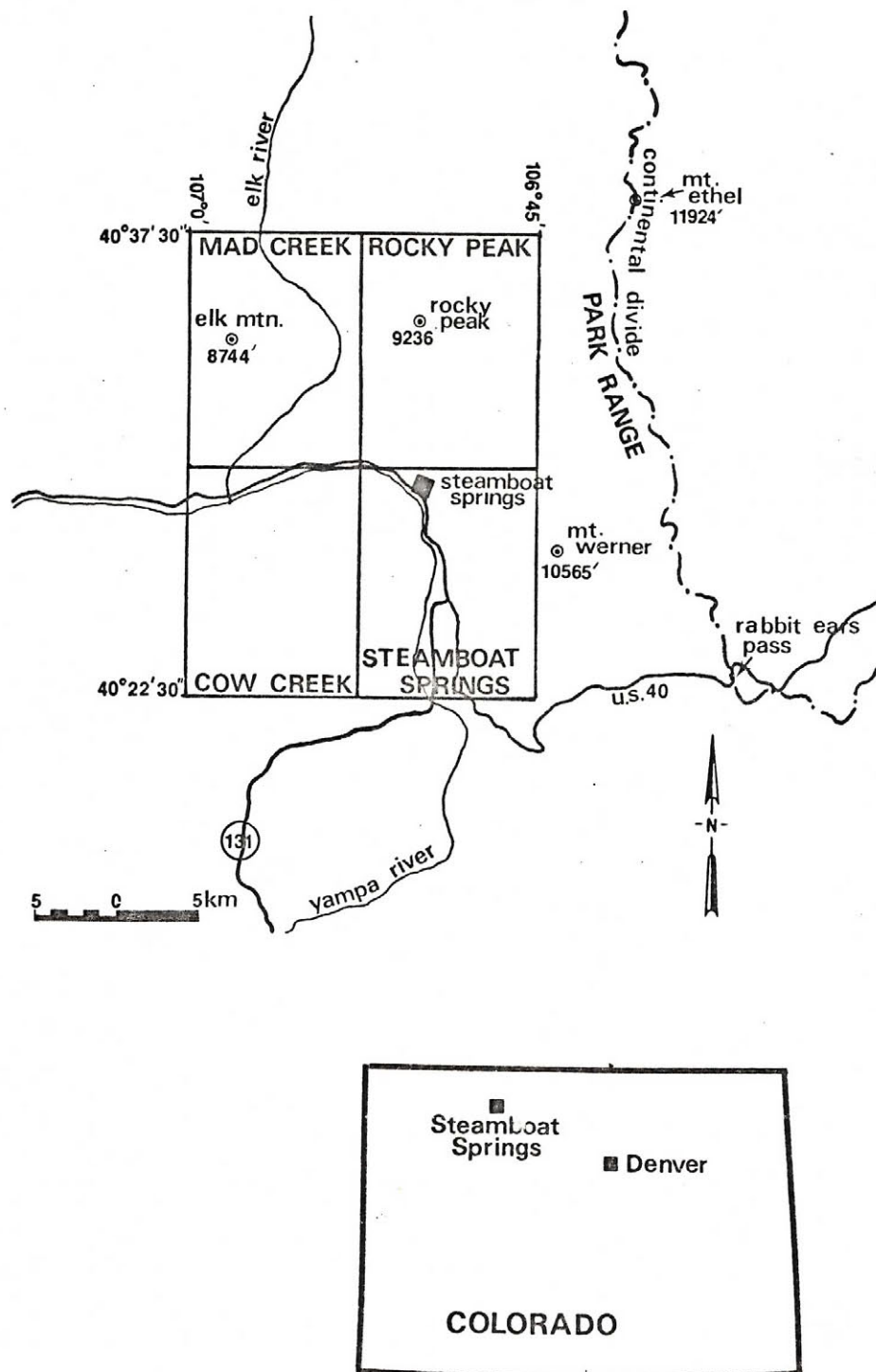


Figure 1. Location of the four-quadrangle study area.



Figure 2. Cow Creek, Colorado 7 1/2' quadrangle.



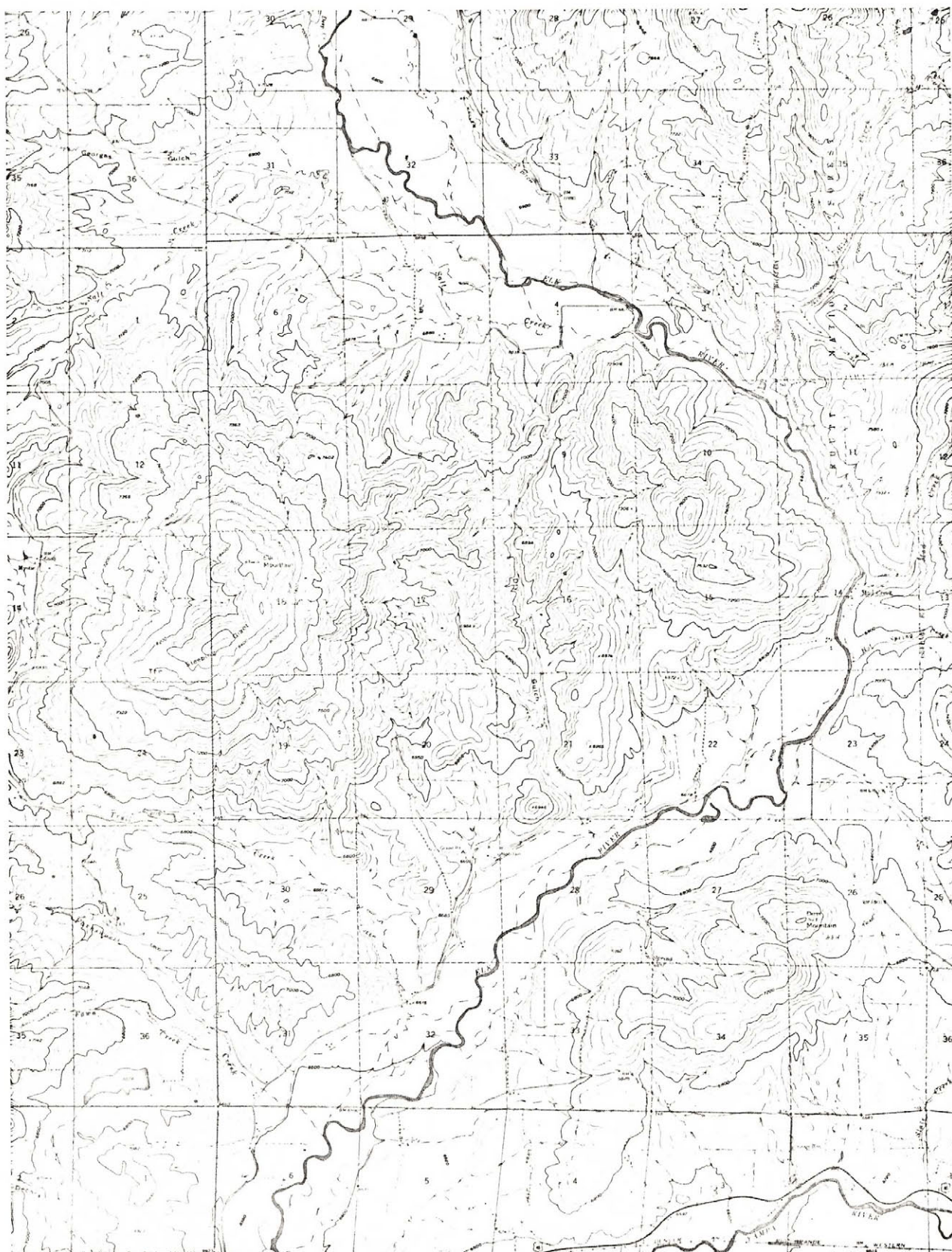


Figure 3. Mad Creek, Colorado 7 $\frac{1}{2}$ ' quadrangle.





Figure 4. Rocky Peak, Colorado 7 $\frac{1}{2}$ ' quadrangle.



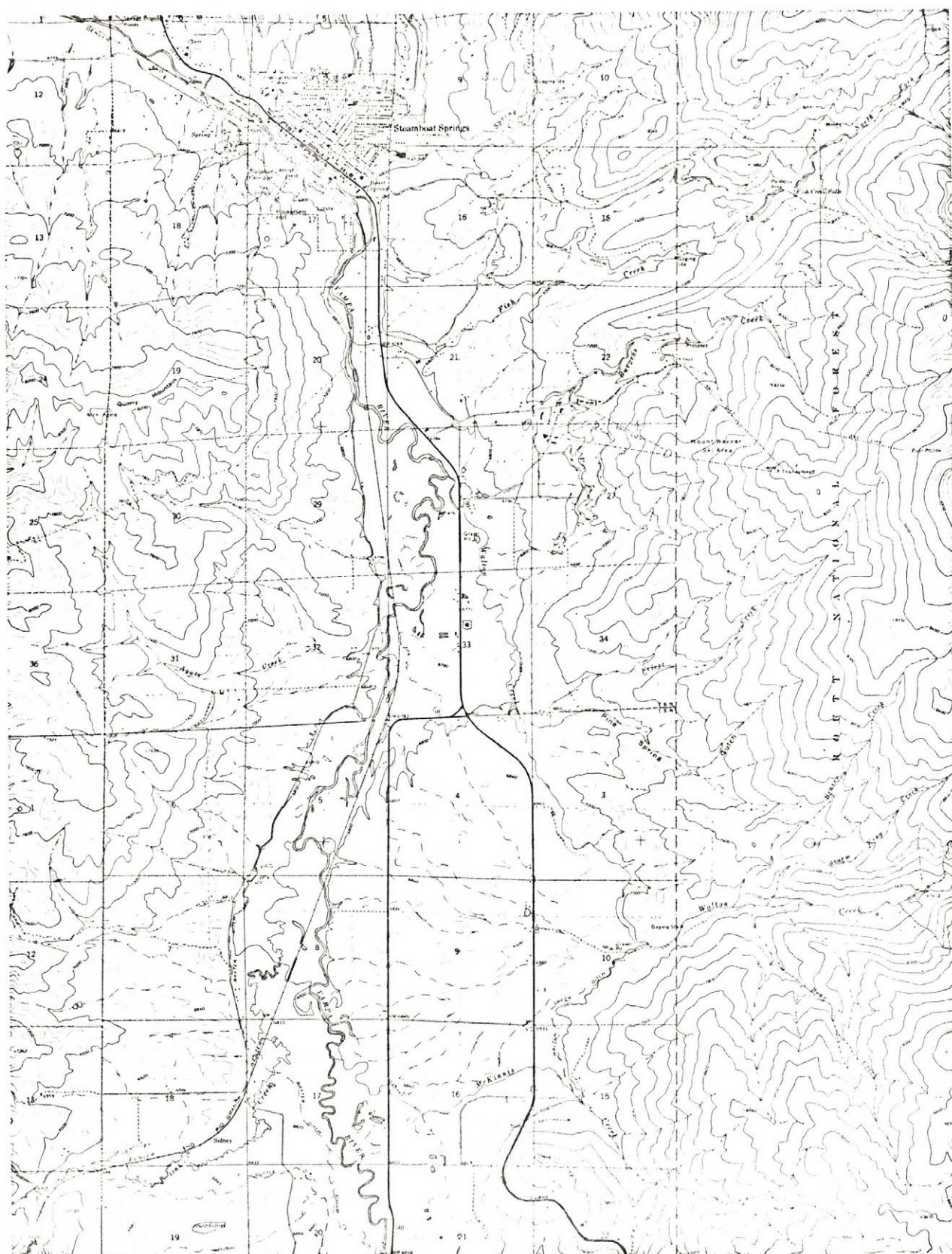


Figure 5. Steamboat Springs, Colorado 7½' quadrangle.



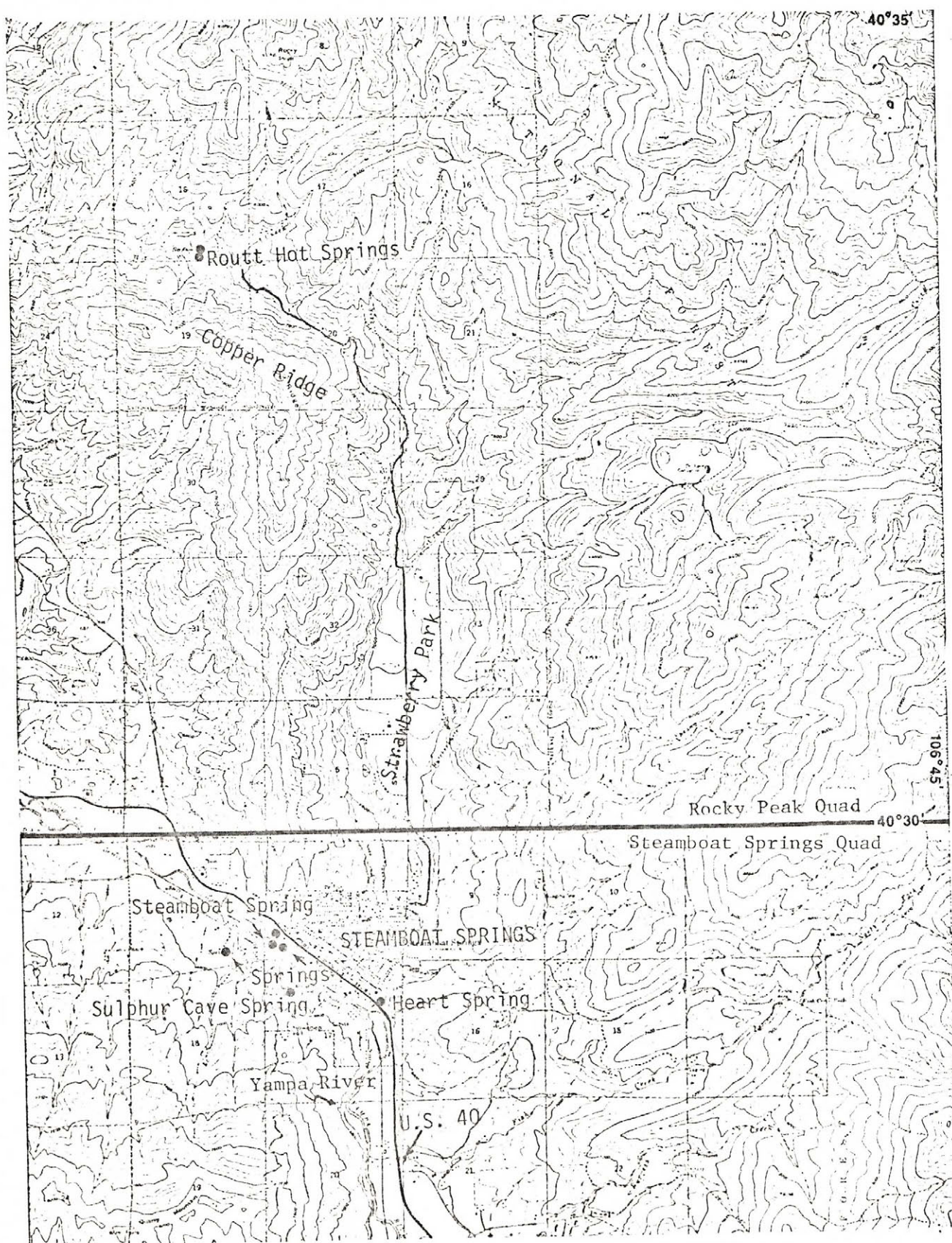


Figure 6. Major springs location map; scale 1:62500.

predominant feature is that Steamboat Springs lies on the west edge of the upthrust of the Park Range where Precambrian crystalline rock is faulted into contact with Mesozoic and Cenozoic sedimentary rocks.

The geophysical techniques used were employed because they are fairly quick and low-cost reconnaissance methods for determining lateral and vertical density and resistivity changes. The areal coverage by these methods was limited by access problems, rough terrain, thick brush, and cultural effects (especially near Steamboat Springs).

This region was chosen for study in cooperation with the Colorado Geological Survey to provide geophysical information for a geothermal assessment of Colorado. The work was funded in part by the Colorado Geological Survey, and by the U. S. Geological Survey, Branch of Electromagnetism and Geomagnetism, which provided most of the equipment, field crews and financial backing.



## GEOLOGY

The geologic maps of the four quadrangles covered in this study are shown in figures 7 through 10 and are followed by an explanation of map symbols and rock types. The maps are adapted mostly from Snyder and in part from Tweto (1976).

The Precambrian exposures are in the north and east of the study area and consist of gneiss, quartz monzonite, granite, metavolcanics, and some pegmatites. Of interest is the contact near Routt Hot Springs where quartz monzonite (pCb) is intruded into gneiss and metavolcanics (pGgn). The west and south parts of the study area lie mainly on Cretaceous Niobrara shale and Tertiary Browns Park sandstone. Quaternary glacial till (Qt), terrace gravels (Qg), alluvium (Qal), and landslide deposits (Ql) represent the cover in the area.

There are areas of outcropping sedimentary rocks of the Cretaceous Benton and Dakota, Jurassic Morrison, and Triassic Chugwater and Chinle formations near Steamboat Springs. A massive intrusive body and an associated dike, both of Tertiary age, underlie a prominent topographic feature called Elk Mountain, in the northwest part of the study area.

Perhaps one of the most prominent structural features of the area is a fairly high-angle reverse fault to the northwest of Steamboat Springs which trends north-northwest and dips east. It brings the Precambrian gneiss into contact with upturned Cretaceous and Jurassic sediments. It is believed (Snyder, 1978) that this reverse fault continues south beneath a cover of Quaternary and Tertiary deposits



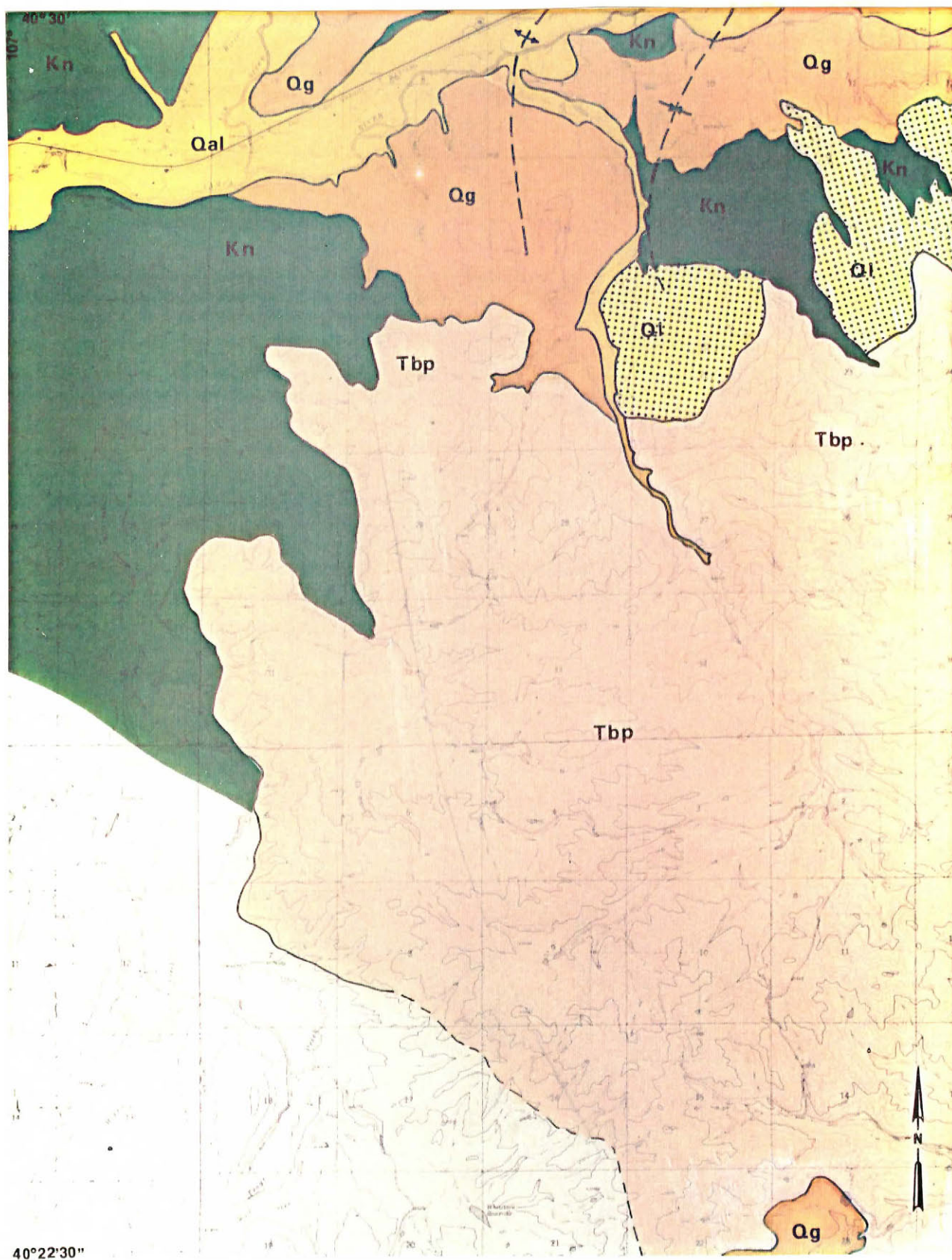


Figure 7. Geologic map of the Cow Creek quadrangle.





Figure 8. Geologic map of the Mad Creek quadrangle.



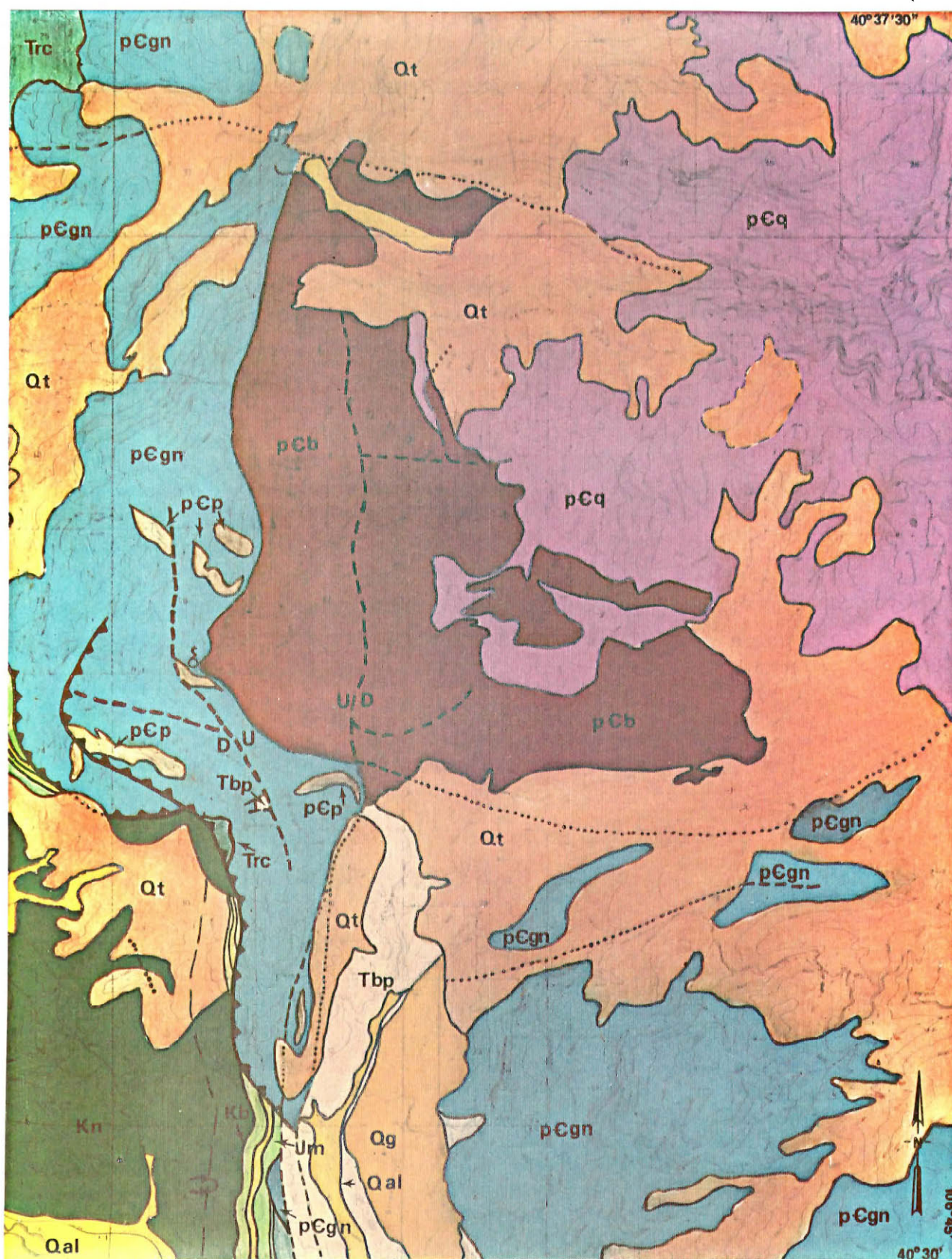
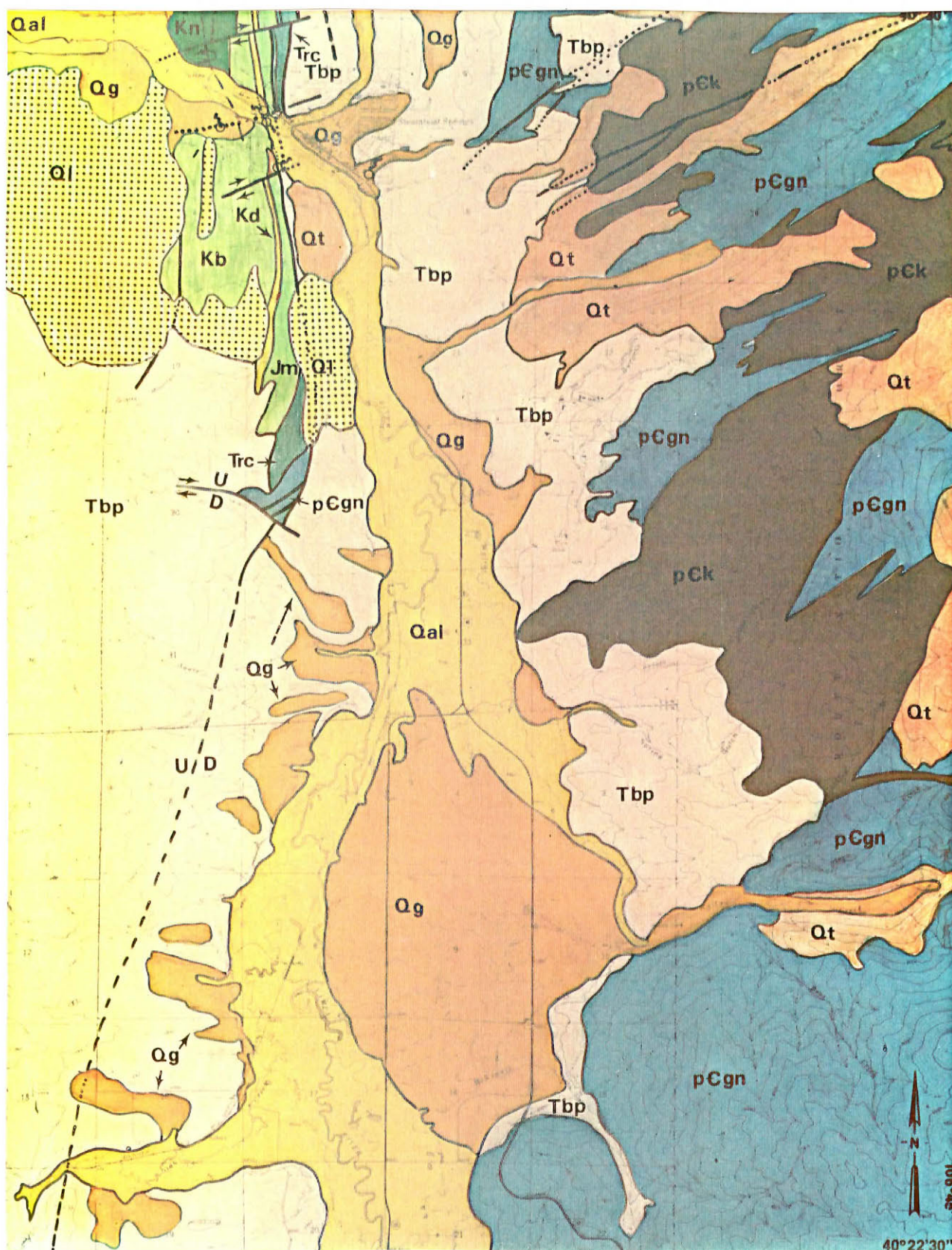


Figure 9. Geologic map of the Rocky Peak quadrangle.





and is exposed again south of the study area. The fault is dated (by lithologic relations) as post-Cretaceous (Niobrara) and pre-Tertiary (Browns Park).

A pair of normal faults with easterly dip trend north from Steamboat Springs bringing Precambrian gneiss into contact with the Chugwater and Chinle group. Near Steamboat Springs, the easternmost of the two faults dies out and the western one is offset by three transverse faults. These faults are dated as post-Tertiary (Browns Park) from cross-cutting relationships.

Numerous other faults and some folding are present as indicated on the geologic maps.




## Map Unit Description

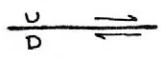
- Qa1 Quaternary Alluvium (Holocene) -- Flood plain sands and gravel deposits, and alluvial fans of primarily Precambrian, well-rounded clasts, of fine-grain to boulder size. [Map color = yellow]
- Q1 Quaternary Landslide Deposit (Holocene and Pleistocene) -- Jumbled soil and rock debris. [Stippled yellow]
- Qg Quaternary Terrace Gravels (Holocene and Pleistocene) -- Gravels in terraces from zero to 110 meters above modern flood plains, ranging in thickness from a few meters to several tens of meters. [Gold]
- Qt Quaternary Till (Holocene and Pleistocene) -- Mostly morainal material of angular to sub-rounded clasts, of clay to boulder (up to five meters diameter) size. [Medium brown]
- Ti Tertiary Intrusive (Pliocene or Miocene) -- Porphyry of intermediate to basaltic composition. [Red]
- Tbp Tertiary Browns Park Formation (Miocene) -- Mainly buff calcareous to non-calcareous siltstone, sandstone, and conglomerate of alluvial (mostly fluvial) colluvial, and aeolian origin. [Tan]
- Kn Niobrary Shale (Upper Cretaceous) -- Blue to dark gray, calcareous, platy shale; 200 to 250 meters thick. [Dark green]


- Kb Benton Shale (Upper to Lower Cretaceous) -- Gray to black non-resistant non-calcareous shale underlain by hard siliceous black shale; 35 to 200 meters thick. [Olive]
- Kd Dakota Sandstone (Lower Cretaceous) -- Buff siliceous sandstone and quartz-pebble conglomerate; some interbedded gray shale; 60 to 120 meters thick. [Lime green]
- Jm Morrison Formation (Upper Jurassic) -- Calcareous purple and green shale and claystone, greenish-white sandstone, gray algal limestone; 150 to 300 meters thick. [Light green]
- Trc Chinle and Chugwater Formations (Triassic and Permian) -- Red calcareous siltstone and shales, some conglomerate in lower part. [Blue-green]
- pEp Pegmatite (Precambrian X and Y) -- Generally small bodies of coarse-grained granite. [Flesh]
- pEb Quartz Monzonite (Precambrian Y) -- Red coarse-grained biotite-hornblende quartz monzonite with large microcline phenocrysts; 1.4 b.y. in age. [Magenta]
- pEq Granite and Quartz Monzonite (Precambrian Y) -- Gray mostly medium-grained biotite granite and biotite quartz monzonite; 1.4 b.y. in age. [Purple]
- pEk Quartz Monzonite Gneiss (Precambrian X) -- Red medium and coarse-grained biotite-hornblende quartz-monzonite gneiss; 1.7 b.y. in age. [Dark brown]

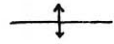
pEgn Felsic Gneiss to Amphibolite Metavolcanics (Precambrian Y)


-- Mainly pink to gray plagioclase-quartz-biotite gneiss, and many types of felsic to mafic green amphibolite, including other gneisses, schists, and quartzite. [Turquoise]


 Contact -- Dashed where approximate, dotted where concealed.

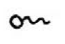
 High-Angle Fault -- Dashed where approximate, dotted where concealed; U = upthrown side, D = downthrown side; arrows denote relative horizontal movement on strike-slip faults.

 Reverse Fault -- Dotted where concealed; sawteeth on upper plate.

 Crest of Anticline

 Crest of Syncline

 Overtaken Syncline

 Hot or warm spring location



## GEOOTHERMOMETRY

Several Steamboat and Routt springs were sampled for geothermometry work along with temperature, discharge rate, and dissolved solids content by Barrett and Pearl (1978). The results of their work are summarized in the following.

### Routt Hot Springs

Several springs issue from both the north and south sides of Hot Springs Creek and are concentrated in a narrow zone. The largest spring, located about 35 meters up the hillside, has a temperature of  $64^{\circ}\text{C}$ , discharges 1.6 to 3.2 liters per second (l/s), and has 518 to 552 milligrams per liter (mg/l) of total dissolved solids (tds). The largest spring on the north side of the creek (about two meters above creek level) has a temperature of  $62^{\circ}\text{C}$ , discharges at 1.9 l/s, and has 539 mg/l of tds. A spring located about 17 meters east of the first spring issues at  $54^{\circ}\text{C}$  and about 0.1 l/s. A fourth spring, located 13 meters southeast of the previous spring, issues at  $51^{\circ}\text{C}$  and also at 0.1 l/s.

For the silica geothermometry, the quartz-silica geothermometer was used since it was determined that quartz was controlling the silica content of the springs. This model indicates a subsurface maximum water temperature of  $125^{\circ}\text{C}$  to  $136^{\circ}\text{C}$ . As per the assumptions for the silica model, the quartz criterion was used for the mixing model geothermometer. Using a cold water fraction of 71 to 76 per cent of spring flow, the indicated

subsurface temperature is 192°C to 231°C. Due to the large seasonal variation of subsurface and surface waters, it cannot be assumed that this model adequately estimates the subsurface temperatures. But the estimates do fall within the range of normal error.

The Na-K (sodium-potassium) and Na-K-Ca (sodium-potassium-calcium) geothermometers indicate subsurface temperatures of 165°C to 170°C and 154°C to 159°C respectively.

From the three models, the best estimate for subsurface temperature is 125°C to 175°C, essentially a combination of the silica, Na-K, and Na-K-Ca geothermometry results which were fairly consistent over four quarter-year samplings.

#### Steamboat Springs

Most of the springs near Steamboat Springs are warm (about 25°C), being cooled by mixing with water from the Yampa River which passes close to most of them. Steamboat Spring, on the west end of town, has a temperature of 26°C, a discharge of about 1.3 l/s, and 6170 mg/l of tds. Sulphur Cave Spring, located up the hill south of town, has a temperature of 20°C, a discharge of 0.6 l/s, and 4530 mg/l of tds. Heart Spring, at the southeast edge of Steamboat Springs, is the source of hot water for the recreational pool. It issues at 39°C, 8.8 l/s, and contains 903 mg/l of tds.

Geothermometry could not be used for Steamboat and Sulphur Cave Springs because of their surface temperatures. Thus all geothermometer estimates are for Heart Spring.

The quartz-silica geothermometer gave a subsurface temperature estimate of  $101^{\circ}\text{C}$ . The quartz-silica mixing model with a cold water fraction of 81 per cent gave an estimate of  $179^{\circ}\text{C}$ . Both of these results may be in error because of the low silica content of the spring. The Na-K and Na-K-Ca geothermometers gave estimates of  $148^{\circ}\text{C}$  and  $141^{\circ}\text{C}$ , which are fairly close to the subsurface temperature estimates for Routt Hot Springs. Therefore the best estimate for subsurface temperature for Heart Spring is  $125^{\circ}\text{C}$  to  $130^{\circ}\text{C}$ .

## GRAVITY

Gravity measurements were obtained at 114 stations in the four quadrangle area. The stations were spaced approximately one and one-half kilometers apart where possible, although this was limited by inaccessibility to vehicles and poor accessibility on foot because of thick brush and rough terrain.

Readings were taken with LaCoste-Romberg gravity meter G-235. Elevations were determined from benchmarks and spot elevations at road junctions, road bends, bridges, peaks, passes, and section corners. Some elevations were estimated by location and contours on 1:24,000 scale topographic maps.

A temporary base station, SBT-2, was tied into twice daily to check for meter drift. The survey was also tied into the International Gravity Base Station, ACIC 3903-2, in Steamboat Springs (designated as SBT-IGN) which has an observed gravity value of 979576.59 milligals and an elevation of 2040.64 meters.

The data were reduced with the U. S. Geological Survey computer program Gravity Reduction (Godson et al, 1978). Linear meter drift and tides were removed from the meter reading (in milligals) to obtain observed gravity values for each station. The theoretical gravity at each station was calculated by the 1967 International Gravity Formula which derives the gravity at sea level as a function of latitude,  $\phi$  by:

$$\begin{aligned} \text{Theoretical gravity} &= 978.0318 (1 + 0.0053024 \sin^2 \phi \\ &\quad (\text{in gals}) \\ &\quad - 0.0000059 \sin^2 2\phi) \end{aligned}$$

Free-air corrections were applied to each station to reduce the measured gravity value to the datum plane (sea level) without accounting for the mass between the station elevation and the datum. This correction is made by:

$$\text{Free-air correction} = (0.30855 + 0.00022 \cos 2\phi)h - 0.000000072 h^2$$

(in milligals)

where h is the station elevation in meters.

Simple Bouguer corrections were made to account for the attraction of mass between the station elevation and datum plane, assumed to be an infinite slab with a density of 2.67 grams/cubic centimeter (g/cc). This correction is calculated by:

$$\text{Simple Bouguer correction} = 0.01040 h$$

(in milligals)

Complete Bouguer corrections were also applied to account for the attraction of mass caused by topographic relief on the top surface of the infinite slab. These were calculated by the U. S. Geological Survey computer program, Bouguer (Godson, 1978), using elevations digitized from topographic maps at 15" intervals. The corrections were applied from Hayford-Bowie zones A through O (outer radii of 2 meters to 166.7 kilometers), using an average density of 2.67 g/cc. Curvature corrections were also calculated (to account for the earth's curvature) and averaged about 1.50 mgals.



The complete Bouguer anomaly is found by:

$$\begin{aligned} \text{Complete Bouguer anomaly} = & \text{Observed gravity} - \text{theoretical gravity} \\ & + \text{free-air correction} \\ & - \text{simple Bouguer correction} \\ & + \text{terrain correction} \\ & - \text{curvature correction} \end{aligned}$$

The values for each station are given in appendix A. The complete Bouguer anomalies are plotted and contoured and shown in the map in the inside back cover. Station locations are designated by open squares, and highs and lows are labeled by capital letters.

Eleven stations of the Department of Defense (DOD) gravity network were repeated and compared to check for consistency between the two surveys. The average difference in observed gravity values is  $\pm 0.27$  milligals. Fifteen DOD stations were reduced and incorporated in the complete Bouguer anomaly maps to fill in areas of sparse data.

Bouguer anomaly values are more negative when gravitational attraction lessens in response to lack of lower density beneath an area. To help in the interpretation of the Bouguer anomalies, some average densities for rock types exposed in the Steamboat Springs area are given below (after Telford et al, 1977). Although no density measurements were made near Steamboat Springs, these values should give a rough idea of expected contrasts.

<u>Rock Type</u>	<u>Density (g/cc)</u>	
Alluvium	1.98 (wet)	1.54 (dry)
Glacial drift	1.80 (wet)	
Gravels	2.00 (wet)	1.95 (dry)
Sandstones	2.35 (wet)	2.24 (dry)
Shales	2.40 (wet)	2.10 (dry)

Granite	2.64 avg. (ranges 2.50 - 2.81)
Gneiss	2.80 avg. (2.59 - 3.00)
Amphibolite	2.96 avg. (2.90 - 3.04)
Quartz Diorite	2.79 avg. (2.60 - 2.96)

The Bouguer lows A and B decrease to the northwest and southwest respectively, coinciding with the thickening sequence of sedimentary rocks (sandstones and shales) away from the mountain front. The Elk Mountain intrusive shows no effect on the contours, although no data were obtained on the intrusive itself, and thus the intrusive is probably local and of no great lateral extent.

Anomaly C, a high of more than -230 mgals, is centered over a topographic high bounded by a major fault to the east. The Browns Park sandstone and Mesozoic sedimentary rock cover is probably thin here and underlain by an upfaulted block (with faults to the southwest, north, and east) of the Precambrian gneiss and metavolcanics (map unit p $\epsilon$ gn) bringing the higher density rock closer to the surface.

The Bouguer low D lies over the Yampa River Valley which is filled with Quaternary alluvium and glacial gravels. The contours get more negative to the south where the valley broadens and sediments thicken.

The high to the southeast, E, contours the mountain front of high density gneisses and metavolcanics (map units p $\epsilon$ gn and p $\epsilon$ k). The -232 mgal contour follows the break in slope and appears to be a typical value for the metamorphic rocks-sedimentary rock contact as evidenced by the gravity trend northwest through highs F, G, and H (following the reverse fault front).

The low, I, lies on the south edge of the reverse fault where less dense sediments are upturned and in contact with the Precambrian rock. The low to the northeast, J, is enclosed by the -236 mgal contour which follows the mapped contact between metamorphics and less dense granite and quartz monzonites (map units pCb and pCq).



## AUDIO-MAGNETOTELLURICS

Readings were taken at thirteen audio-magnetotelluric (AMT) stations in the vicinity of Routt and Steamboat Springs with locations given in figure 11.

The AMT system, developed by the U. S. Geological Survey (Hoover et al, 1976; Hoover and Long, 1975), measures natural and artificial electromagnetic waves at twelve frequencies from 7.5 to 18,600 hertz. The technique has proved to be a fairly effective reconnaissance tool in geothermal areas where used for resistivity mapping.

For each station, the electric (E) and magnetic (H) fields are measured in orthogonal directions at each frequency. Two simultaneous soundings are made with the 100-meter electric field lines (using copper-clad steel stakes as electrodes) and the coils oriented east-west and north-south. The apparent resistivity is determined as:

$$\rho_a = \frac{1}{5f} \left| \frac{E_x}{H_y} \right|^2 \quad (1)$$

where:  $\rho_a$  = apparent resistivity in ohm-meters

$f$  = frequency in hertz

$E_x$  = horizontal x-directed electric component in  
millivolts/kilometer

$H_y$  = horizontal y-directed magnetic field in gammas

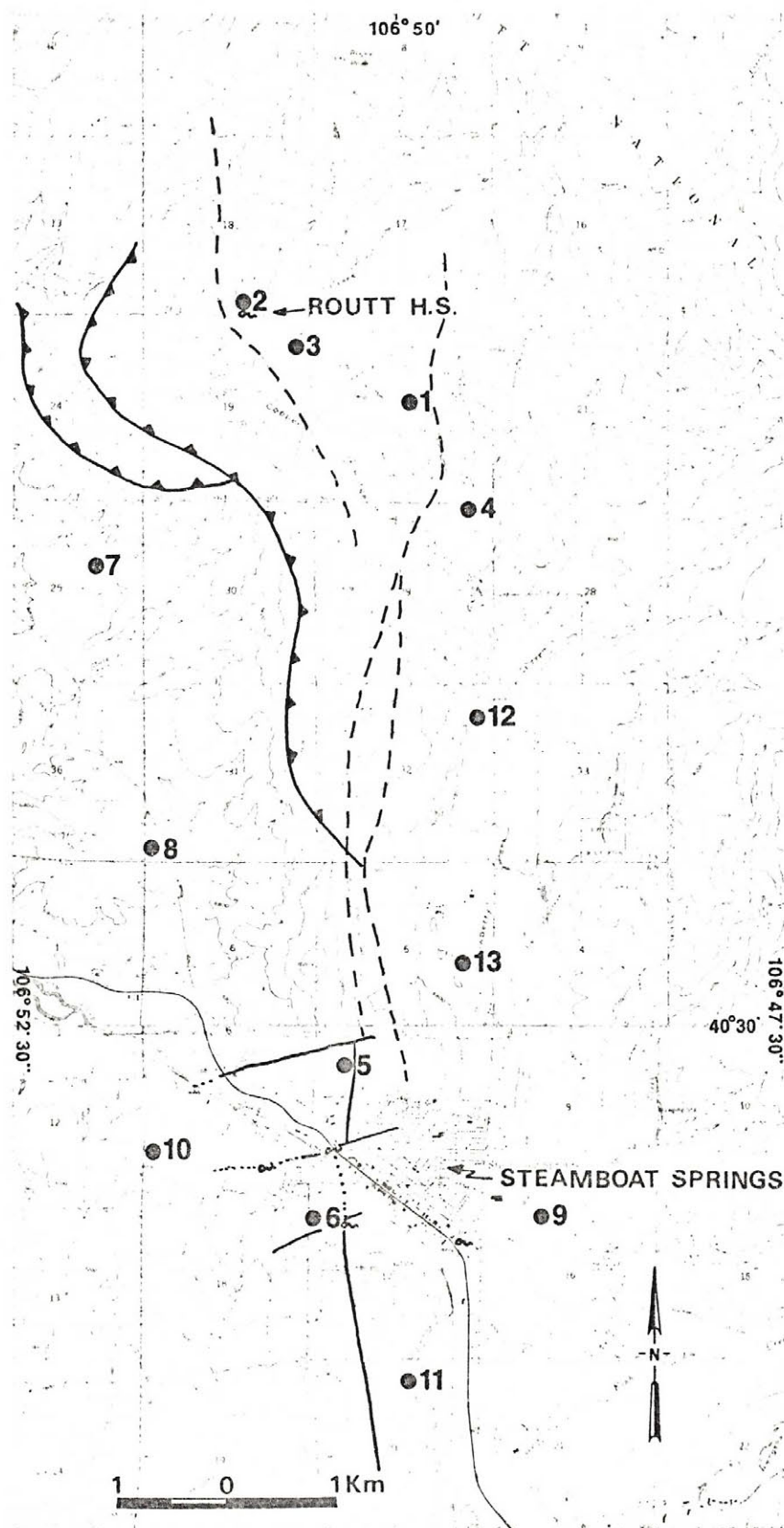


Figure 11. Audio-magnetotelluric station location map.

The source for most of the natural electromagnetic fields for the AMT data is lightning storms, with the largest and most frequent storms occurring at equatorial latitudes. Man-made VLF (very low frequency) signals are employed at the 10,200 and 18,600 hertz levels. In most cases the results at the middle frequencies (285, 685, 1200, 3300 hertz) are poor or unattainable because of low signal strength and cultural noise.

If they are far enough from the source, the electromagnetic waves can be treated as plane waves and penetrate the earth to a depth determined by frequency and the earth's resistivity. The skin depth, that depth where signals are attenuated to  $1/e$  (37%), may be determined at various frequencies to indicate the approximate depth of investigation. Also, boundaries more than one-half skin depth distant will not be detected. The following relation obtains:

$$\delta = 503 \sqrt{\rho/f} \quad (2)$$

where:  $\delta$  = skin depth in meters

$\rho$  = resistivity in ohm-meters

$f$  = frequency in hertz

The relative strengths of the electric and magnetic fields are recorded, the ratio between orthogonal E and H fields calculated, and resistivity determined by equation 1. Generally, enough ratios are calculated at each frequency to give a standard deviation of less than ten per cent of the apparent resistivity.

This relatively quick method then gives a rough idea of resistivity changes with depth (since the lower frequencies penetrate deeper).

The results of the Steamboat Springs soundings (apparent resistivity with frequency) are given in appendix B. These results were plotted and contoured at 7.5 and 27 hertz. The 7.5 hertz data were log averaged because in part the data scatter is greater due to a poorer signal to noise ratio. The 27 hertz data were plotted separately in the north-south and east-west E-line orientations, a method that can distinguish lateral variations in resistivity. For example, with the E-line oriented north-south, east-west trending structural features can be more easily detected than with an east-west orientation. These two frequencies were contoured because they are usually the strongest in signal strength and provide the deepest information. The contour maps are shown by figures 12, 13, and 14 depicting lateral resistivity changes. The contour interval is logarithmic because of the wide variation of resistivity.

The contour maps all show sharply increasing resistivity gradients toward the north and east, indicative mostly of lithologic change (from primarily sedimentary to crystalline rocks). They also show an increase in resistivity between the depths sampled at 27 and 7.5 hertz. The low resistivities to the west may be the result of thick sequences of Cretaceous shales. The steep gradient to the south may be exaggerated on the 7.5 hertz map but also appears on the 27 hertz map with the E-line oriented east-west. This probably is the result of Precambrian basement under a thin sedimentary cover.

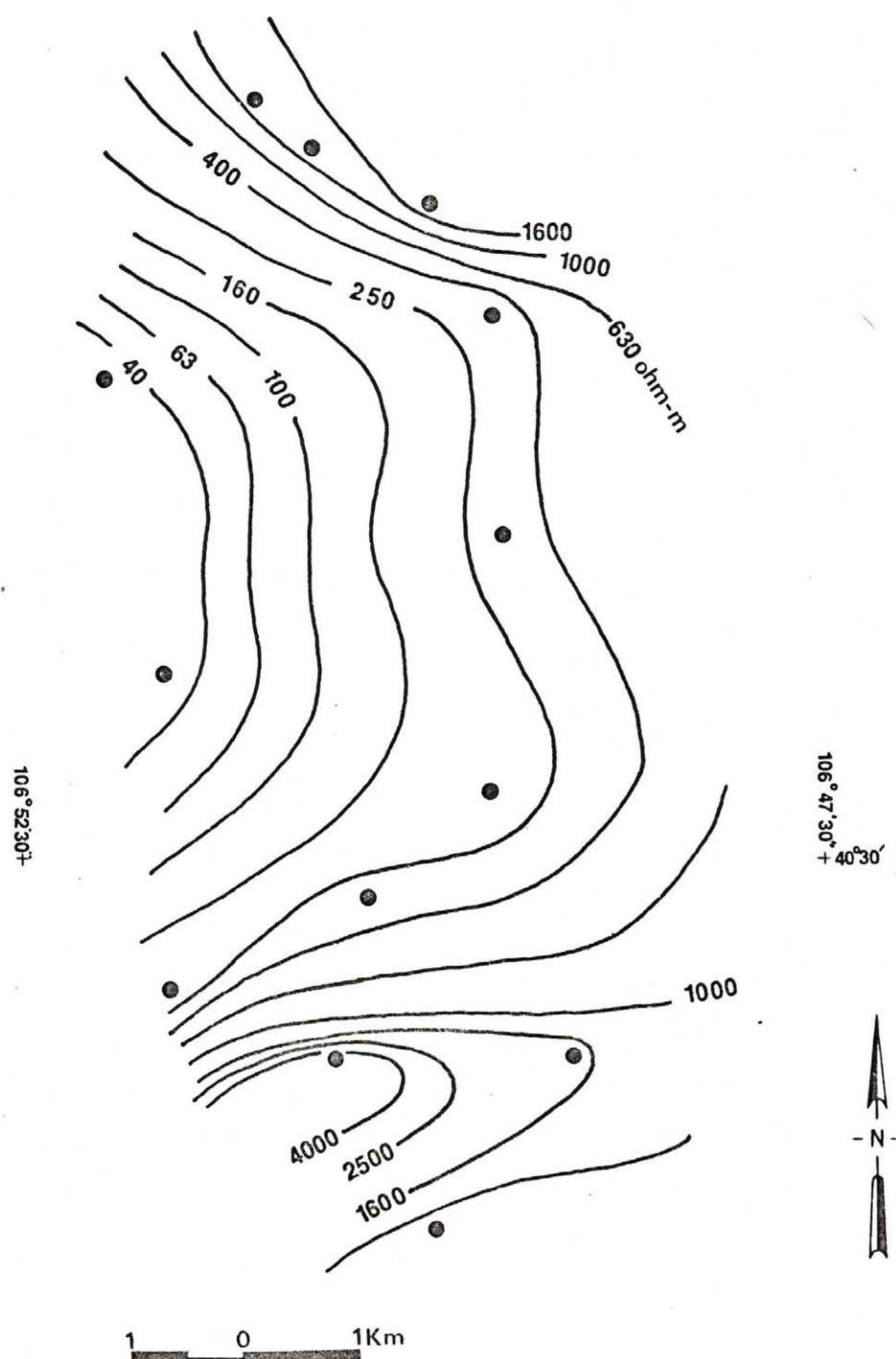


Figure 12. AMT apparent resistivity map at 7.5 hertz.



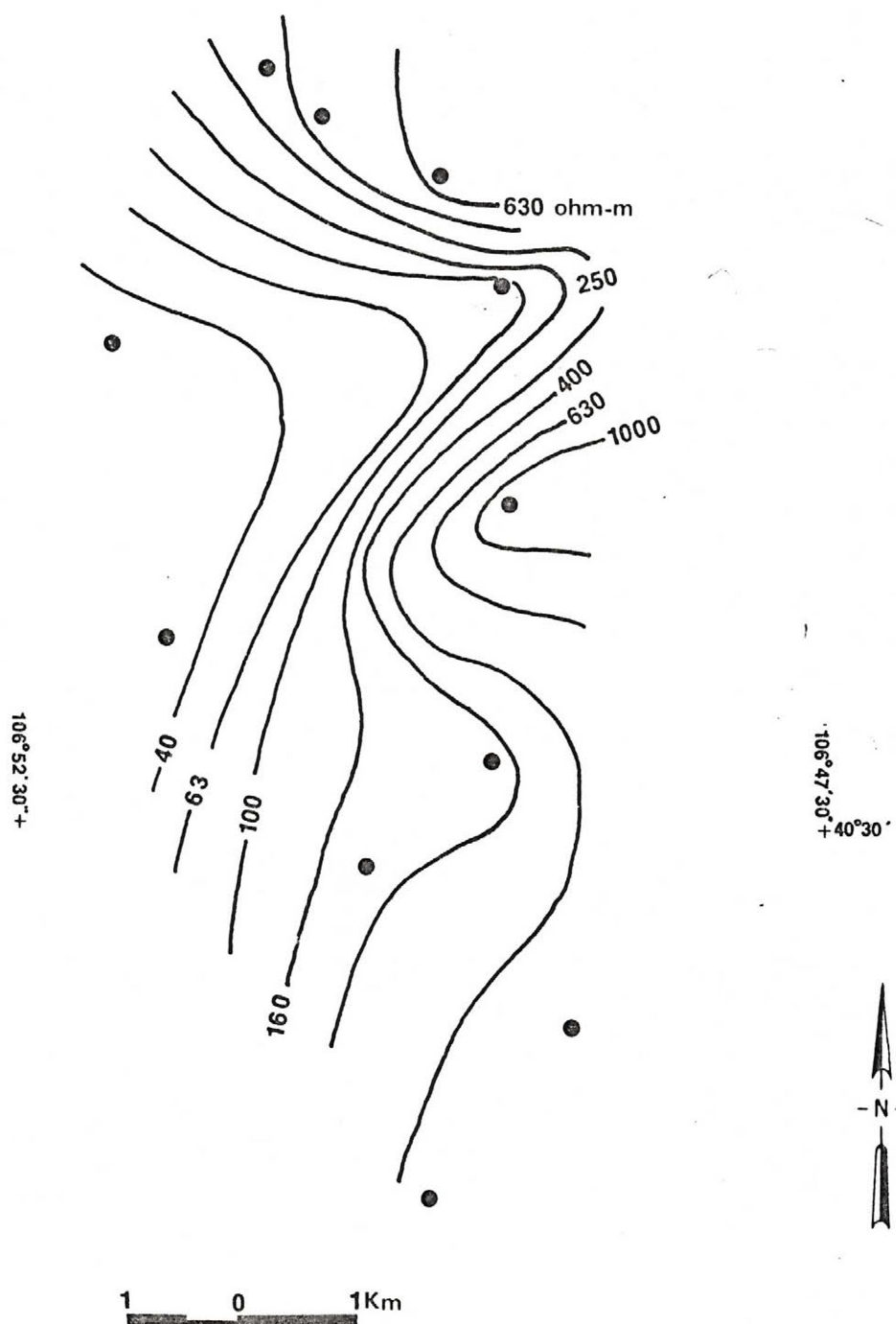


Figure 13. AMT apparent resistivity map at 27 hertz, E-line N-S.

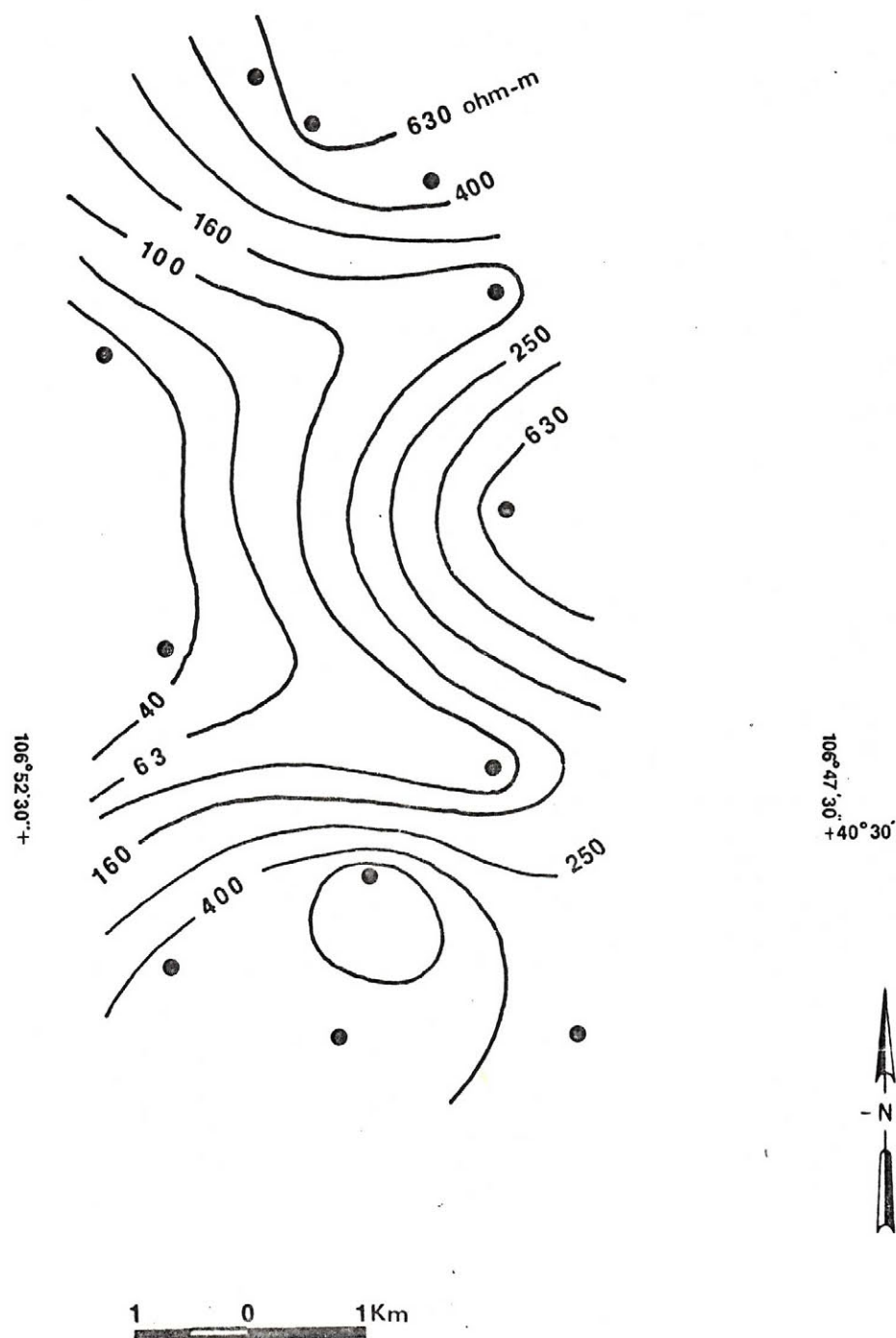


Figure 14. AMT apparent resistivity map at 27 hertz, E-line E-W.

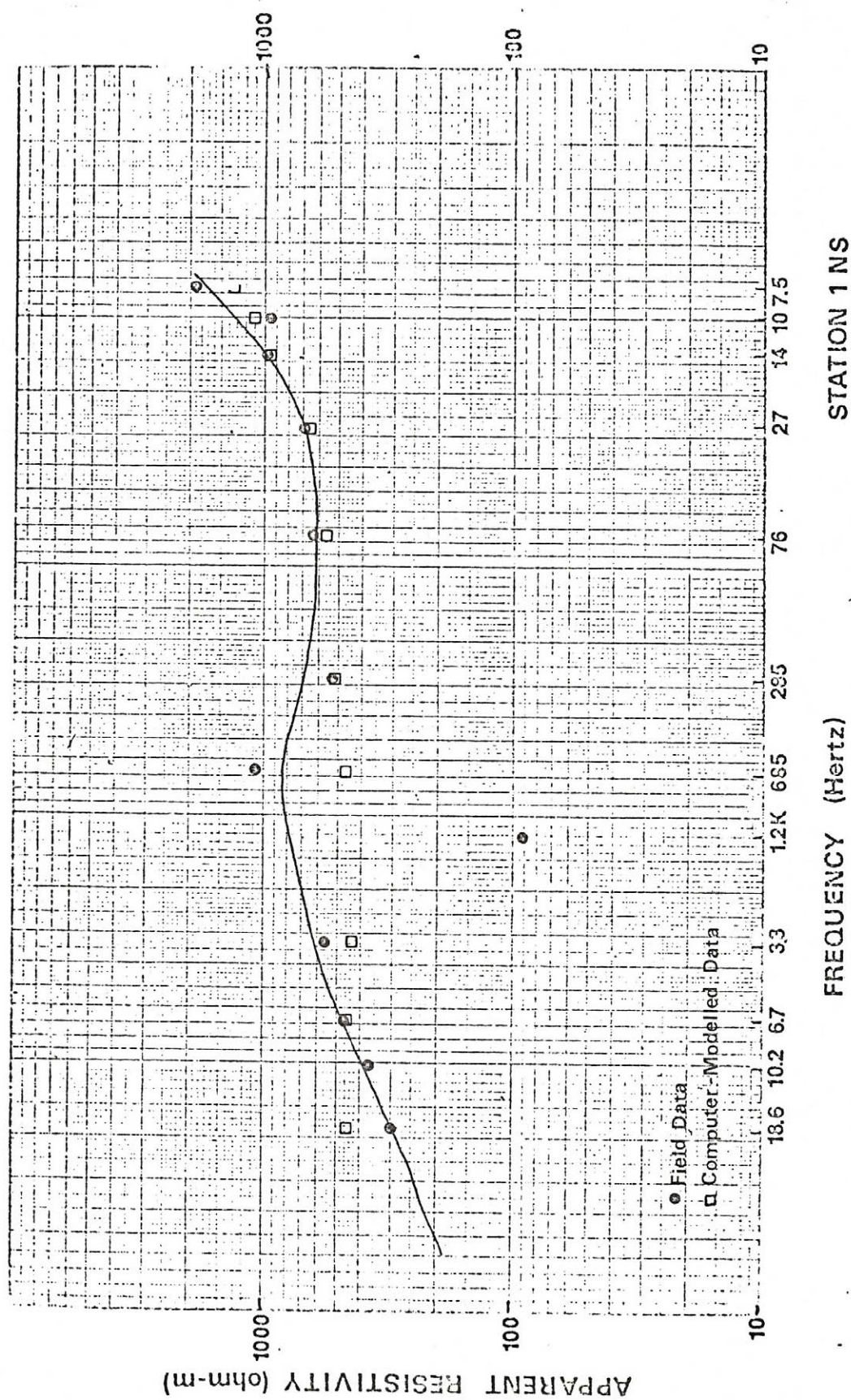


Figure 15. AMT sounding curve, station 1 NS



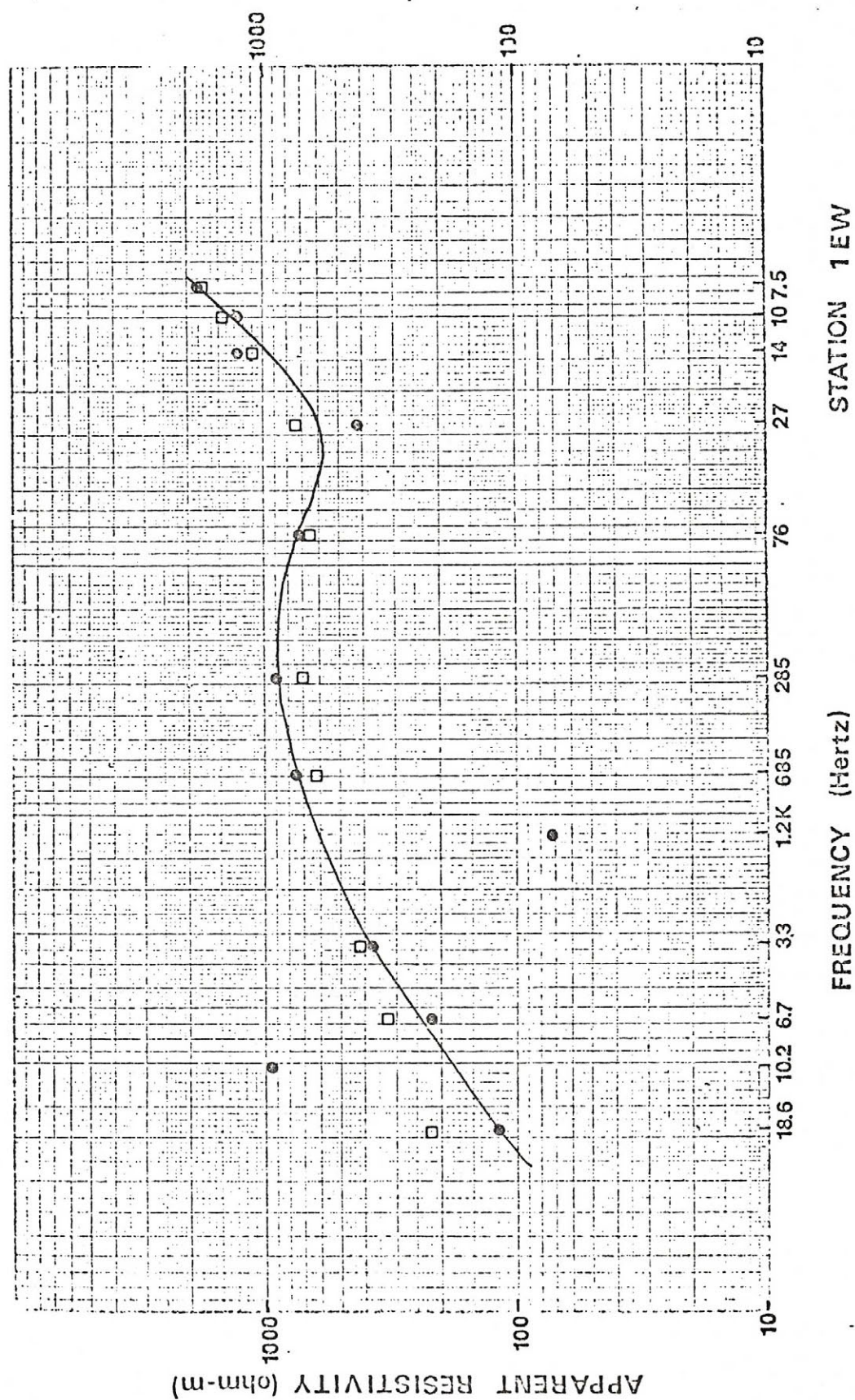


Figure 16. AMT sounding curve, station 1EW



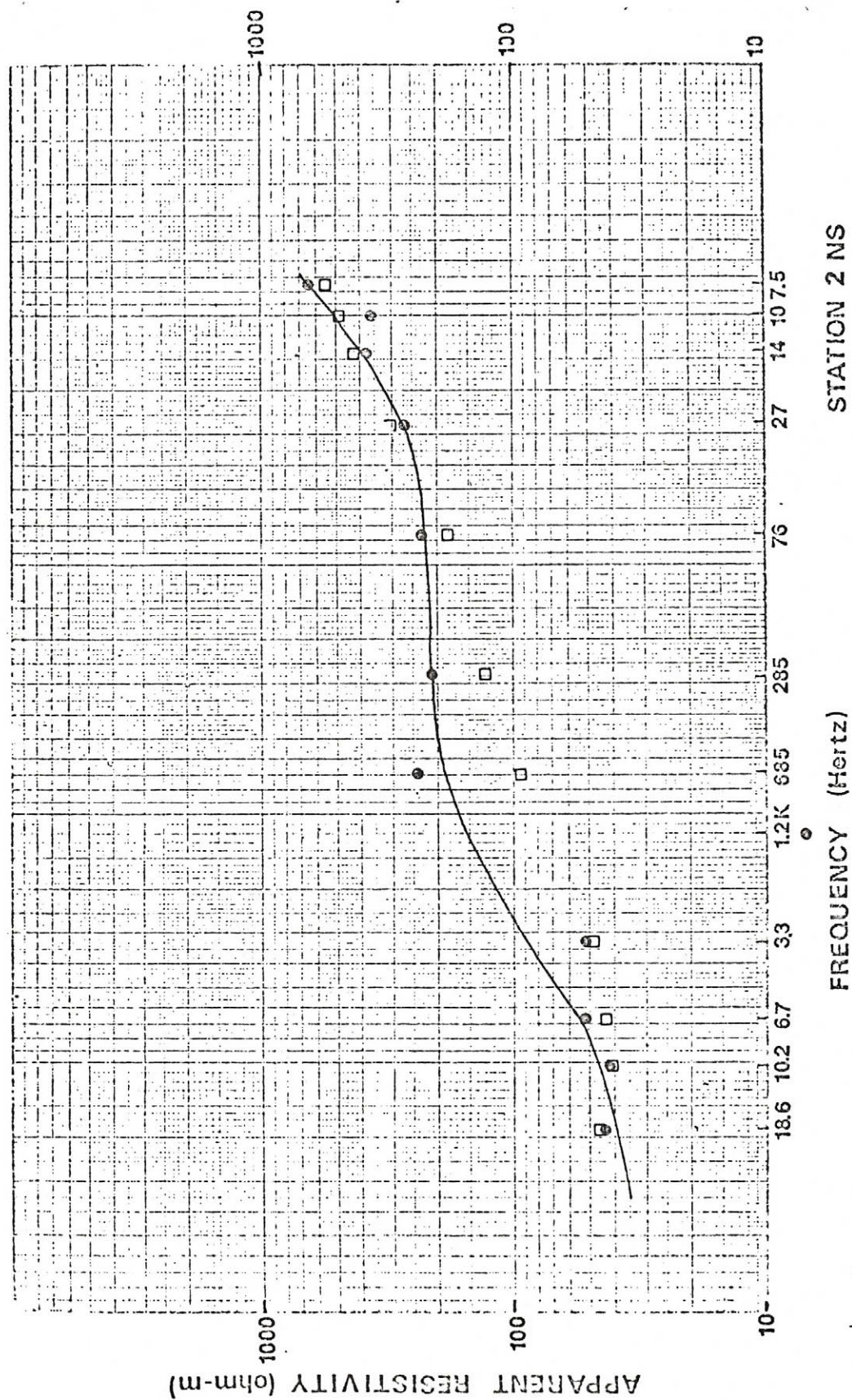


Figure 17. ANT sounding curve, station 2NS



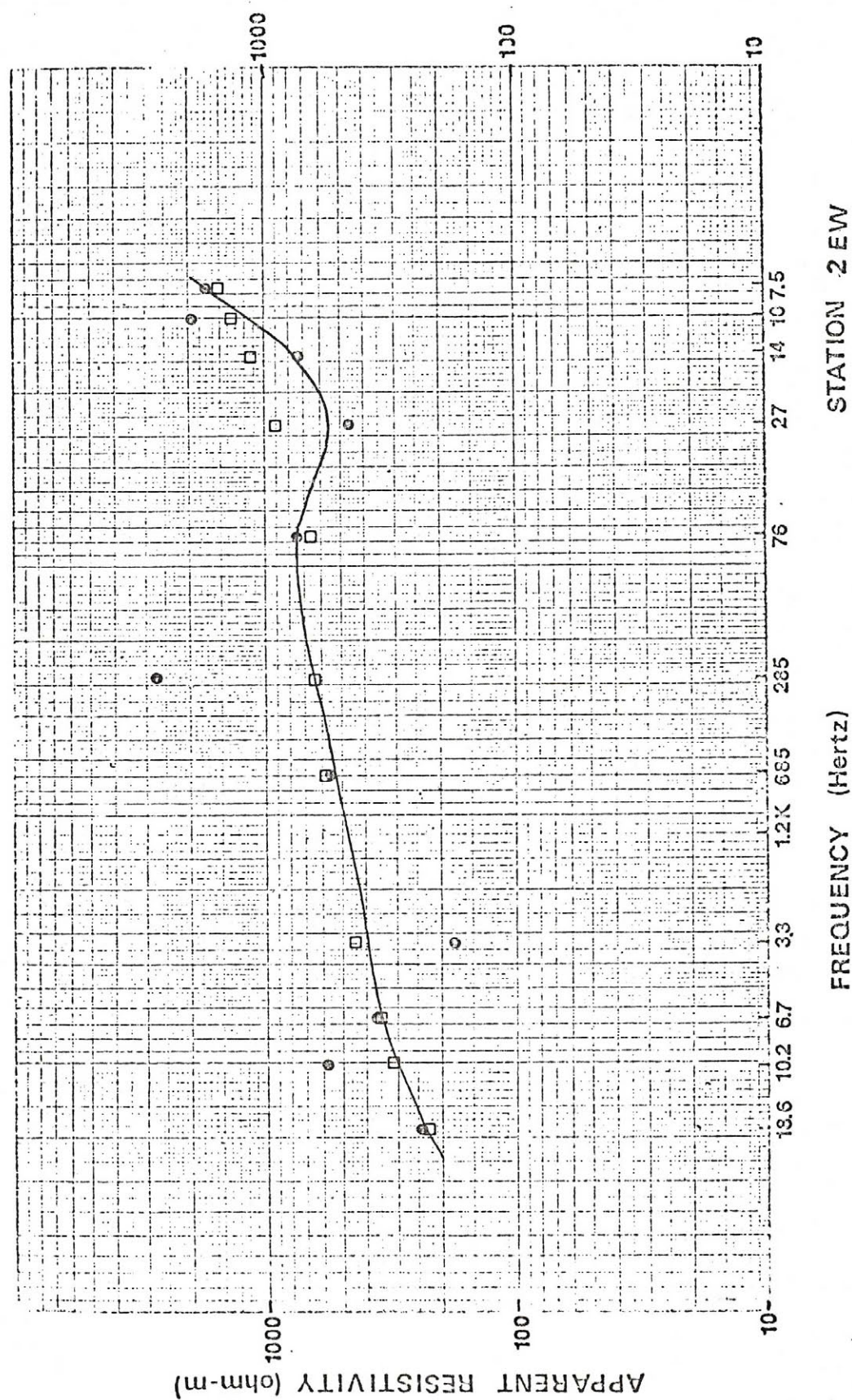


Figure 18. AMT sounding curve, station 2EW



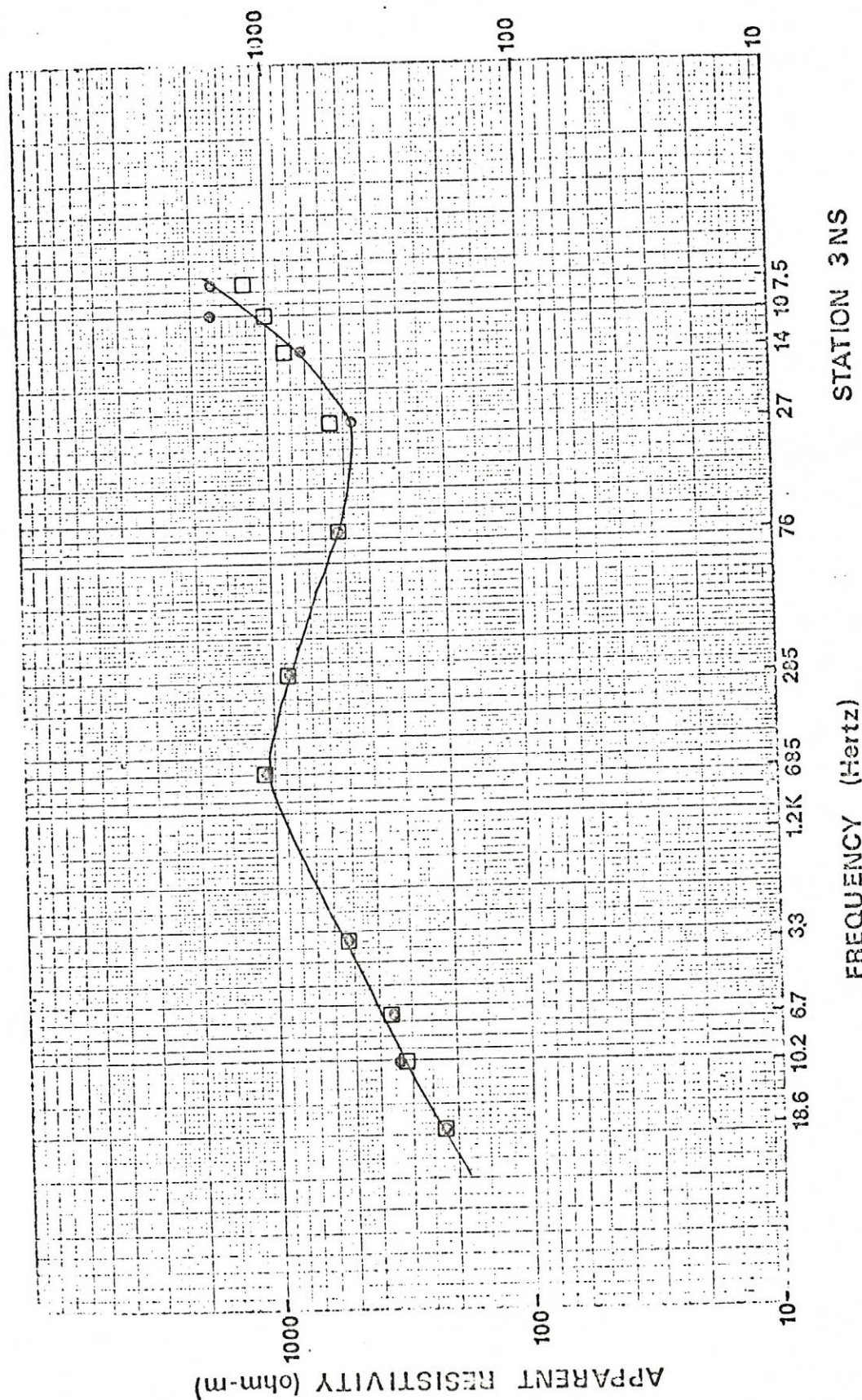


Figure 19. AMT sounding curve, station 3NS



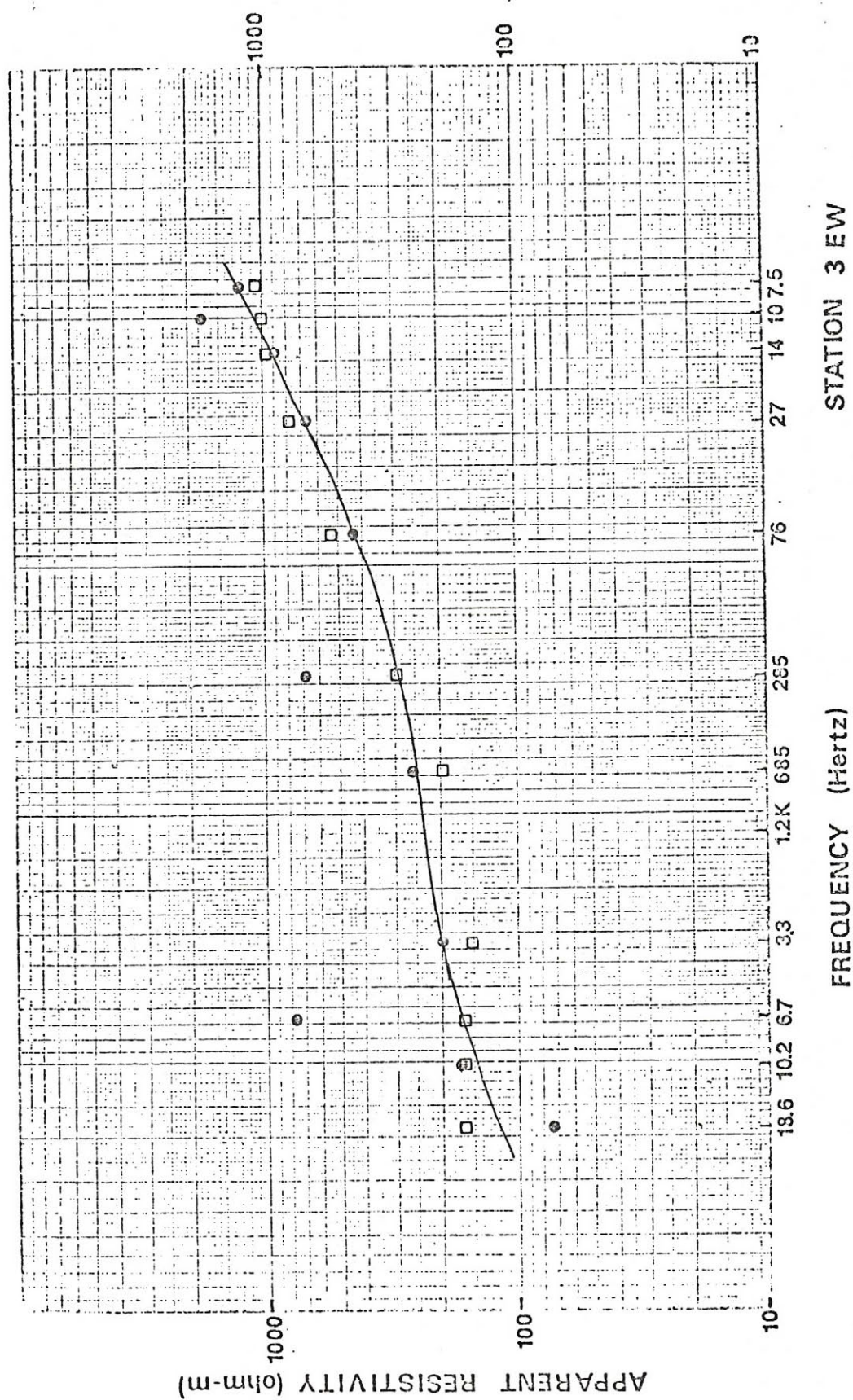


Figure 20. AMT sounding curve, station 3EW



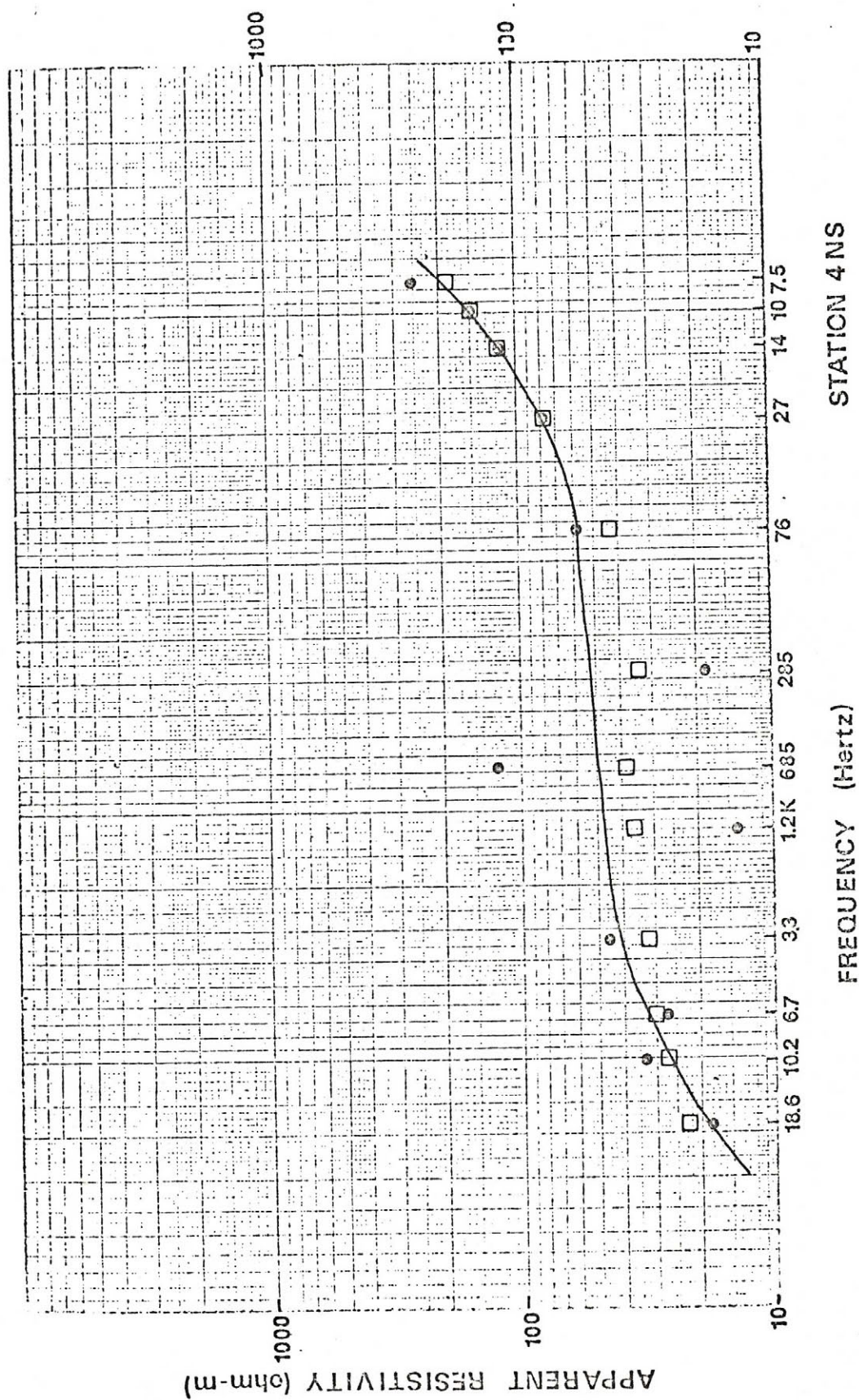


Figure 21. AMT sounding curve, station 4NS



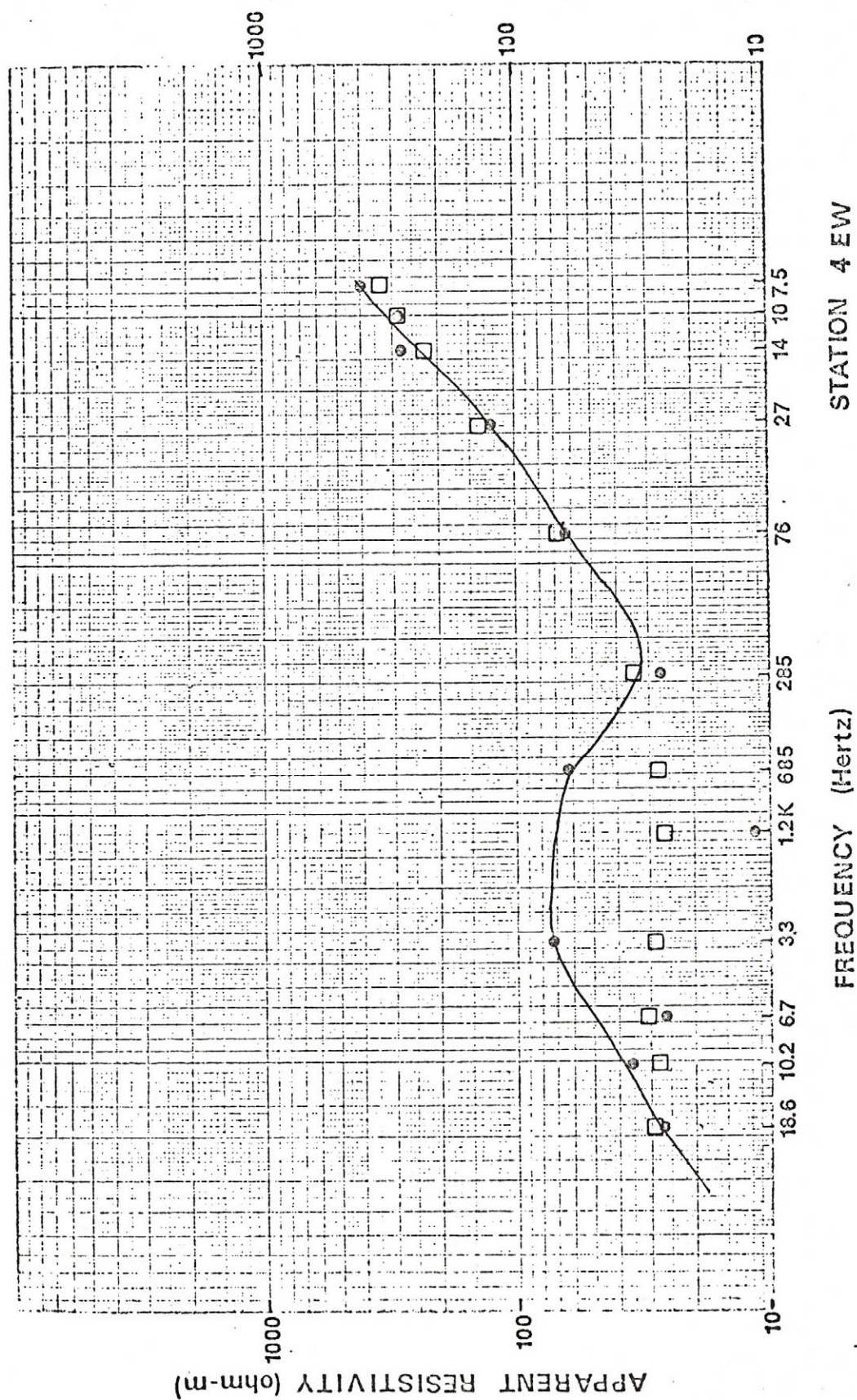


Figure 22. AMT sounding curve, station 4EW



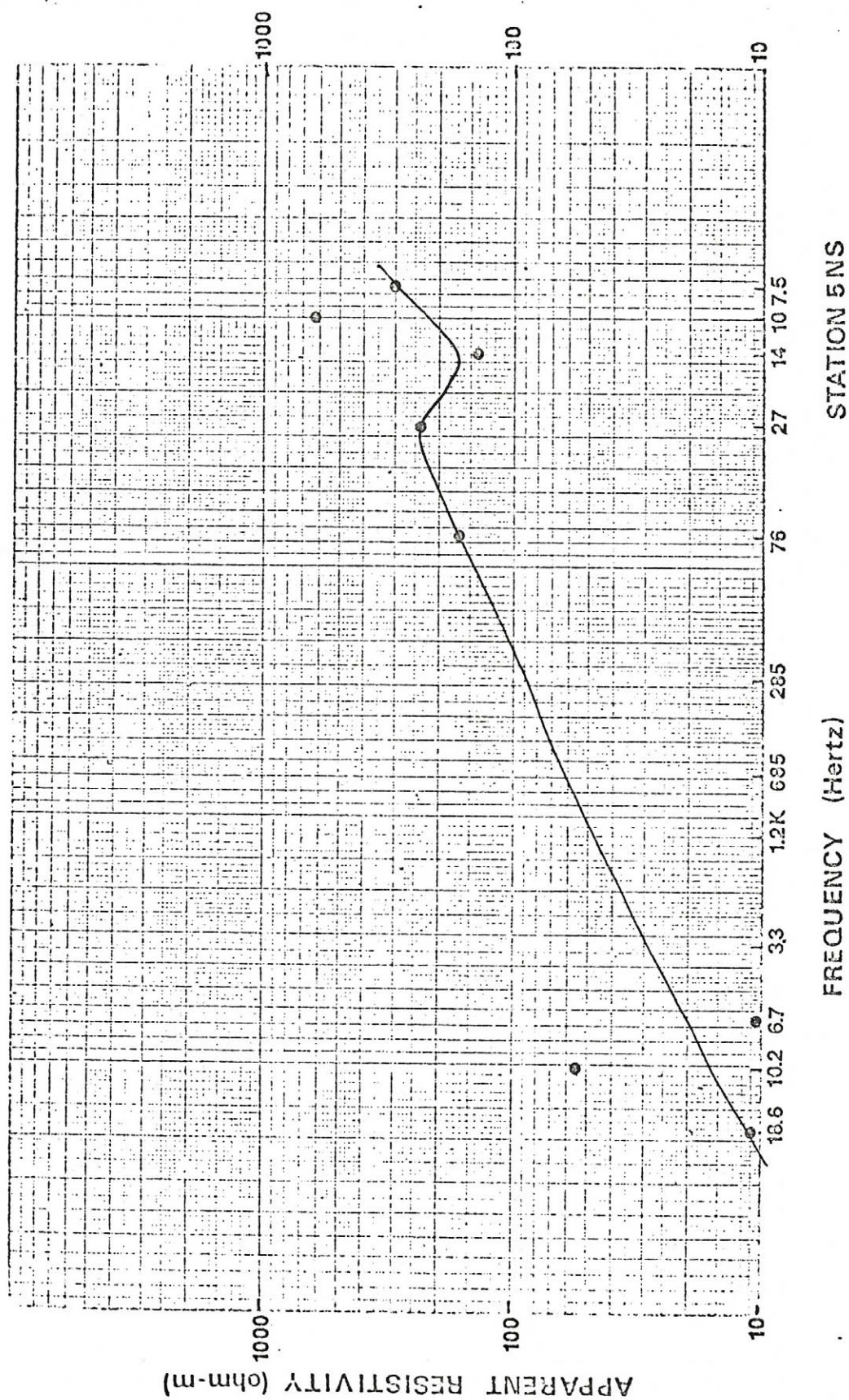


Figure 23. AMT sounding curve, station 5NS



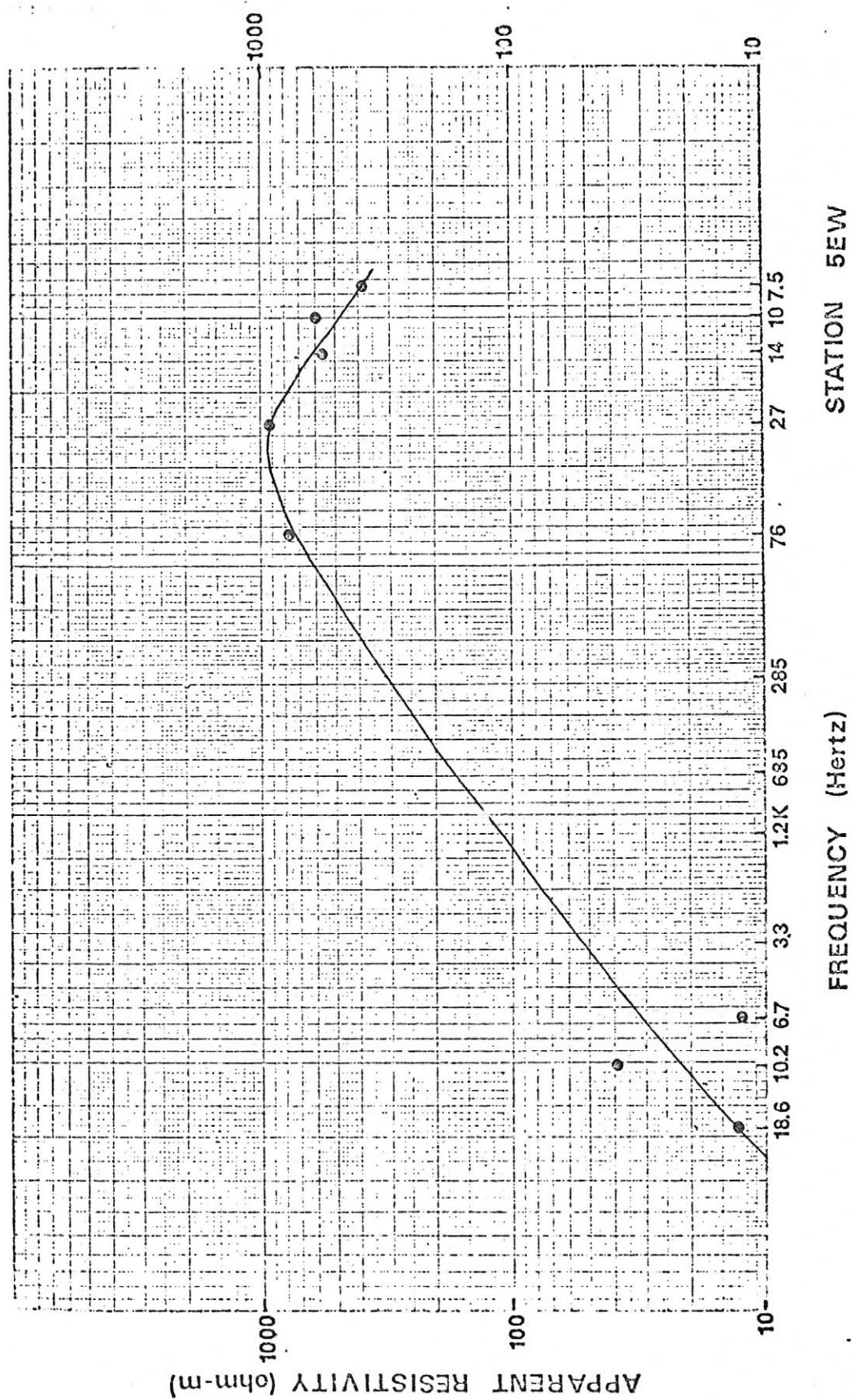


Figure 24. AMT sounding curve, station 5EW



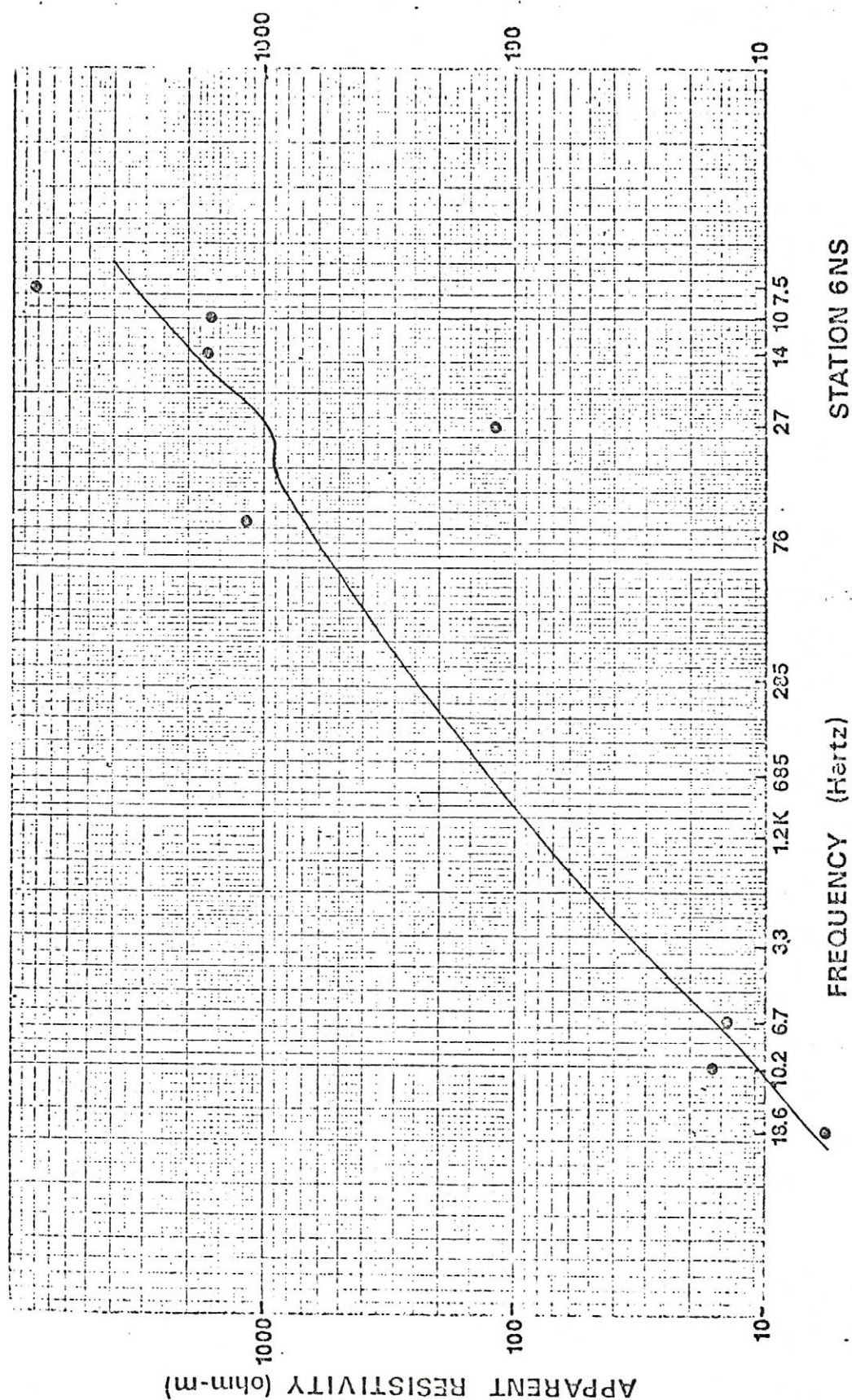


Figure 25. AMT sounding curve, station 6NS



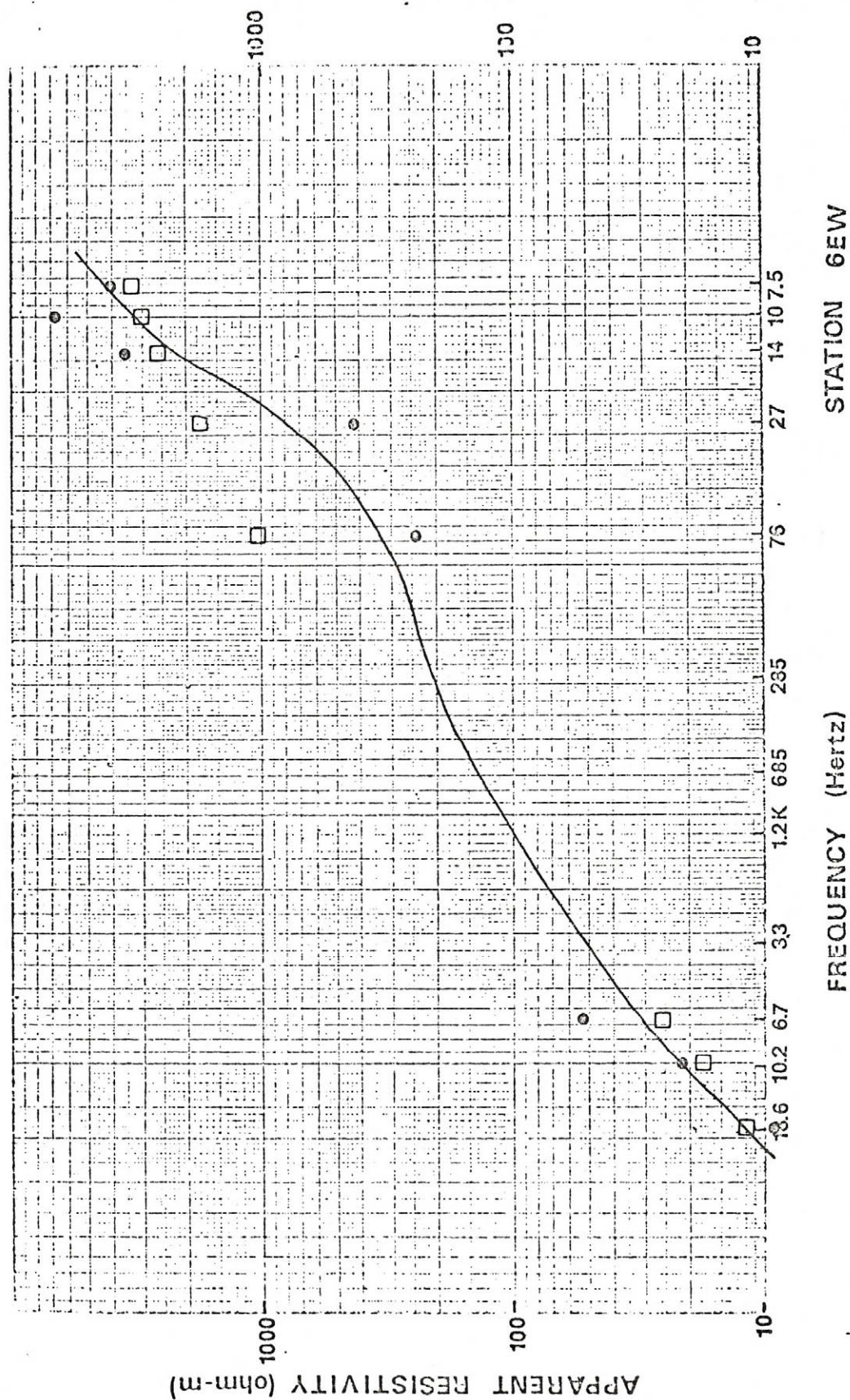


Figure 26. AMT sounding curve, station 6EW



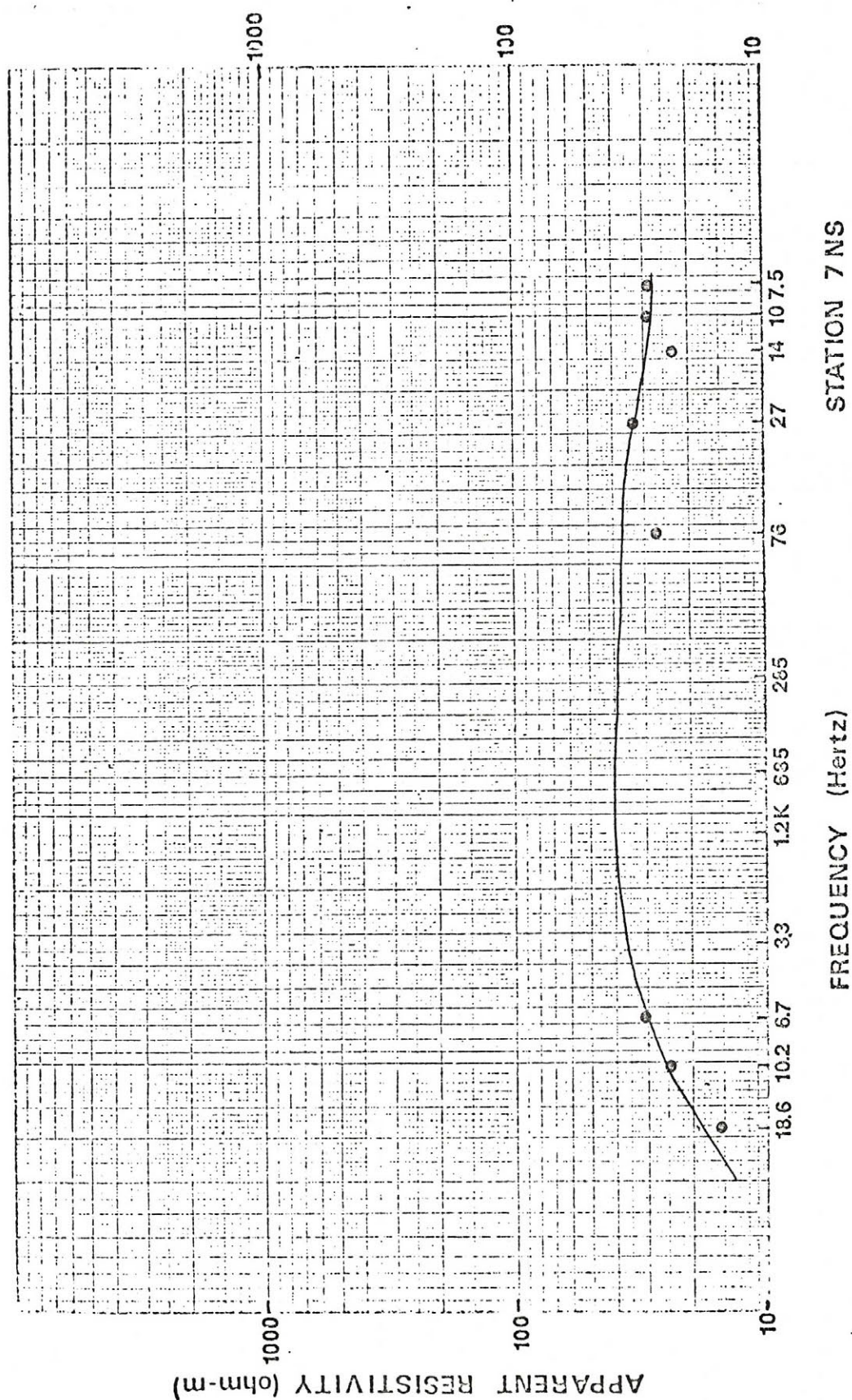


Figure 27. AMT sounding curve, station 7NS



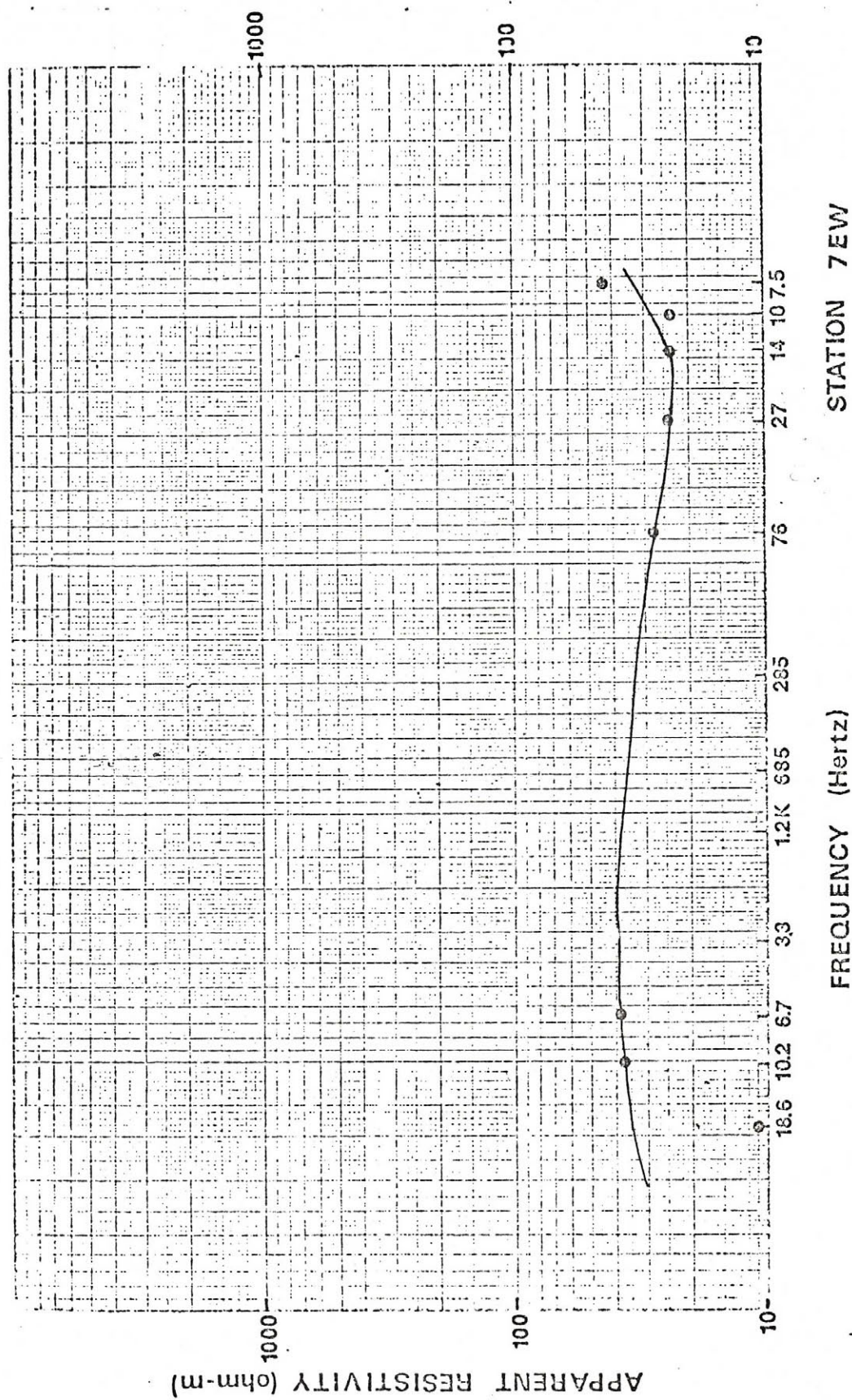


Figure 28. AMT sounding curve, station 7EW



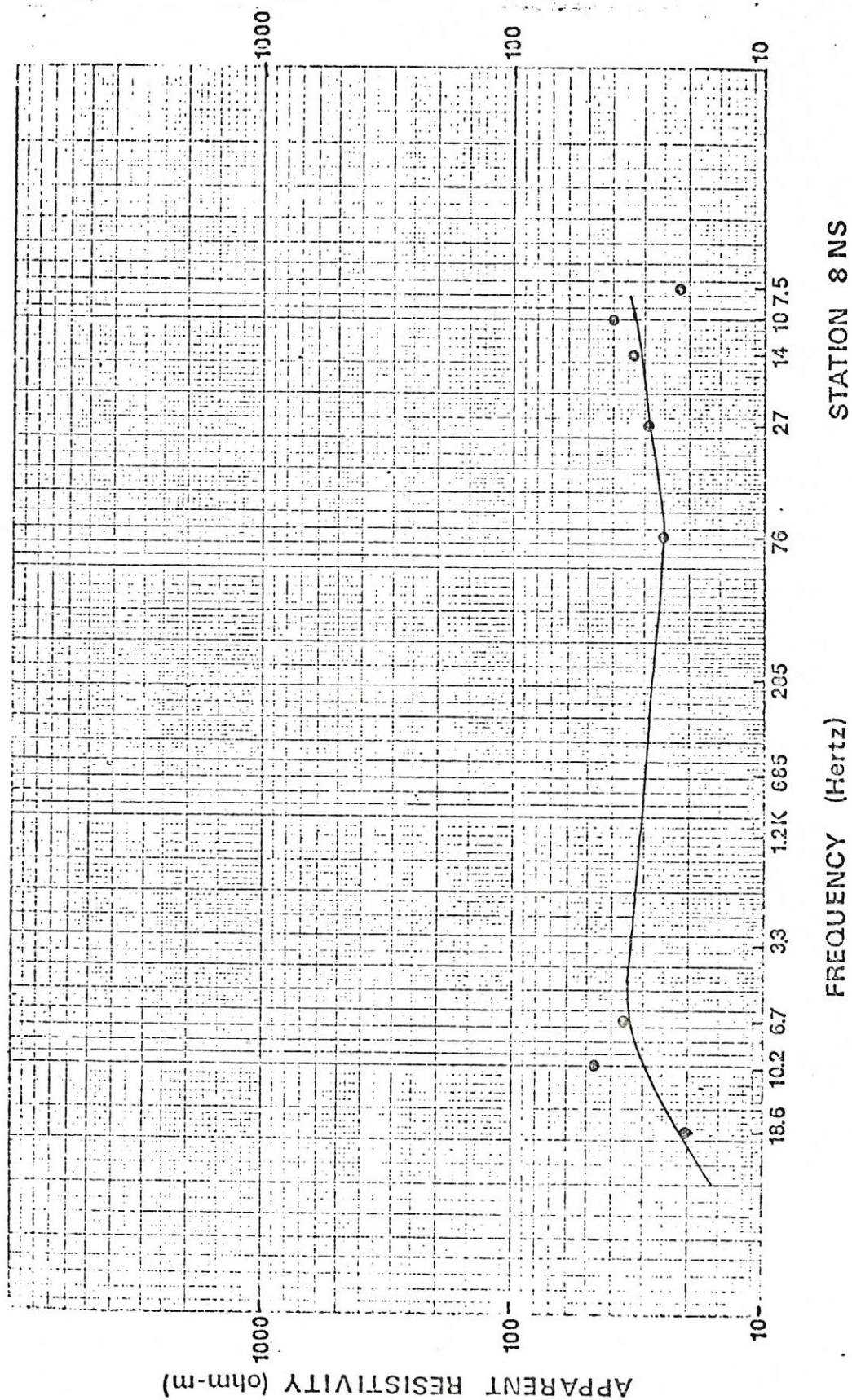


Figure 29. AMT sounding curve, station 8NS



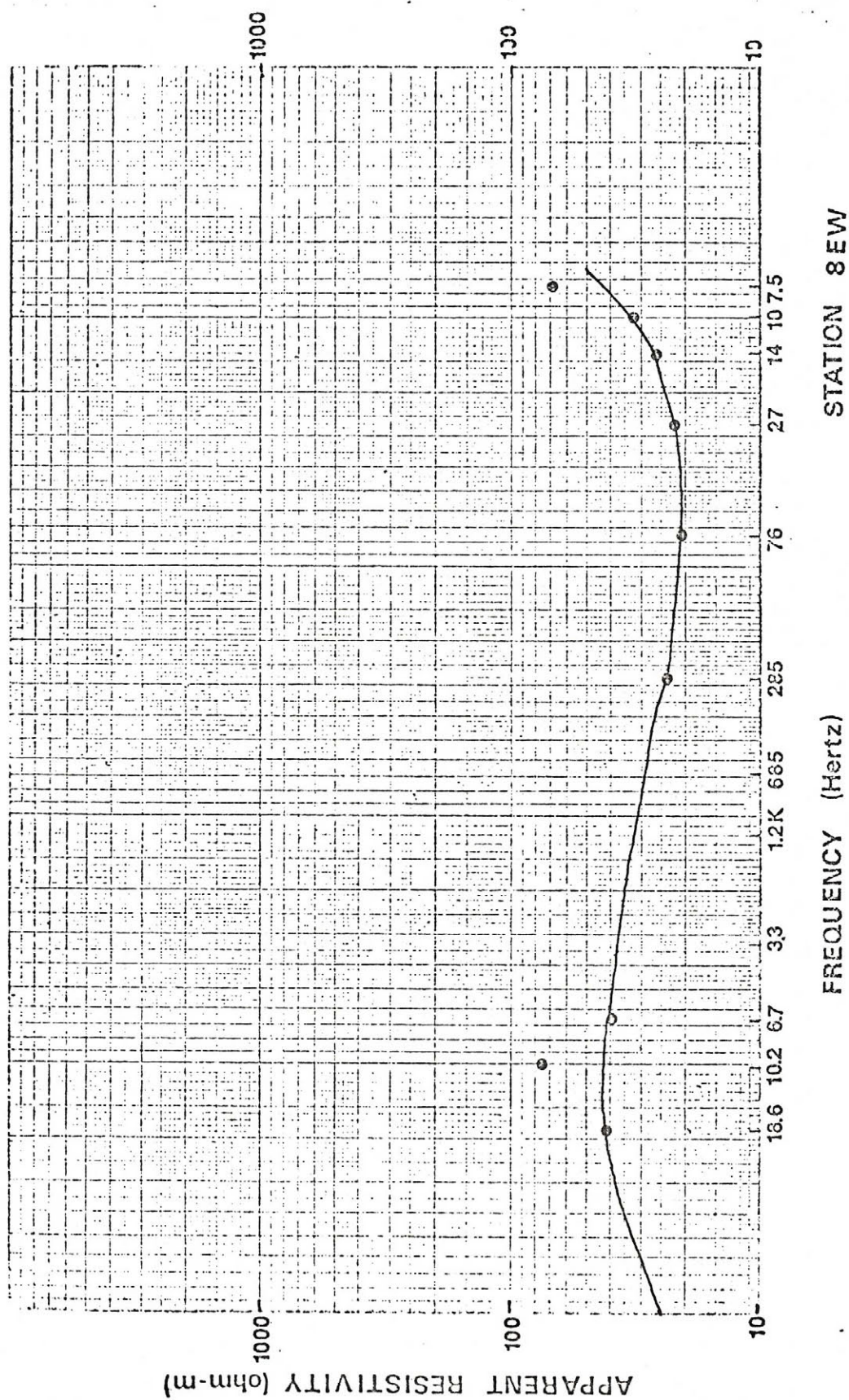
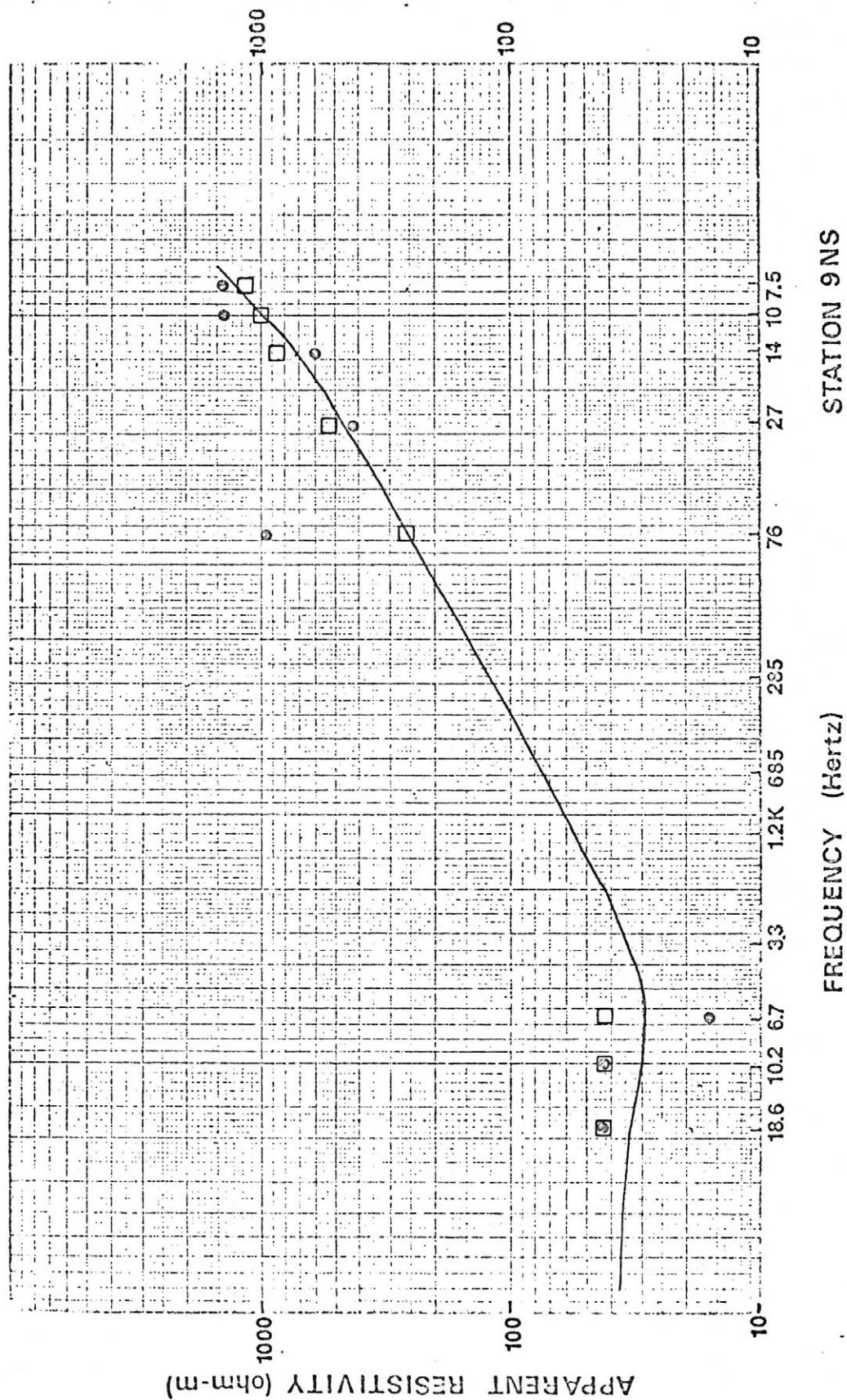


Figure 30. AMT sounding curve, station 8EW







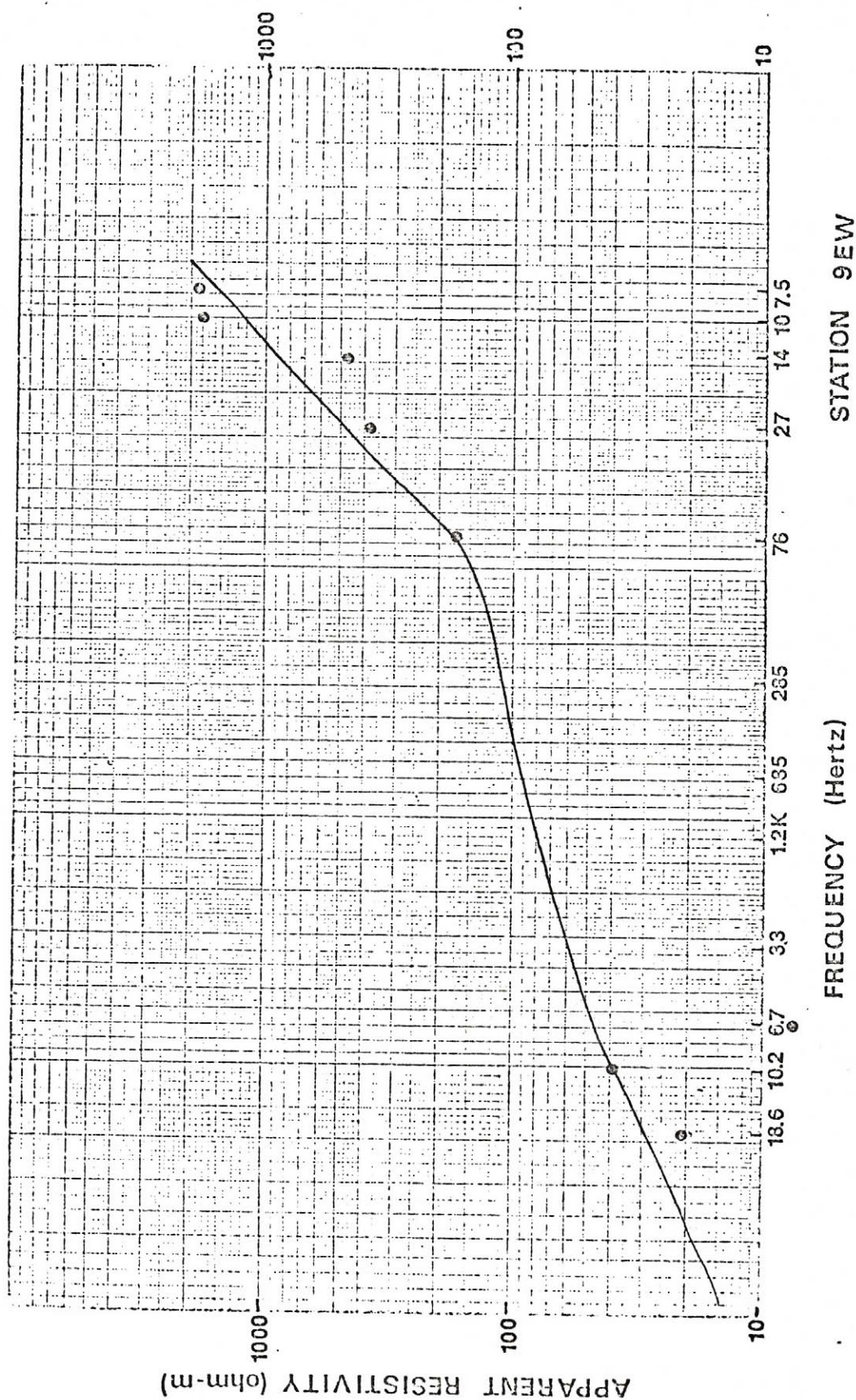


Figure 32. AMT sounding curve, station 9EW



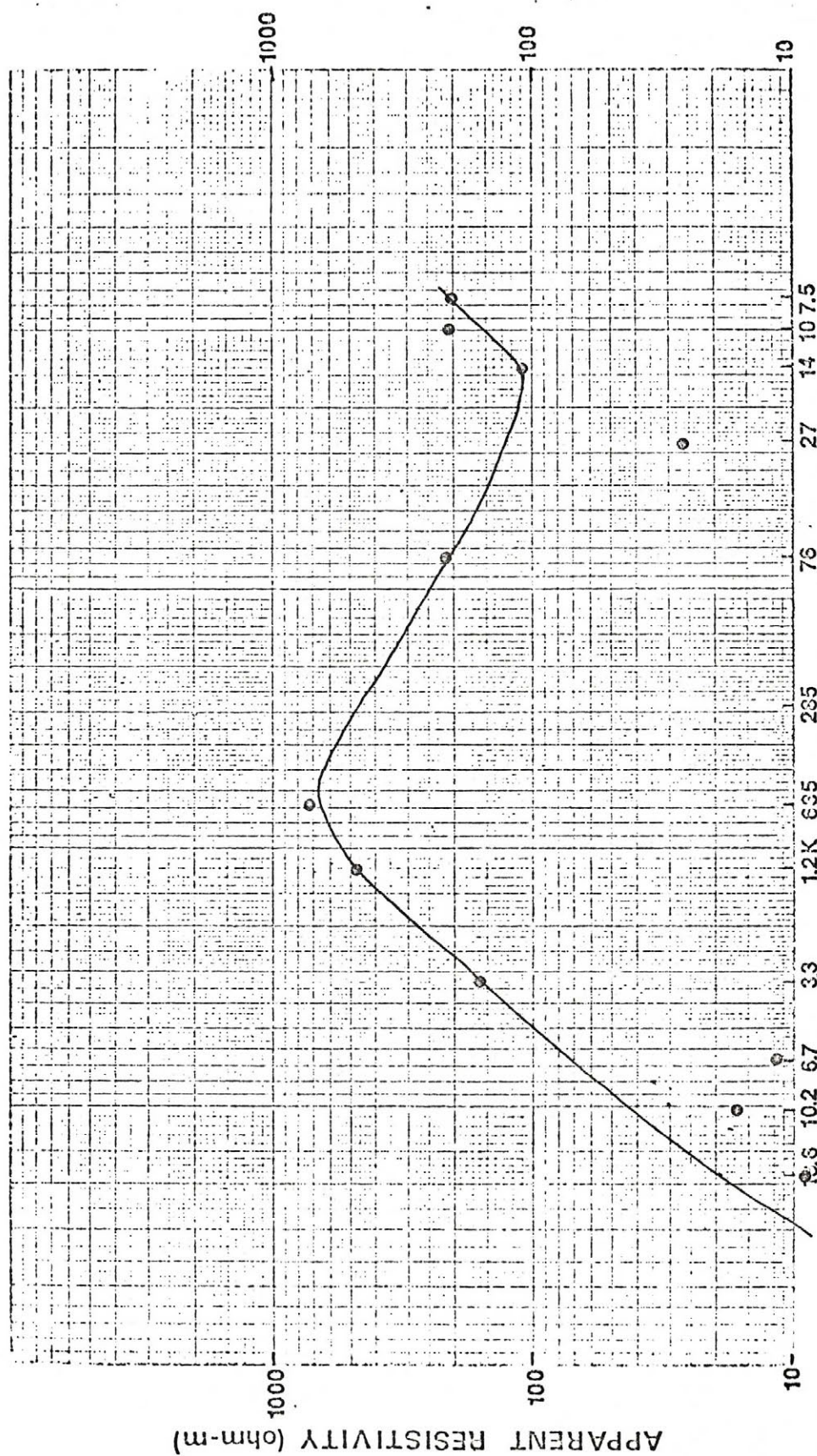


Figure 33. ANT sounding curve, station 10NS



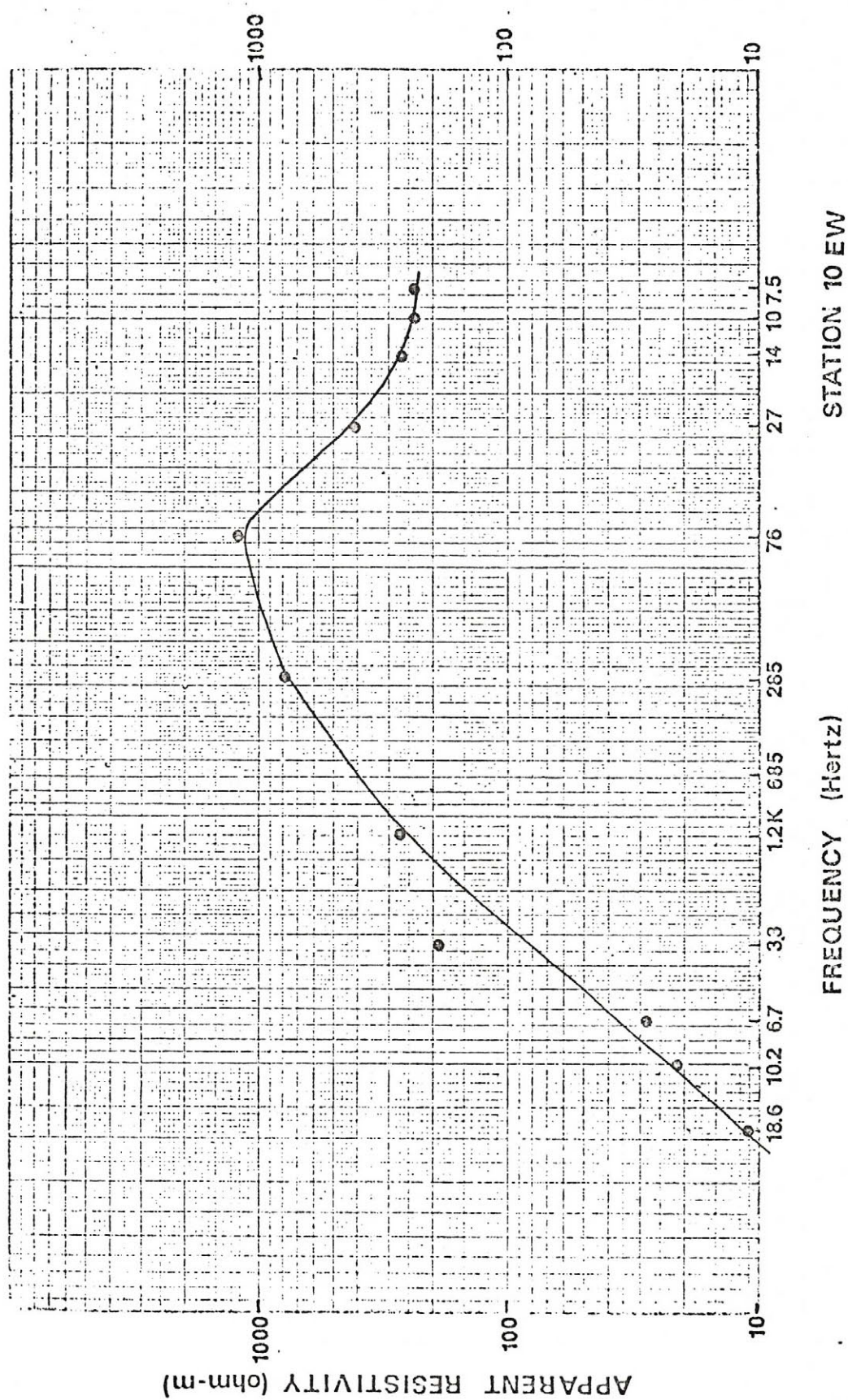
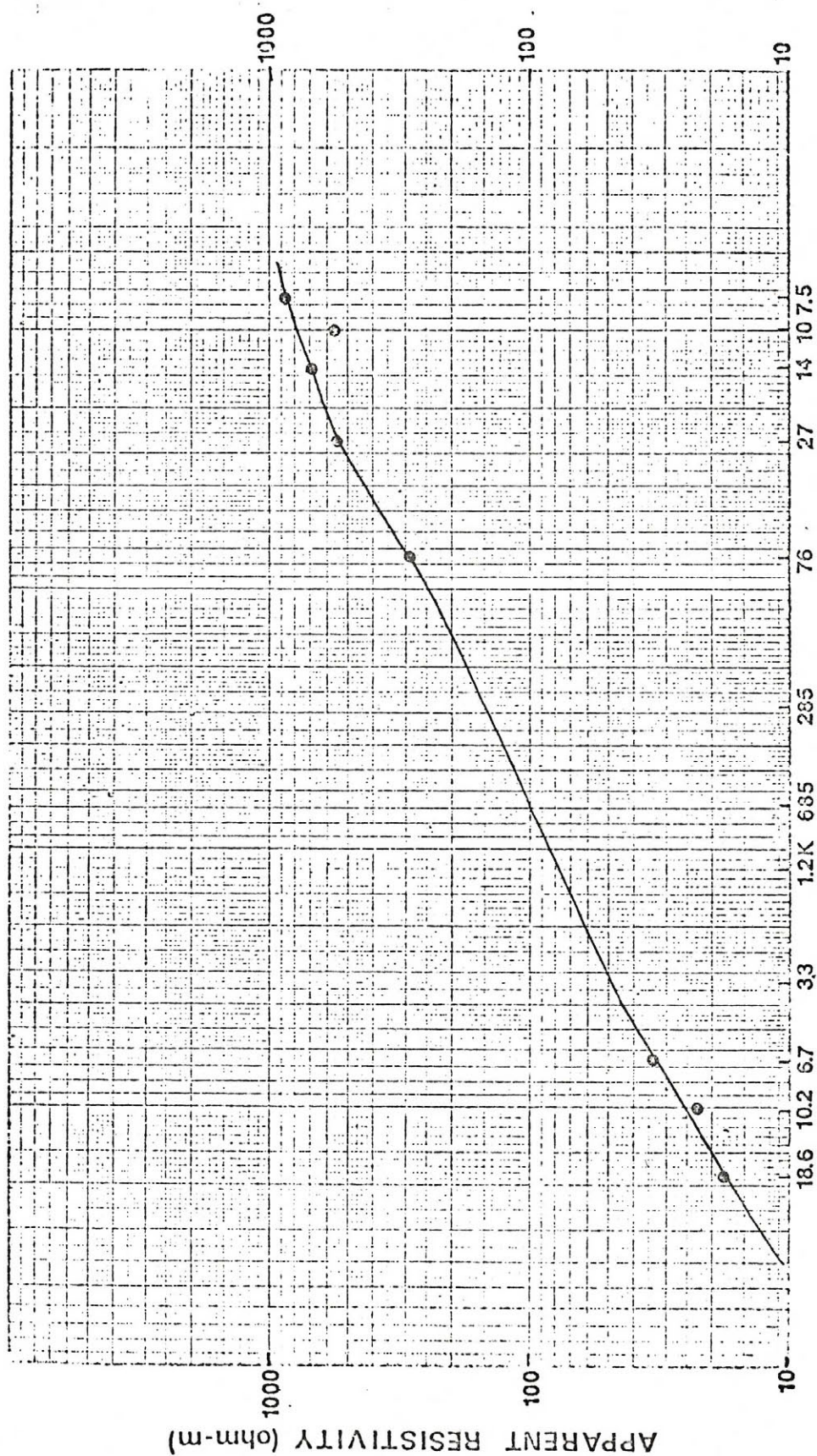


Figure 34. AMT sounding curve, station 10EW





STATION 11 NS  
FREQUENCY (Hertz)

Figure 35. AMT sounding curve, station 11NS



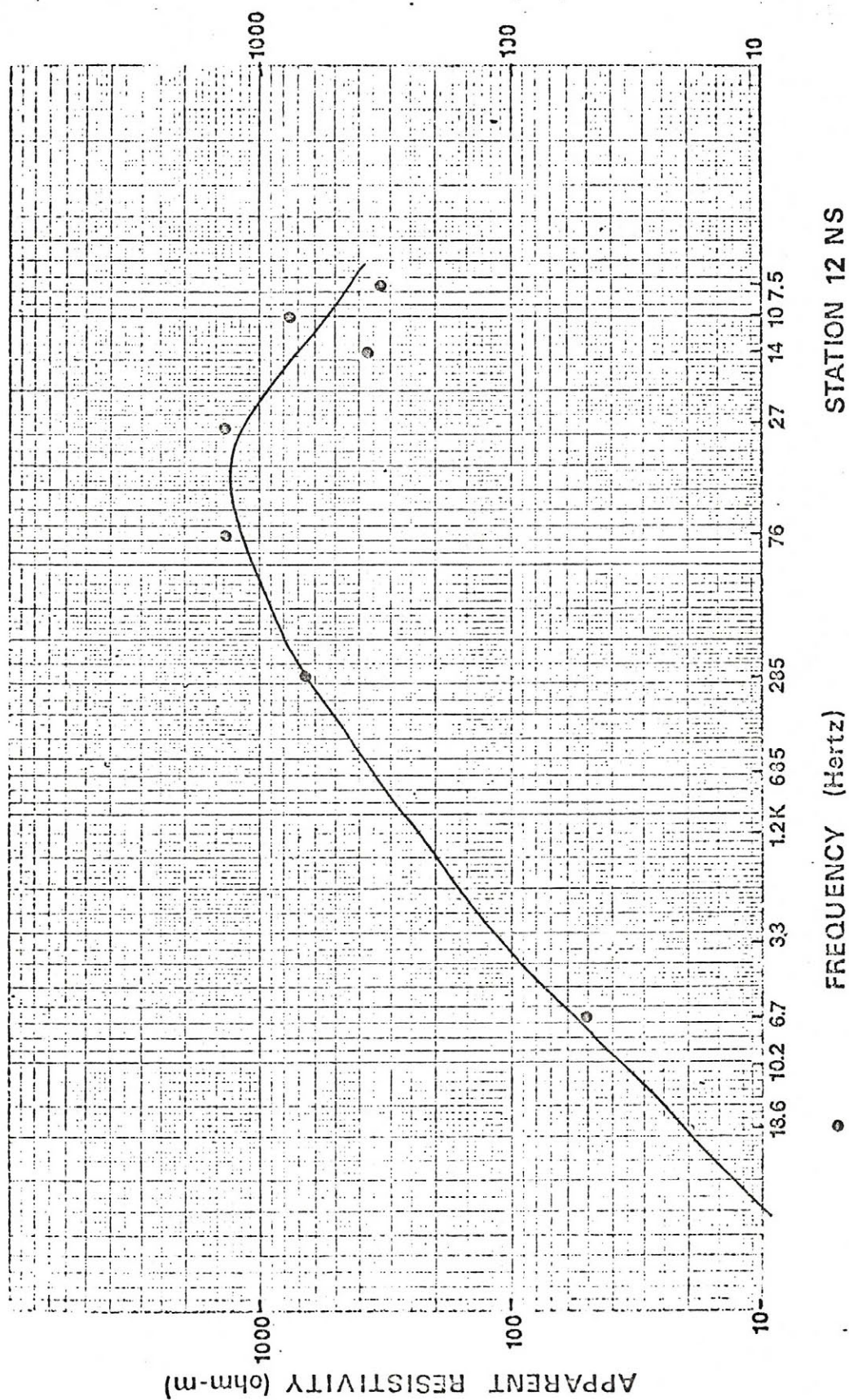


Figure 36. AMT sounding curve, station 12NS



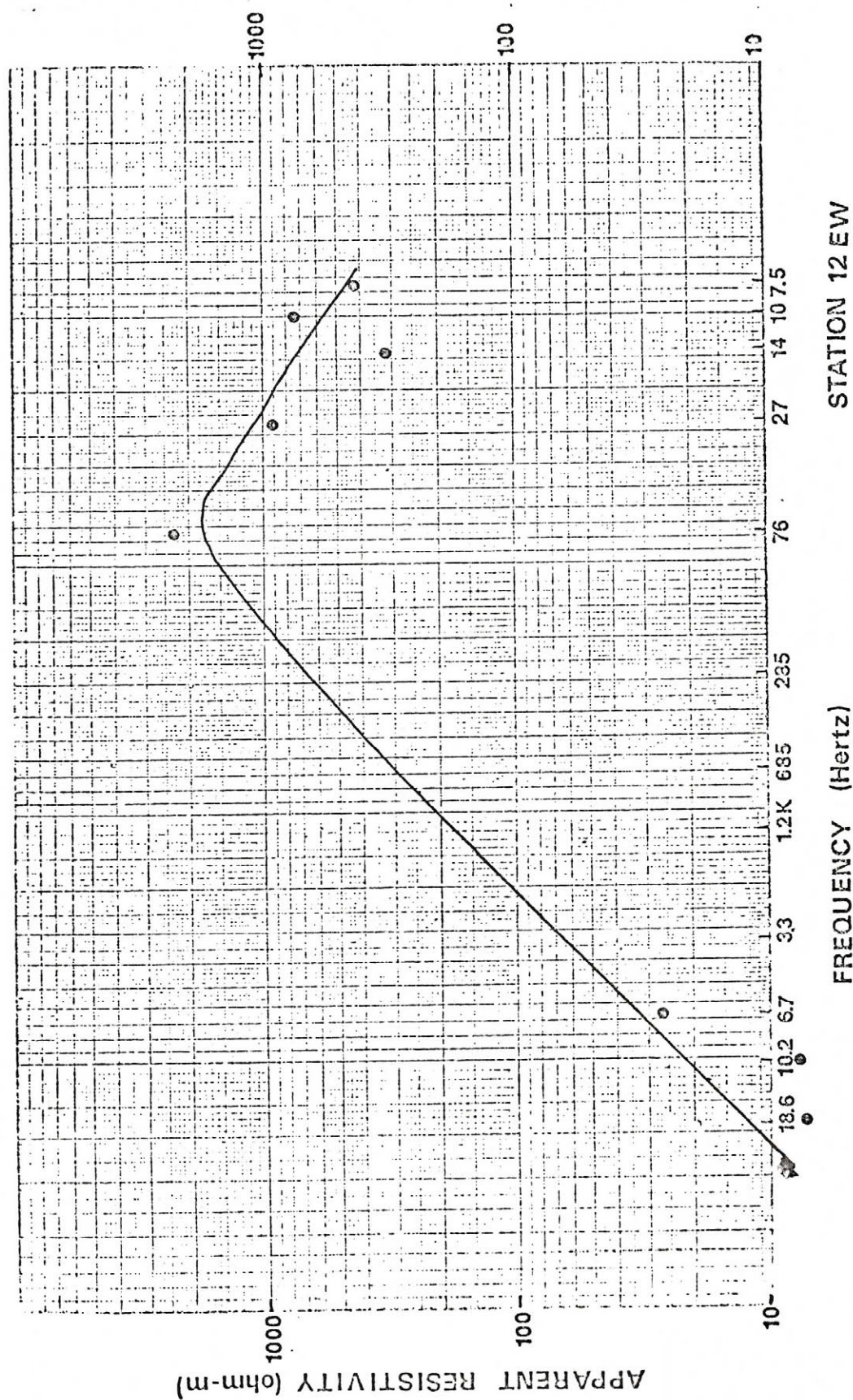


Figure 37. AMT sounding curve, station 12EW



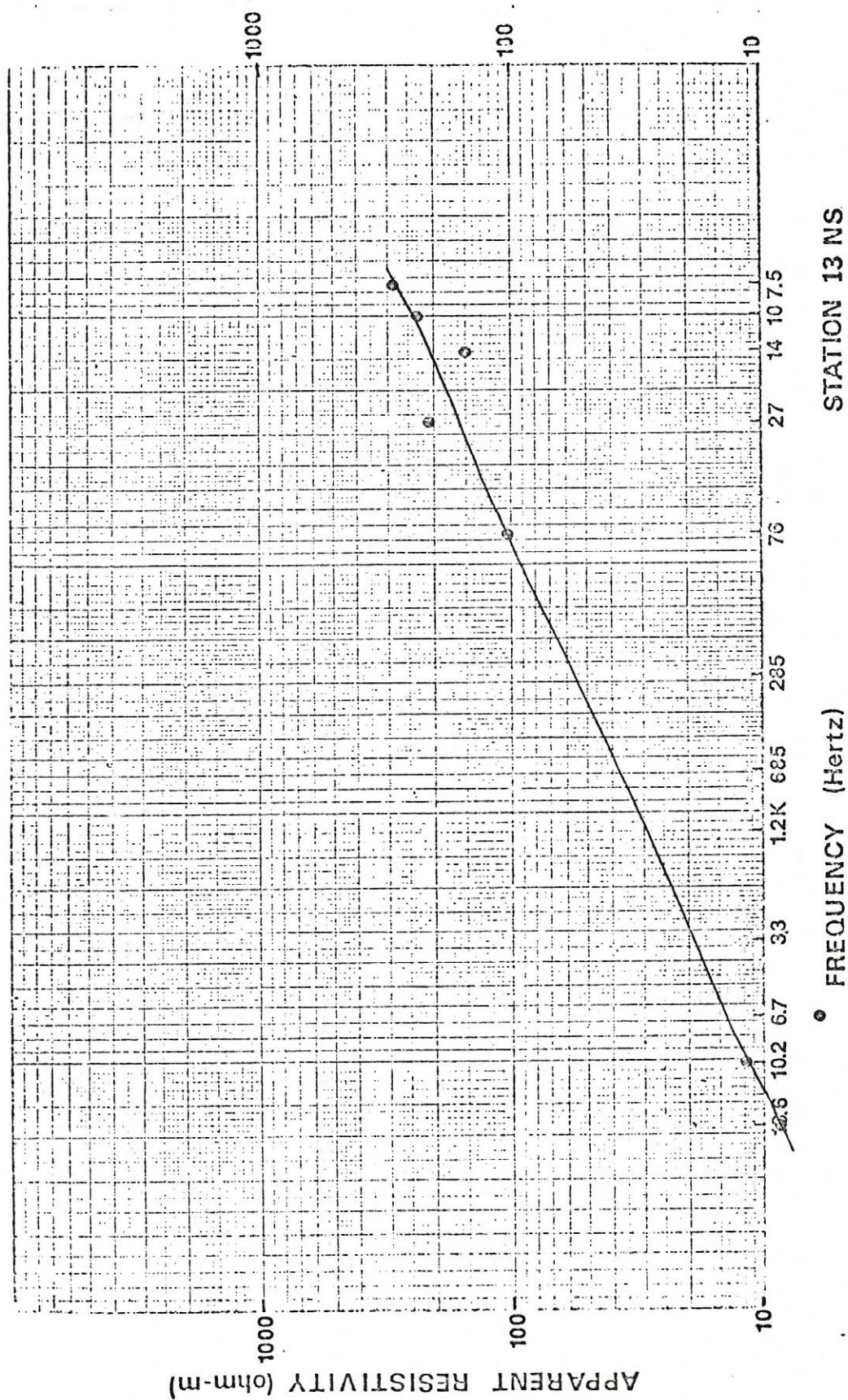


Figure 38. AMT sounding curve, station 13NS



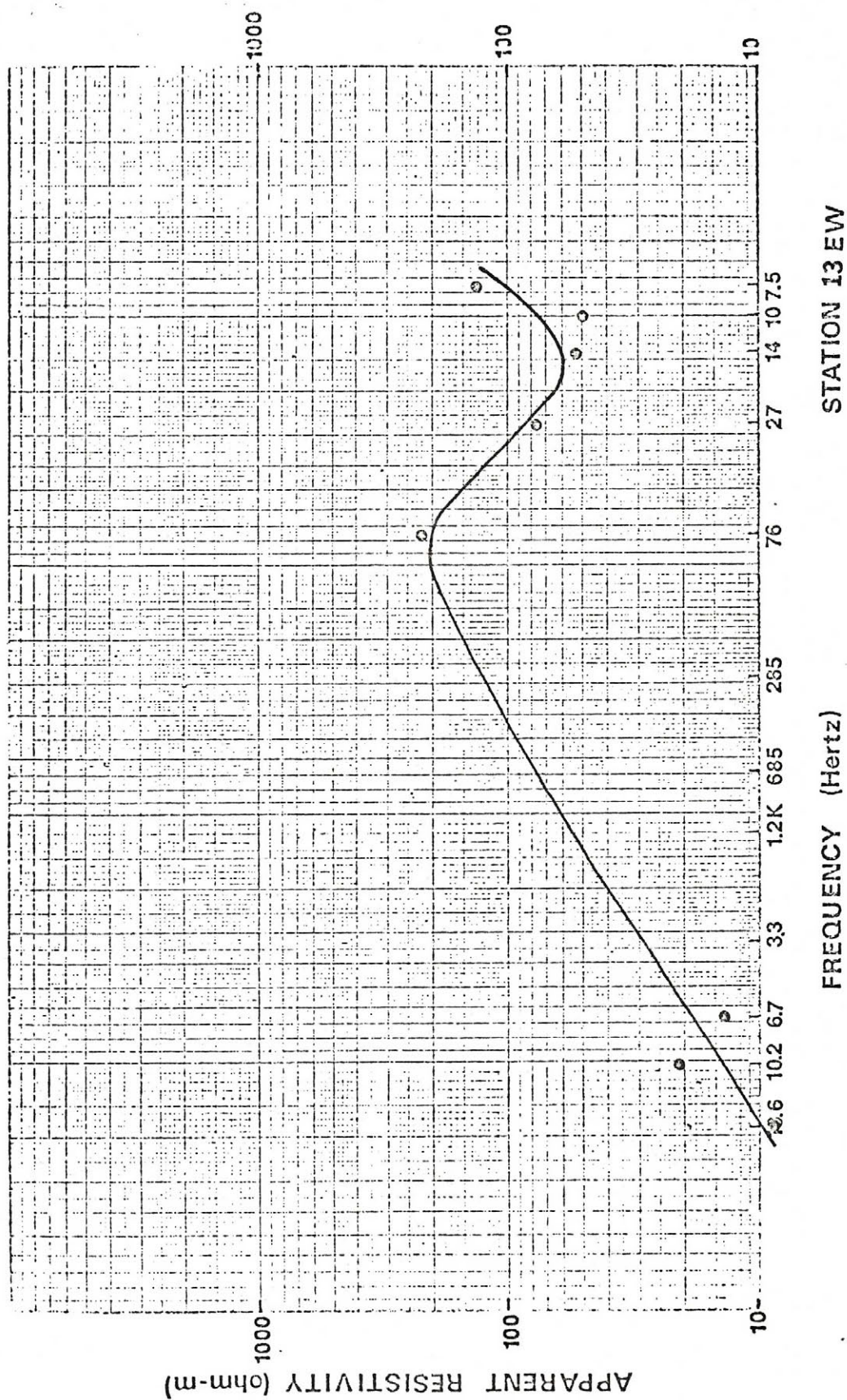


Figure 39. AMT sounding curve, station 13EW



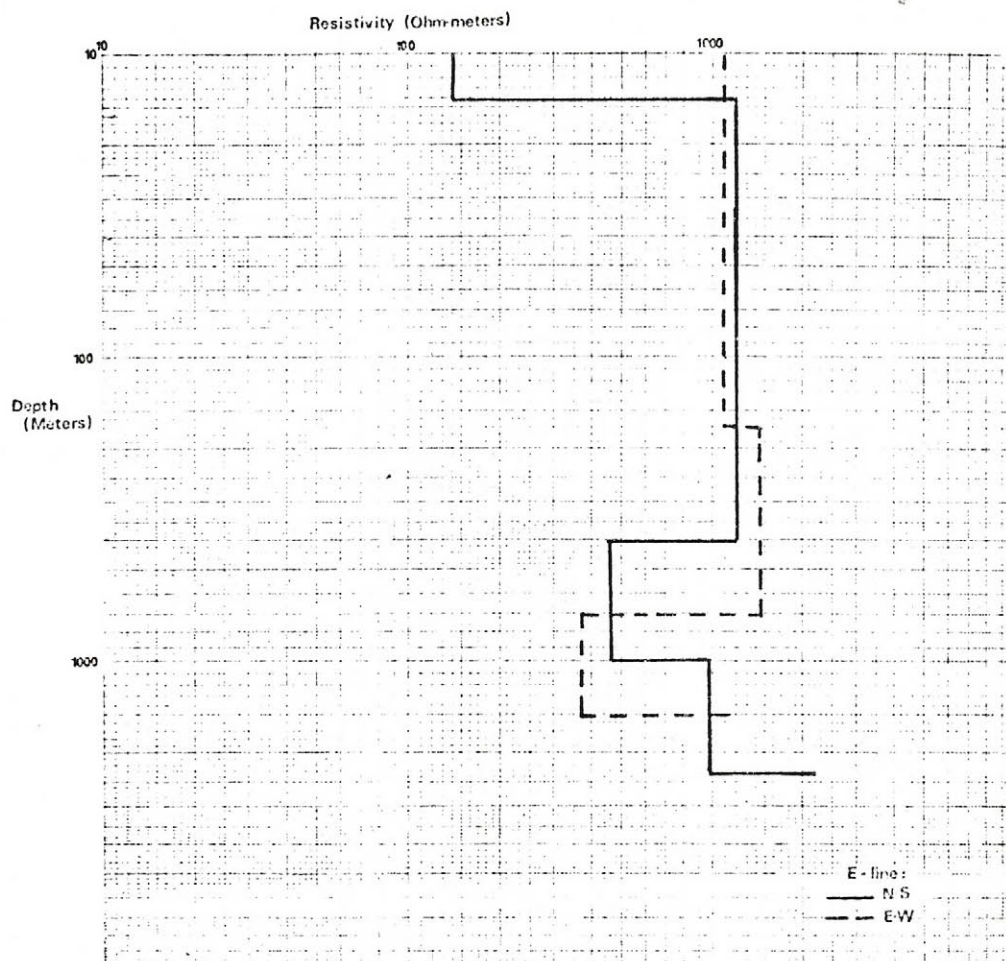


Figure 40. AMT depth versus resistivity plot,  
Bostick inversion, station 1.

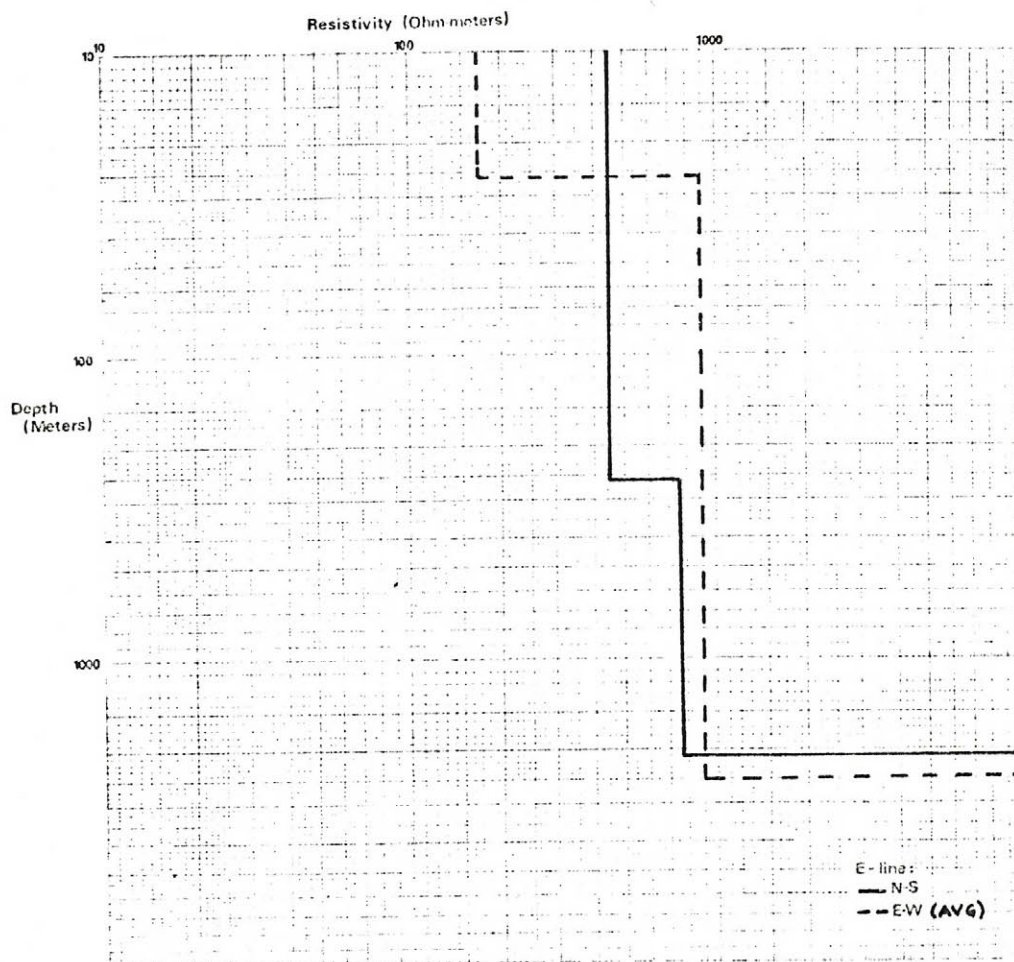


Figure 41. AMT depth versus resistivity plot,  
computer inversion, station 1.



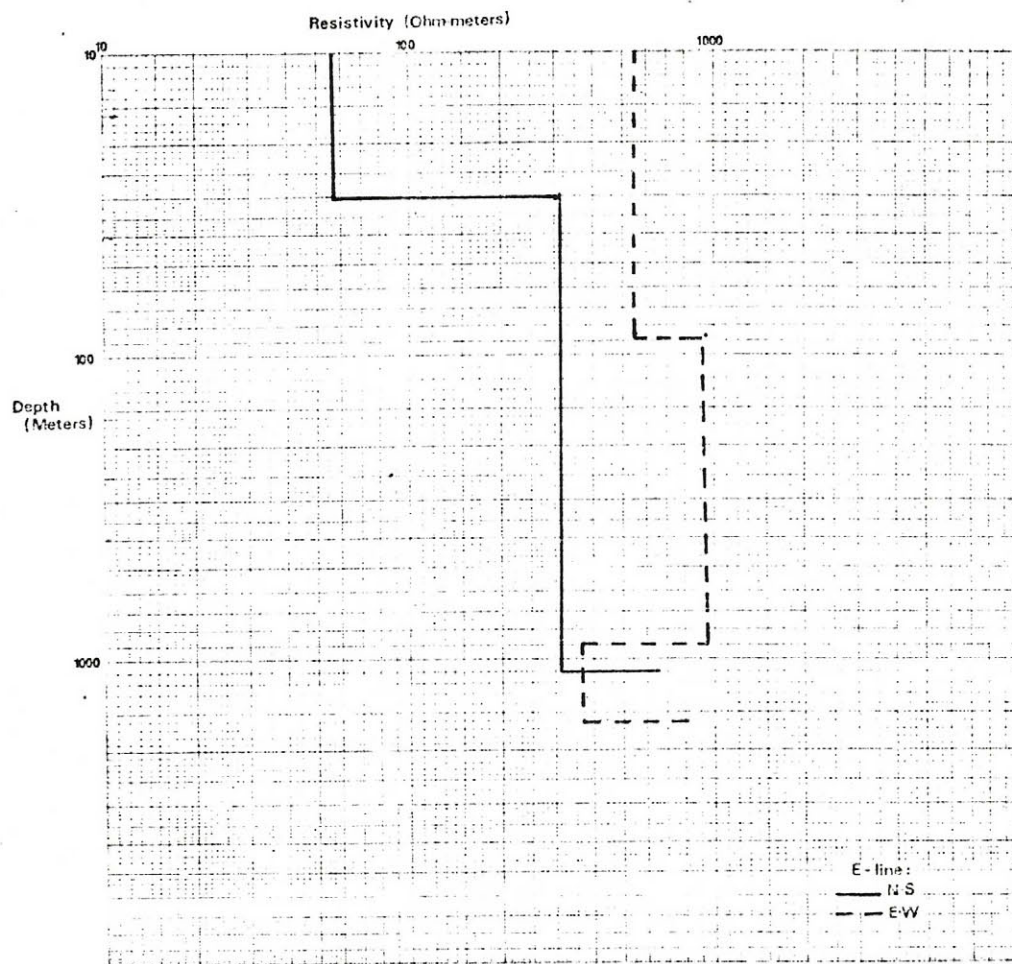


Figure 42. AMT depth versus resistivity plot,  
Bostick inversion, station 2.

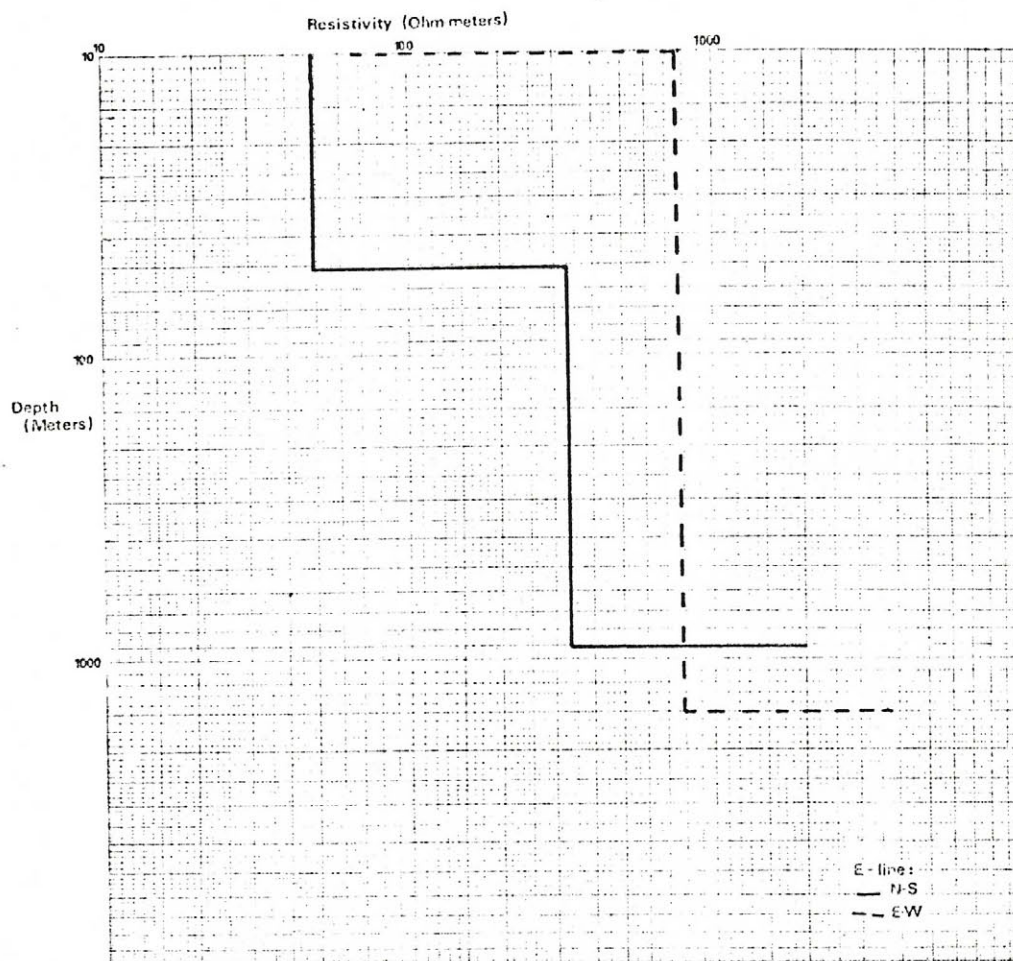


Figure 43. AMT depth versus resistivity plot, computer inversion, station 2.



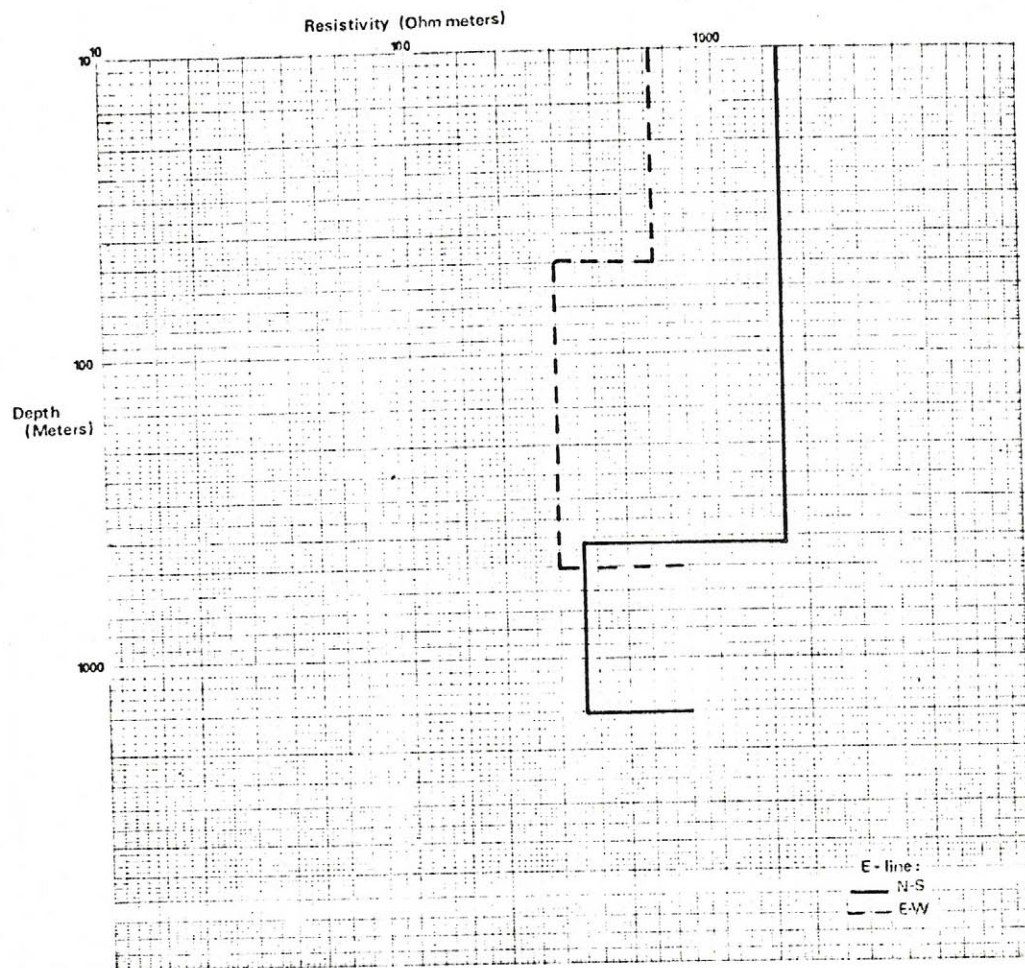


Figure 44. AMT depth versus resistivity plot,  
Bostick inversion, station 3.

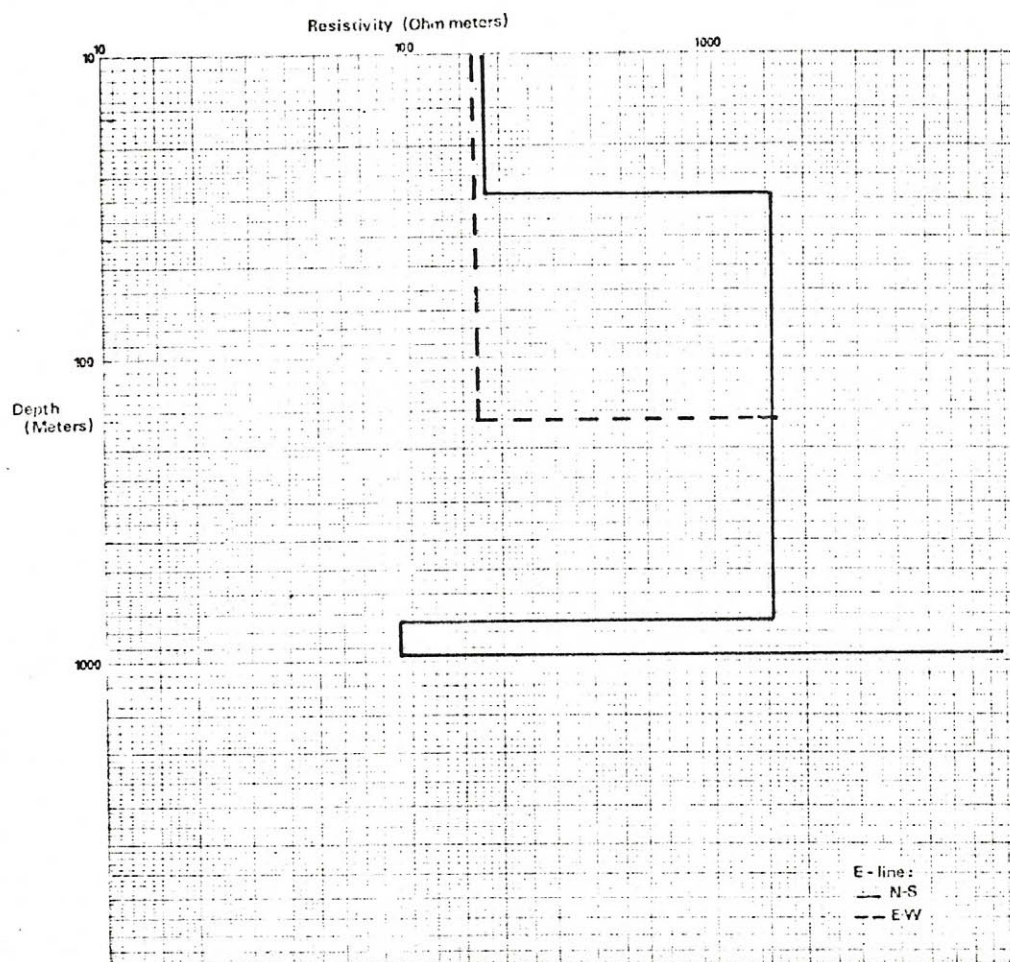


Figure 45. AMT depth versus resistivity plot, computer inversion, station 3.



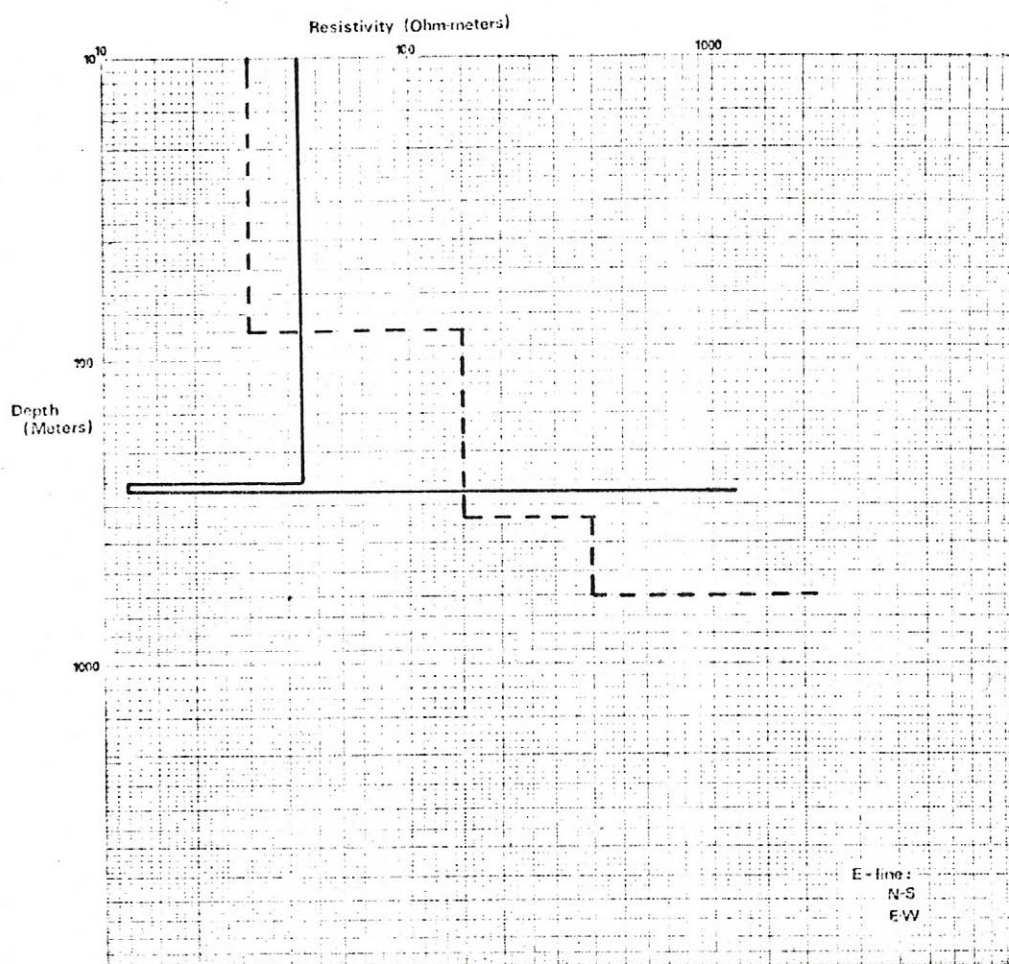


Figure 46. AMT depth versus resistivity plot, computer inversion, station 4.

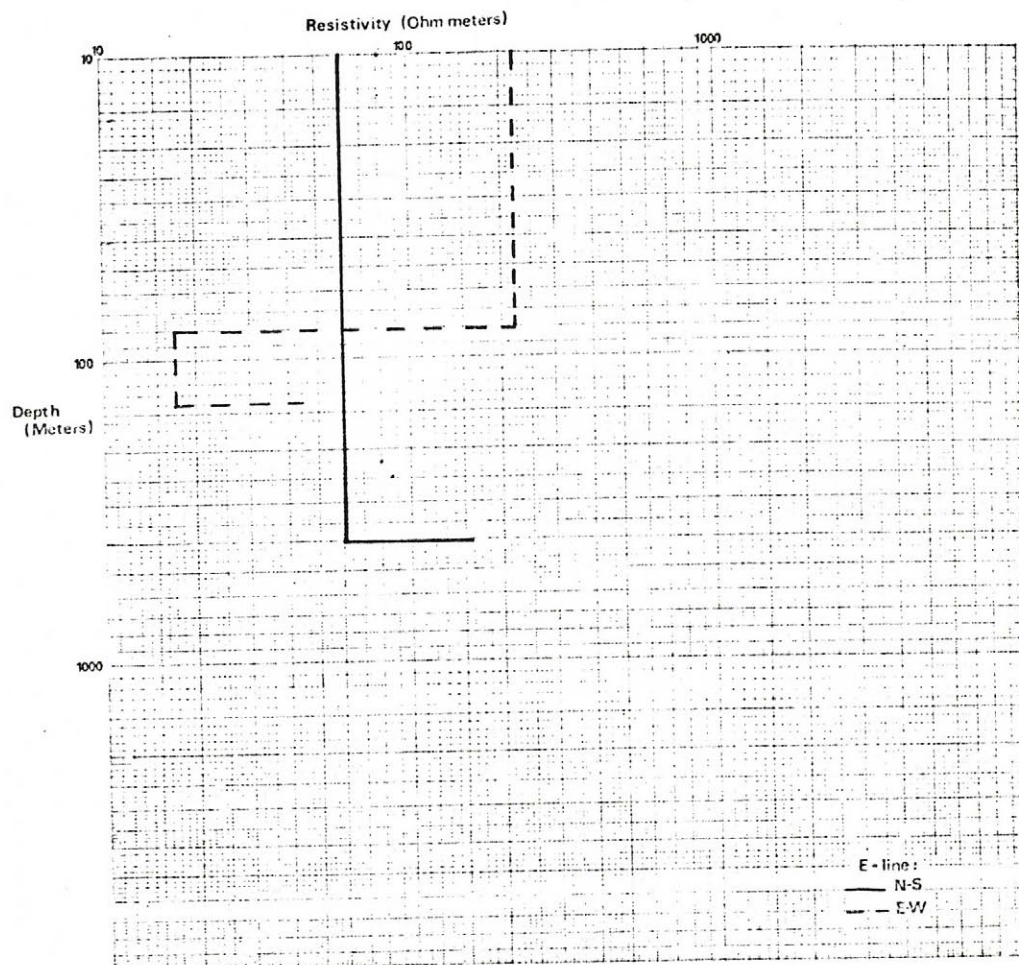


Figure 47. AMT depth versus resistivity plot,  
Bostick inversion, station 4.



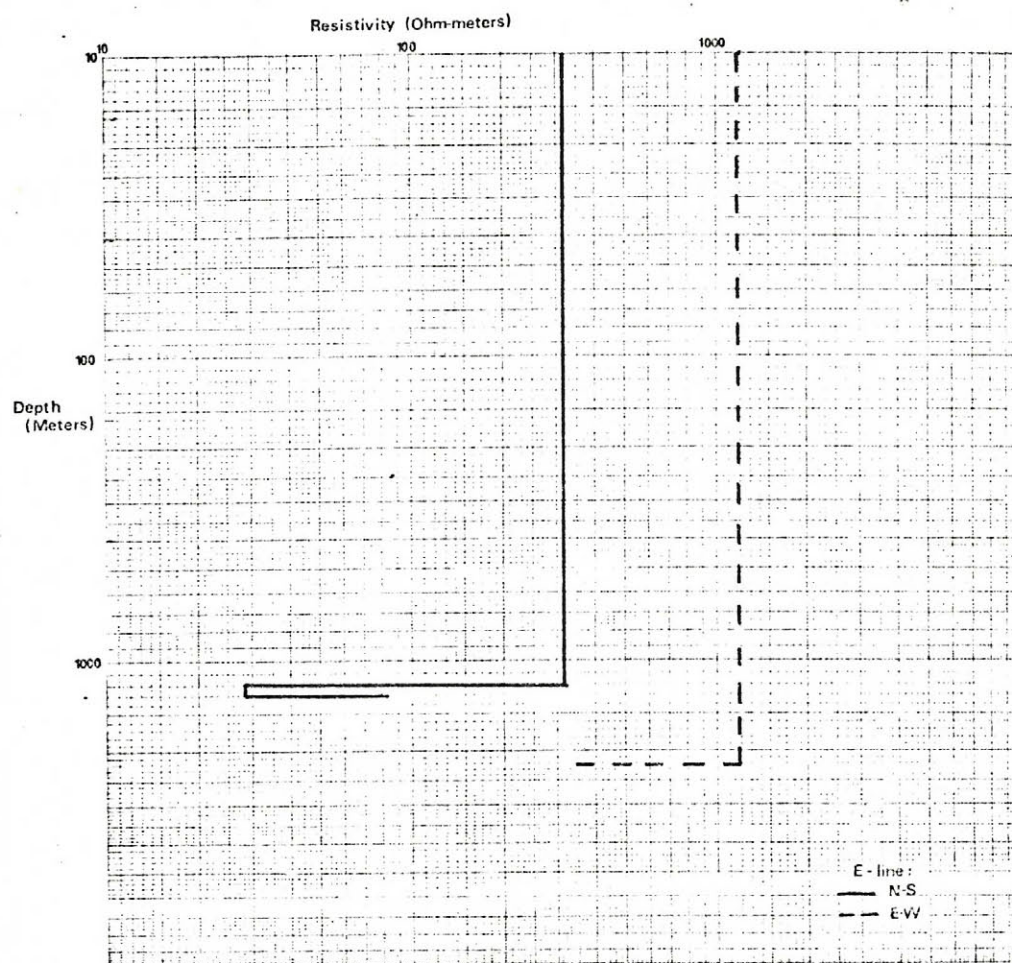


Figure 48. AMT depth versus resistivity plot,  
Bostick inversion, station 5.

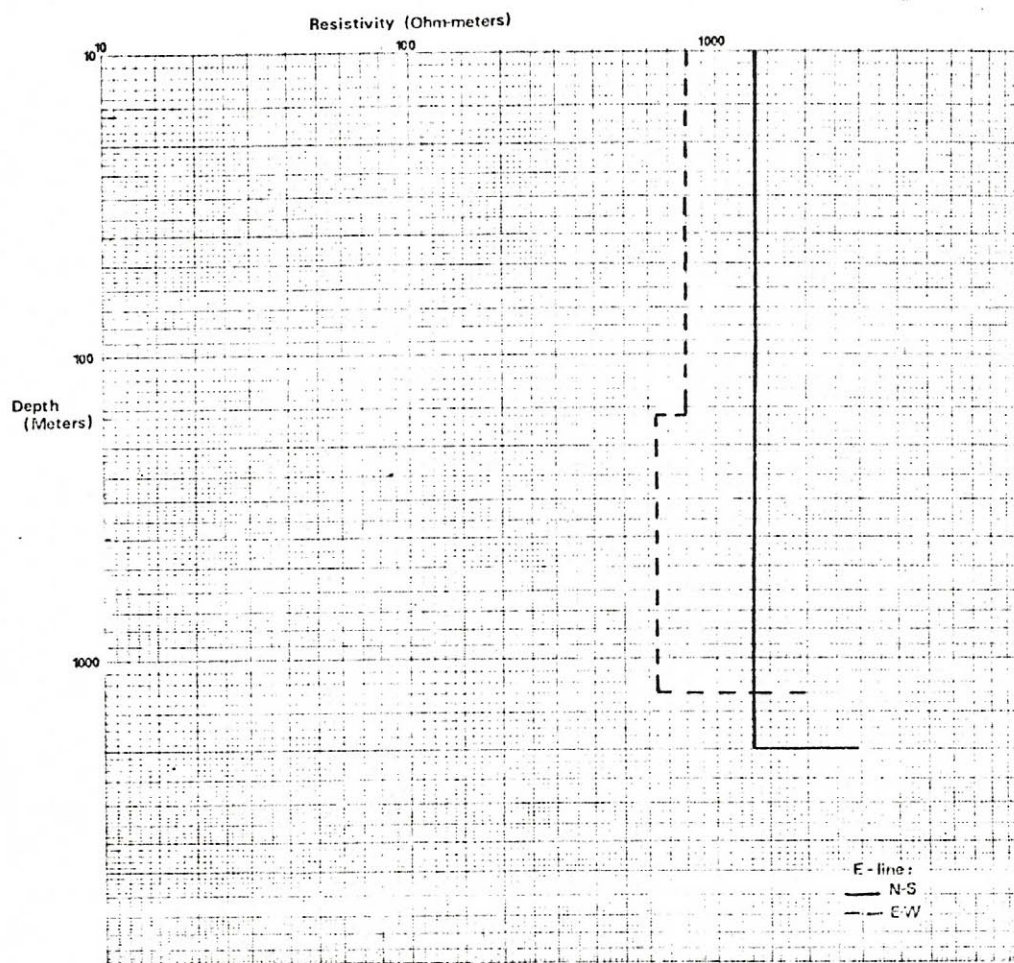


Figure 49. AMT depth versus resistivity plot,  
Bostick inversion, station 6.



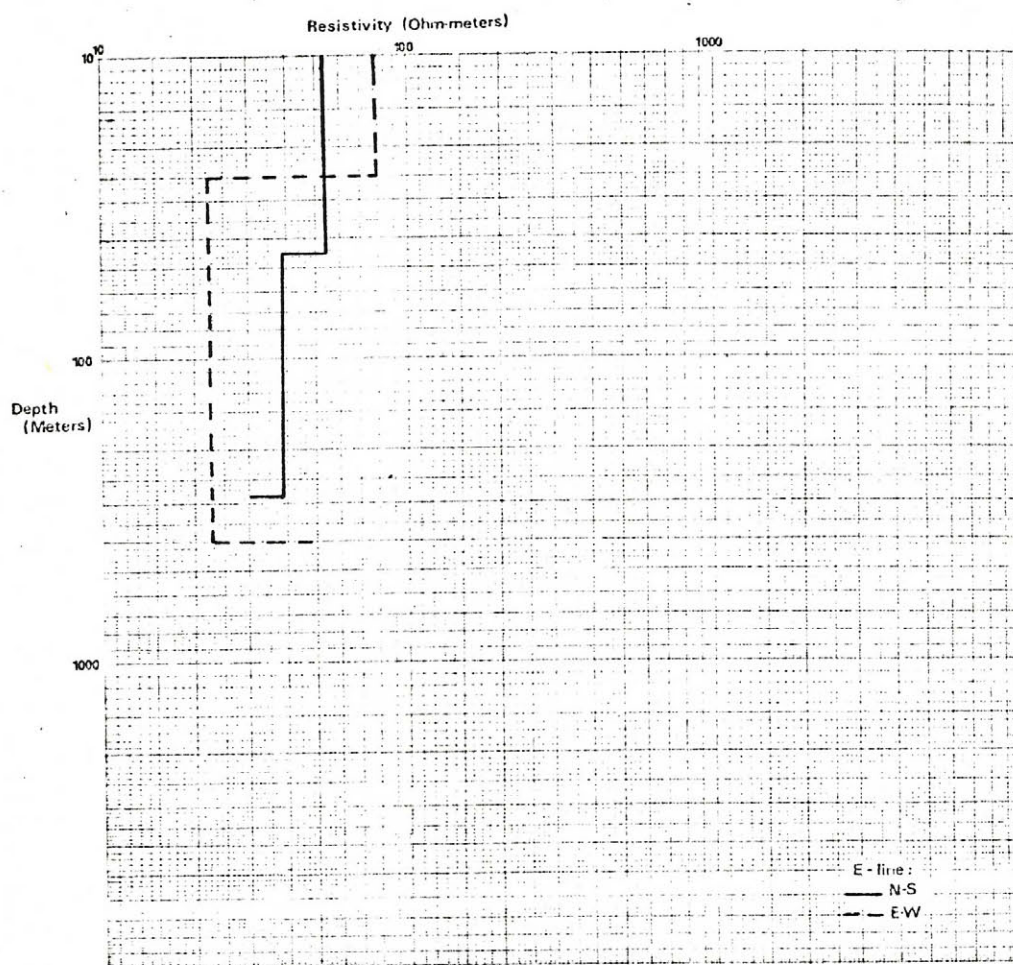


Figure 50. AMT depth versus resistivity plot,  
Bostick inversion, station 7.

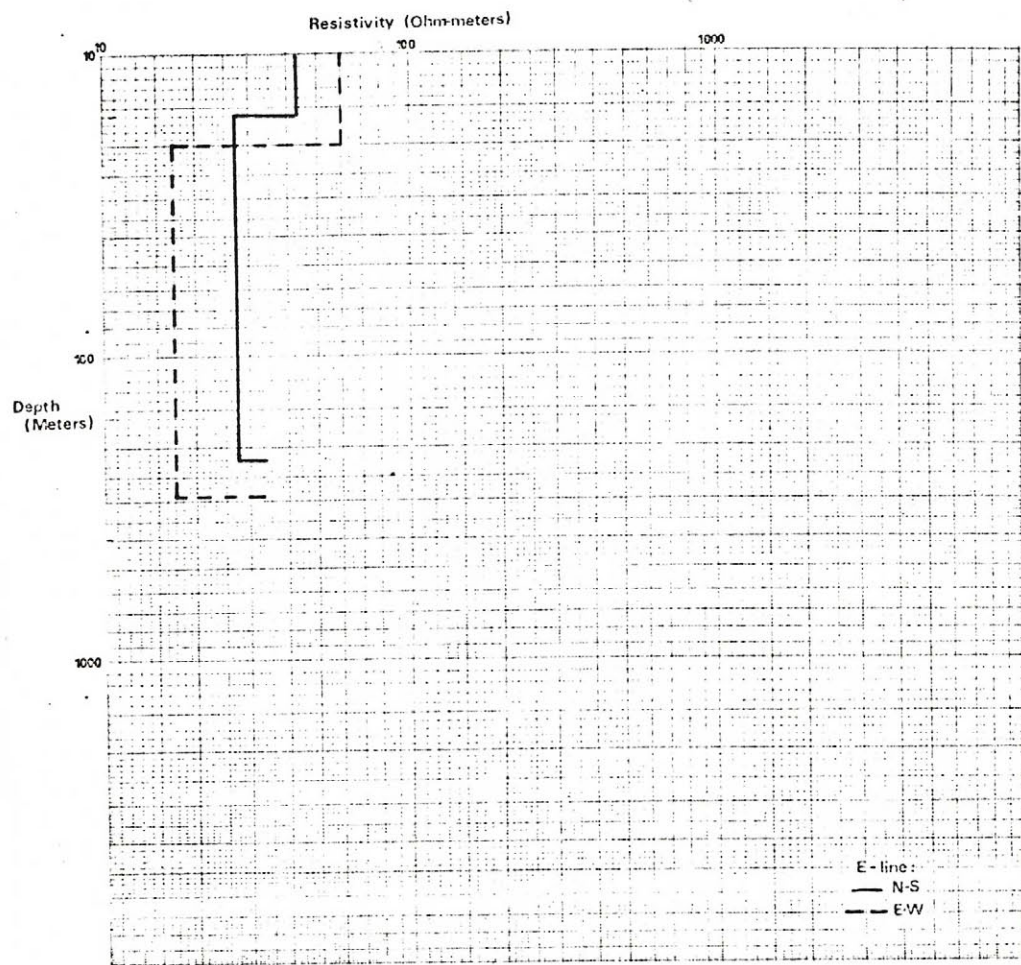


Figure 51. AMT depth versus resistivity plot,  
Bostick inversion, station 8.



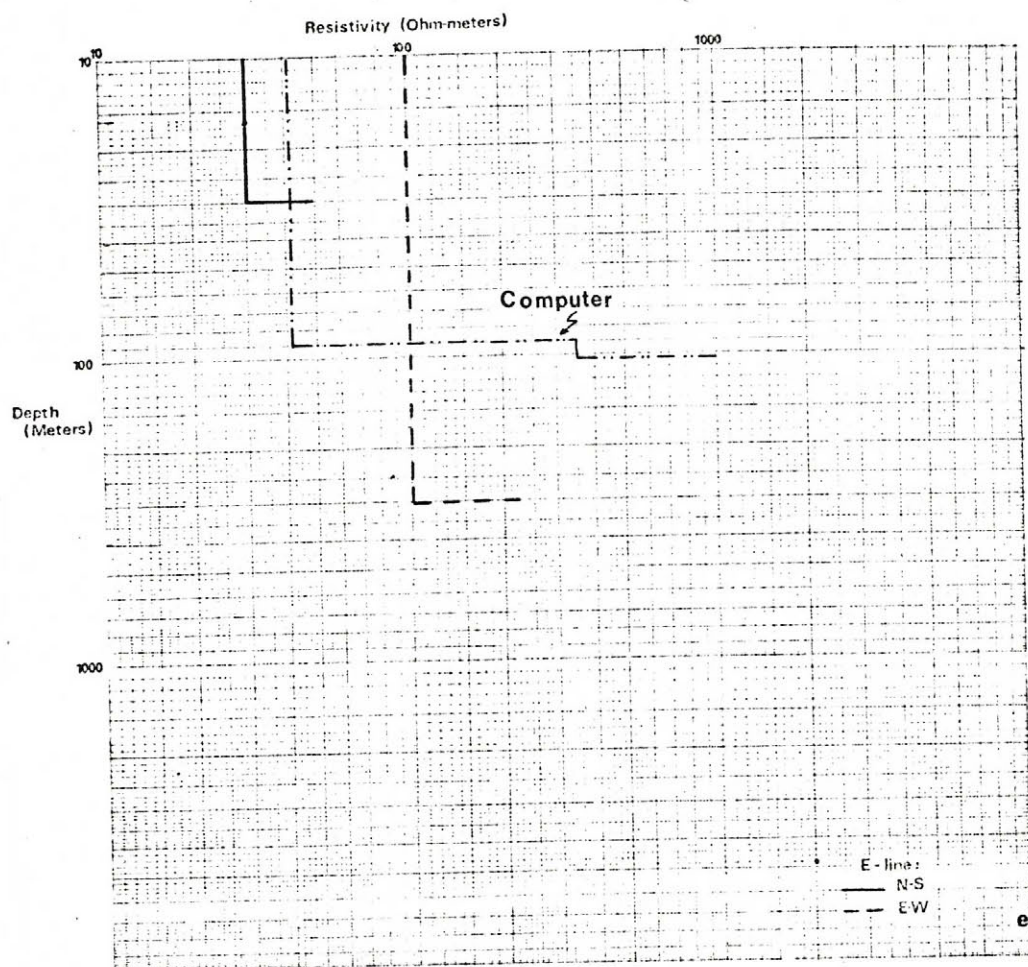


Figure 52. AMT depth versus resistivity plot,  
Bostick and computer inversions, station 9.

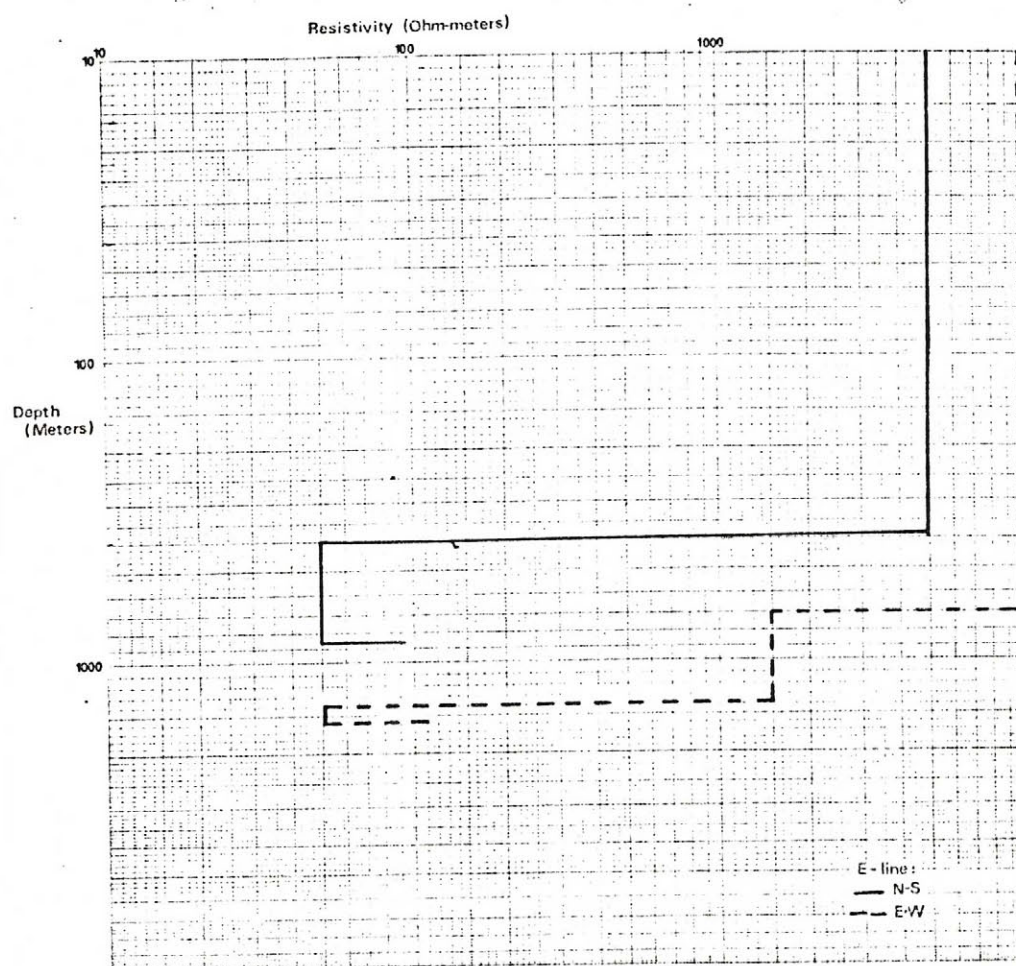


Figure 53. AMT depth versus resistivity plot,  
Bostick inversion, station 10.



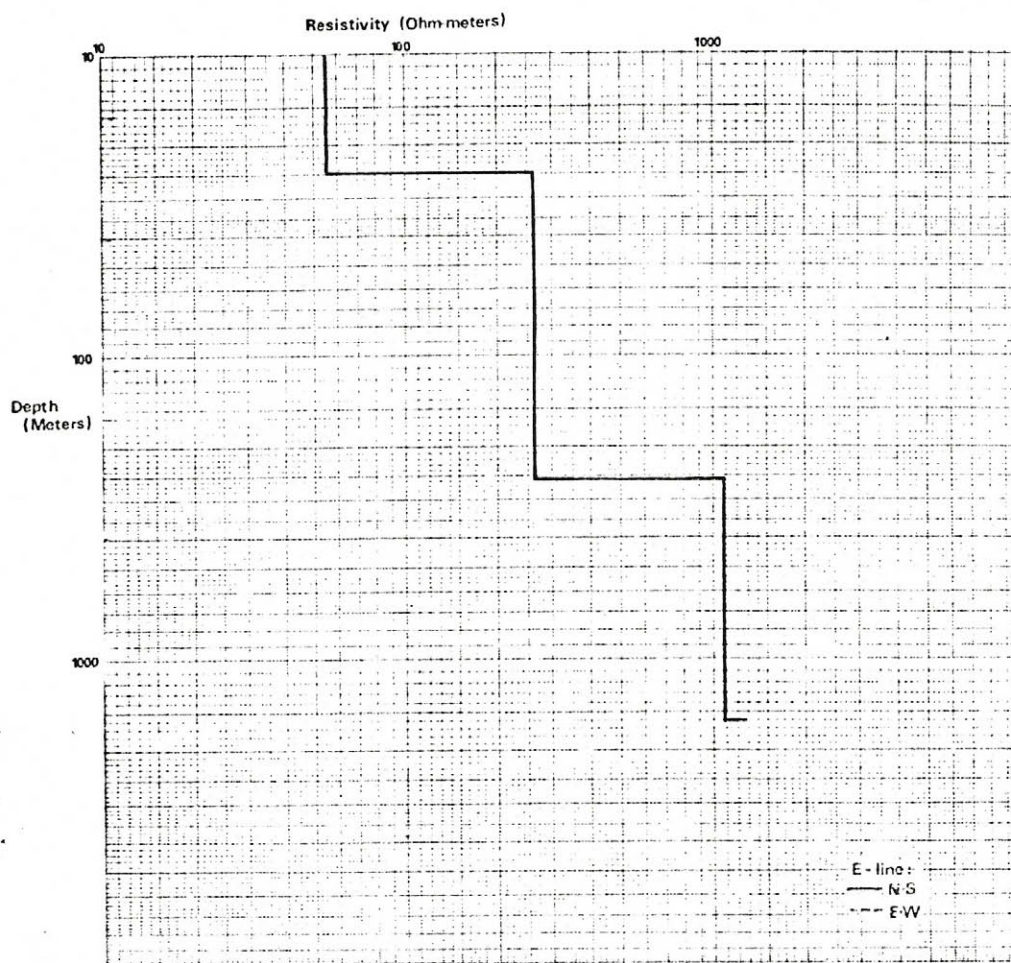


Figure 54. AMT depth versus resistivity plot,  
Bostick inversion, station 11.

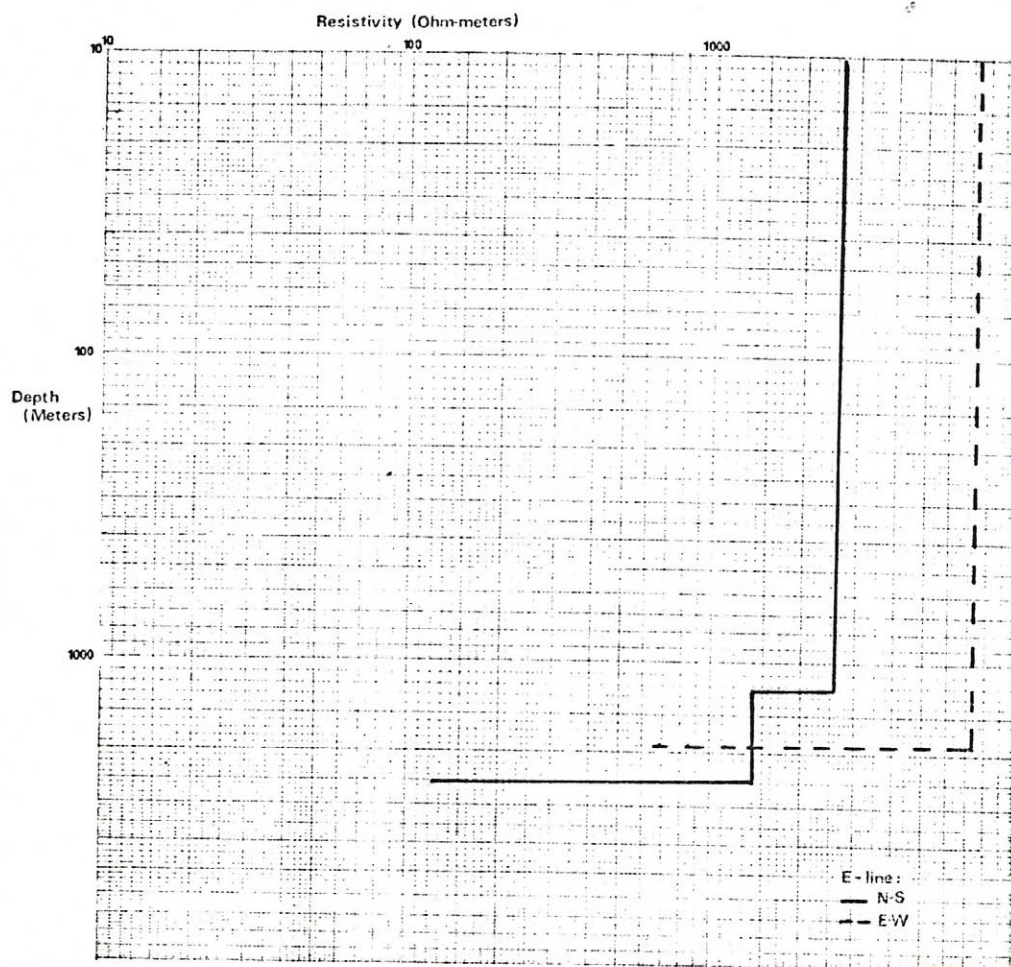


Figure 55. AMT depth versus resistivity plot,  
Bostick inversion, station 12.



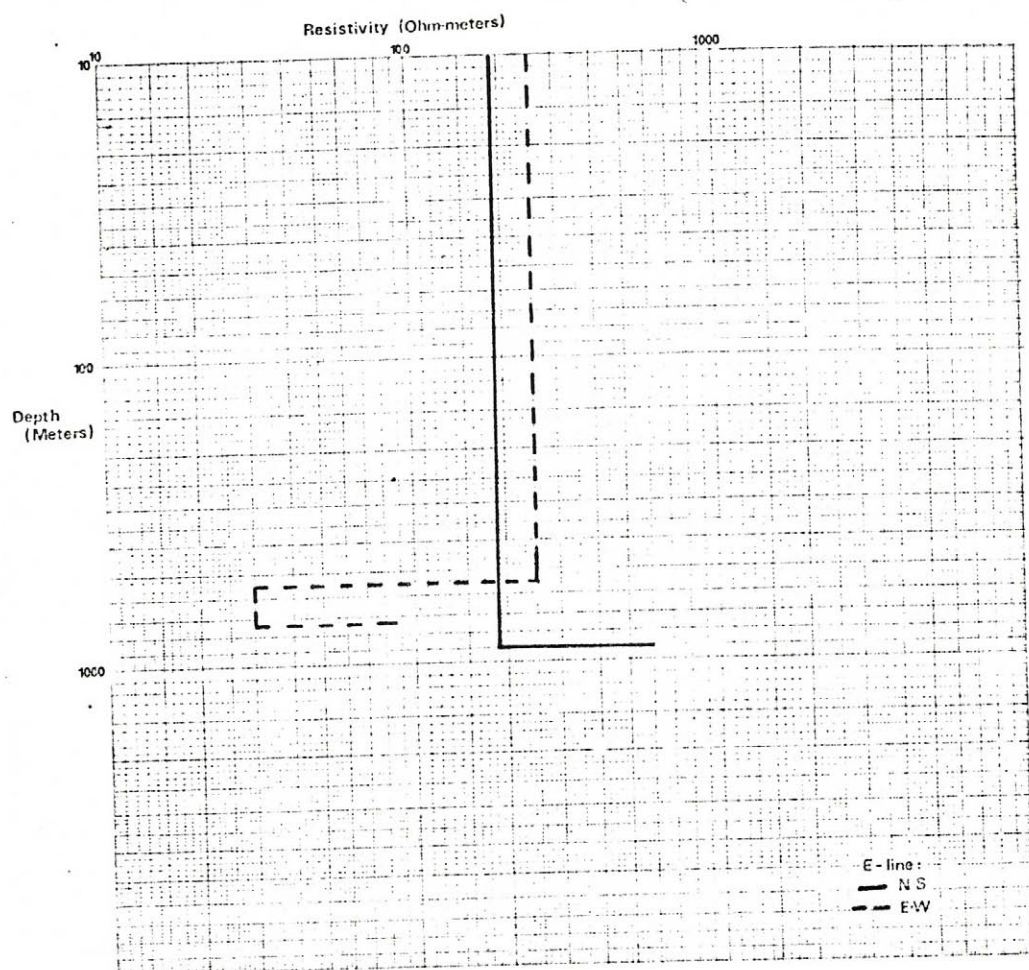


Figure 56. AMT depth versus resistivity plot,  
Bostick inversion, station 13.

For each sounding, the results were plotted as apparent resistivity versus frequency. These sounding curves were plotted separately by E-line orientation since at many stations there was a marked difference between the two directions caused by geologic structure. The curves were smoothed to best fit the data points and then inverted to give a rough idea of true resistivity change with depth. The inversions were done by a method devised by Bostick (1977) which is an approximate solution. Some soundings were also inverted with the computer program MARQPW (Anderson, 1978).

The sounding curves are given in figures 15 through 39. The solid circles represent collected data points, the solid lines are the smoothed curves through these points, and the open squares are the modelled points to fit the computer profile. The resulting plots of depth and true resistivity are shown in figures 40 through 56. The two soundings at each station were plotted on the same graph so as to compare results in the orthogonal directions.

As shown in the depth-resistivity plots, station 1 consists of fairly high resistivity (1200 to 1500 ohm-meters) from near the surface to a depth of 400 to 700 meters, underlain by a 350 to 460 ohm-meter zone extending to 940 to 1500 meters depth and by rocks of increasing resistivity below that. The two soundings are fairly consistent in character and also agree roughly with the computer model, although the computer fit did not model the shallow high resistivity layer.



The station 2 curves are similar in profile, but the north-south line shows lower resistivity above 1100 meters than does the east-west line. The computer profiles also indicate this difference. The resistivity low is centered at 1000 to 1600 meters and resistivity increases with depth below that.

The north-south sounding of station 3 models a resistivity low at 400 to 1500 meters whereas the east-west profile shows a shallower low resistivity zone. This is probably caused by the north-south trending contact of the gneiss and quartz monzonite near this station.

All of the above differences in resistivity between orthogonal soundings are probably due to lateral inhomogeneities in geologic structure. The resistivity changes with depth are interpreted as reflecting changes within Precambrian rock, such as hydrothermal alteration and more intense fracturing. Presence of thermal water may also contribute as at station 2.

Station 4 shows resistivities lower than in the previous plots and at less than 400 meters deep, with an increase below that. It is inferred that this is caused by a layer of Browns Park on Precambrian basement at the station.

The two soundings of station 5 are similar in character down to 1200 meters depth where the north-south sounding reaches a low of 30 ohm-meters at 1300 meters and then increases, whereas the east-west line peaks at 2200 meters depth and then decreases. This station was situated close to several north-trending faults and north-south contacts between shale, sandstones, and gneiss which may account for the drop in east-west resistivity.

The resistivity at stations 6 and 9 increases uniformly with depth as best determined without middle frequency data. The resistivity at stations 7 and 8 is constant at 30 to 70 ohm-meters to a depth of 800 meters, which may be attributed to a thick sequence of shales and sandstones.

A low resistivity layer lies between two higher ones at station 10 where landslide deposits and glacial gravels cover Niobrara shale. The resistivity increases to a depth of 400 to 700 meters (base of the alluvium?), then decreases to 50 ohm-meters at 900 to 1500 meters depth (base of the shale?), and increases below that where basement is reached.

Station 11 depicts increasing resistivity with depth as it was positioned on a landslide deposit over Browns Park and crystalline basement. No data were available in the east-west orientation because of cultural interference. Stations 12 and 13 were both situated on Browns Park and their geoelectric sections are quite different. Station 12 was located close to the major north-trending normal fault and the drop in resistivity at about 2000 meters depth could be caused by an altered fault zone. Station 13 east-west could also be detecting this fault zone as shown by the resistivity drop at 600 to 700 meters depth. Probably the results of 13 north-south are the best representation of the subsurface geology beneath the two stations showing an increase in resistivity with depth.



## TELLURICS

Two telluric profiles were made north of Steamboat Springs, with the general locations shown in figure 57 and more detailed locations shown in figure 58. They were situated to cross as much variation in geologic structure as possible, while avoiding cultural noise and rough terrain.

The telluric technique employs a co-linear spread of three electrodes (made of lead sheeting) with the recorder at the middle electrode. The electrodes are not watered to minimize noise. The electrodes are connected by equi-length lines (250 meters in this survey) and the method measures the drop in potential created by telluric currents between the middle and outer electrodes. Telluric currents are naturally-occurring, electromagnetic signals in the earth. Long wave length signals were employed in this study corresponding to a period of about 30 seconds, or a frequency of 0.033 hertz. The signals are amplified and filtered, then recorded on an x-y recorder (with x being the voltage between the center and one outer electrode and y the other). The tangent of the angle that the major axis of the ellipse (Lissajous figure) makes with the x-axis is determined, and the ratio of voltages between the two stations derived. By this method, only a relative ratio of voltages between the end electrodes is determined, and by leap-frogging the spread along a traverse, a profile of relative voltages can be made. The square of the voltage is then the relative change in resistivity (see equation 1). Thus the telluric method can determine major lateral changes in resistivity to fairly



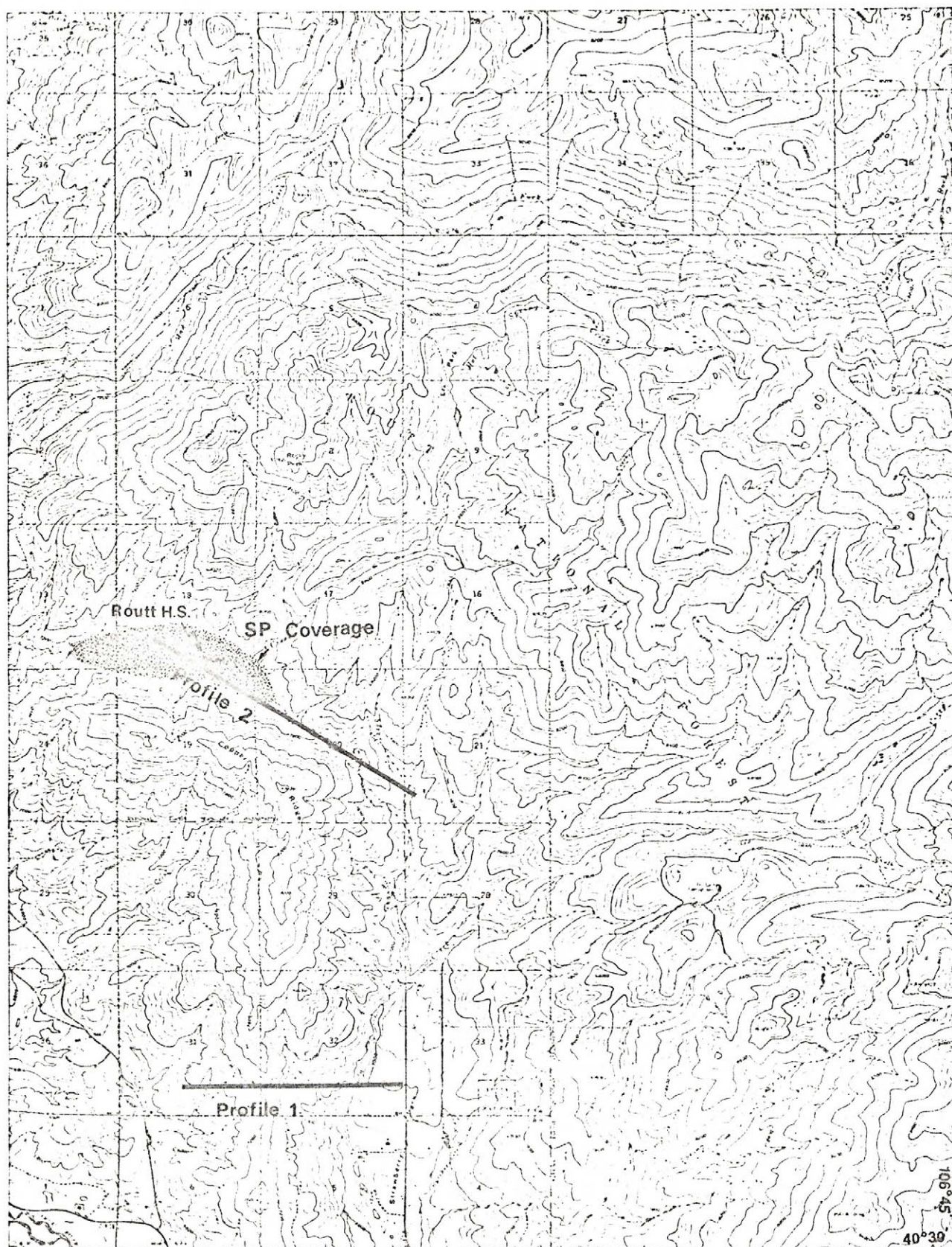


Figure 57. Telluric profile and self-potential survey location map (in Rocky Peak quadrangle); scale 1:62500.



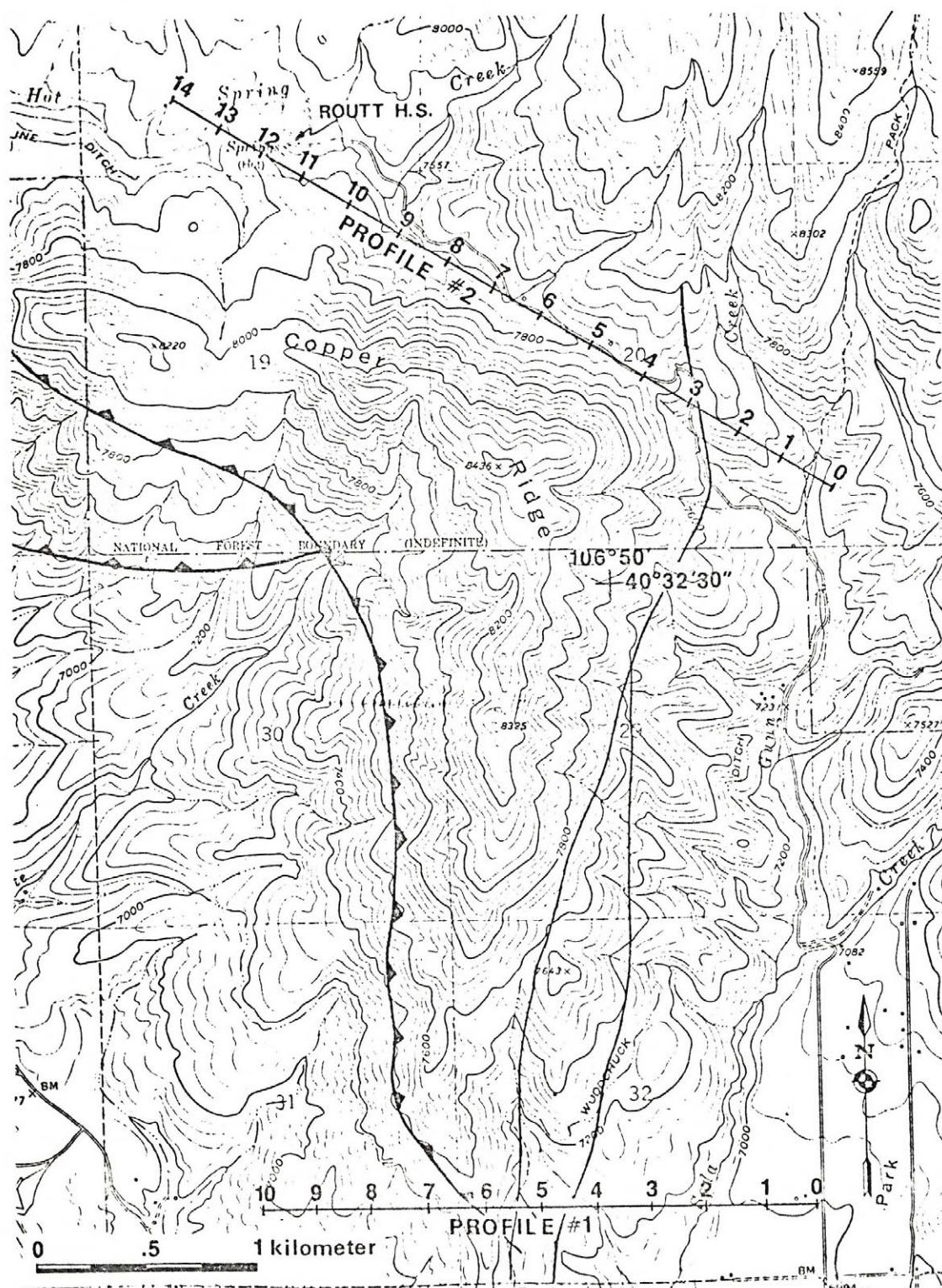


Figure 58. Telluric profiles location map.

great depths (from several to tens of kilometers). For example, assuming a homogeneous 300 ohm-meter earth and a frequency of 0.03 hertz, the skin depth (from equation 2) would be 50 kilometers, although this is lessened by near surface effects and inhomogeneity. For a further discussion of the telluric method see Beyer (1977).

The results of Profile 1 are shown in figure 59. The traverse was run east-west, perpendicular to the major faults and lithology changes, and the profile reflects the resistivity changes associated with the geologic structure. Moving west from a thin (about 100 meters) alluvium and Browns Park cover on Precambrian basement, low resistivity zones are crossed between stations 4 and 5, and 5 and 6 which are interpreted to be faults. A thick sequence of Cretaceous and Jurassic shales and sandstones is encountered between stations 6 and 7. The steep gradient in the profile (dropping off to the west) is probably the result of the sudden lithology change and edge effects from the thick sequence of low resistivity (10 to 30 ohm-meter) shales.

The results of Profile 2 are given in figure 60. This traverse was run near Routt Hot Springs in a northwesterly direction crossing two faults and two lithology changes. The relative voltage is fairly constant in the southeast part of the profile with two minor lows occurring where the traverse crosses glacial till (to the extreme southeast) and near the normal fault (close to station 4). A broad low of 500 to 750



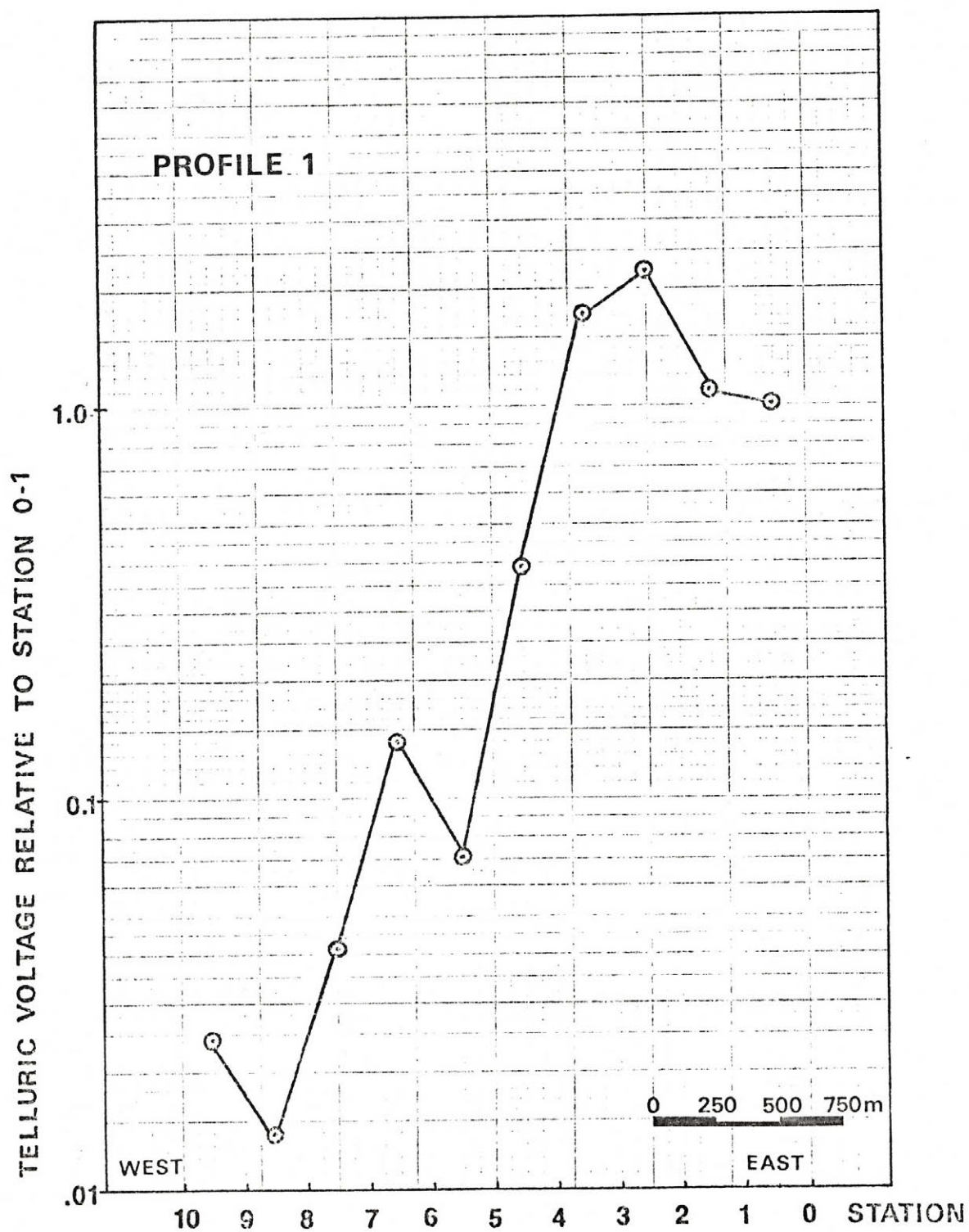


Figure 59. Telluric profile 1.

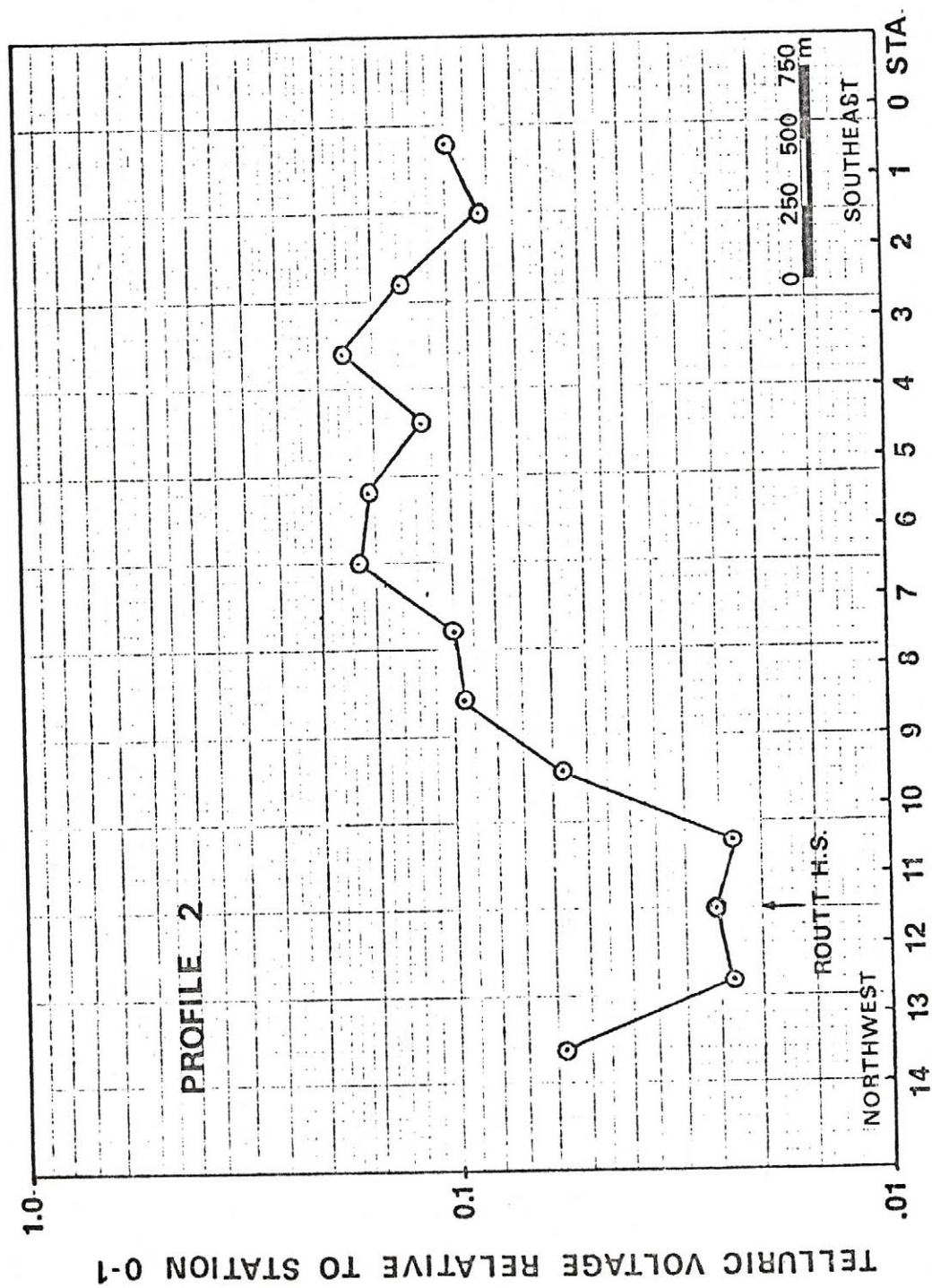


Figure 60. Telluric profile 2.



meters in width and almost a one order of magnitude drop in resistivity is centered over the hot springs area. Considering the high resistivity of the Precambrian rock, this low is probably the result of thermal waters circulating up from great depths through a well-fractured and altered zone of high permeability.

## SELF-POTENTIAL

Self-potential anomalies associated with geothermal areas are generally not well understood, but seem to be the product of higher temperatures and circulating underground fluids relating to three mechanisms. These are discussed at length by Corwin and Hoover (1979) and are discussed briefly here.

Thermoelectric coupling is the result of a voltage gradient created across a section of rock by a temperature gradient imposed on it. The ratio of the voltage change to the temperature change,  $\Delta V/\Delta T$  (where  $V$  = voltage and  $T$  = temperature), is called the thermoelectric coupling coefficient and usually ranges between  $-0.09$  and  $+1.36$  millivolts /  $^{\circ}\text{C}$ .

Electrokinetic coupling is caused by fluid flowing through a porous rock which creates an electric potential gradient (the electrokinetic or streaming potential) along its path due to interaction between the fluid and the electrical (Helmholtz) double layer (charge layers) of the pore surface. The electrokinetic coupling coefficient,  $\Delta E/\Delta P$  (where  $E$  = streaming potential and  $P$  = the pressure drop along the flow path), varies greatly with the resistivity of the pore fluid.

A potential change also exists across most lithologic contrasts but has not been well explained.

Self-potential anomalies in geothermal areas are usually the result of water flow through permeable zones combined with geology and temperature differences. Errors or noise can be the



result of changes in soil moisture or chemistry, diurnal variations, telluric currents, electrode drift, and streaming potential caused by groundwater flow.

A self-potential survey was done in the area of Routt Hot Springs. A 100 meter line was used and the voltage difference was measured (in millivolts) with a multimeter between electrodes at either end. Three pairs of silver-silver chloride electrodes were used in case one pair became faulty and to give a measure of electrode contact noise. The electrodes were leapfrogged (to reduce cumulative error) along two main profiles: stations 0 through 13, and stations 9 to 14 through 20 to 2. The survey area is shown in figure 57 and the station locations are shown in figure 61. The two lines were tied together in several places to check for errors.

The diurnal changes were measured with a self-potential monitor left stationary for the duration of the survey. The self-potentials at the monitor were measured on two orthogonal 100 meter lines with silver-silver chloride electrodes. The diurnal change averaged about  $\pm 4.0$  millivolts during the day and about -10 millivolts overnight.

The two profiles for each electrode pair are shown in figure 62. The voltage change between stations (electrodes) was calculated by setting a value of zero voltage at station 0 and successively adding or subtracting the millivolt difference between stations along the traverse. Thus the voltages in the profiles are relative voltages for each station, assuming

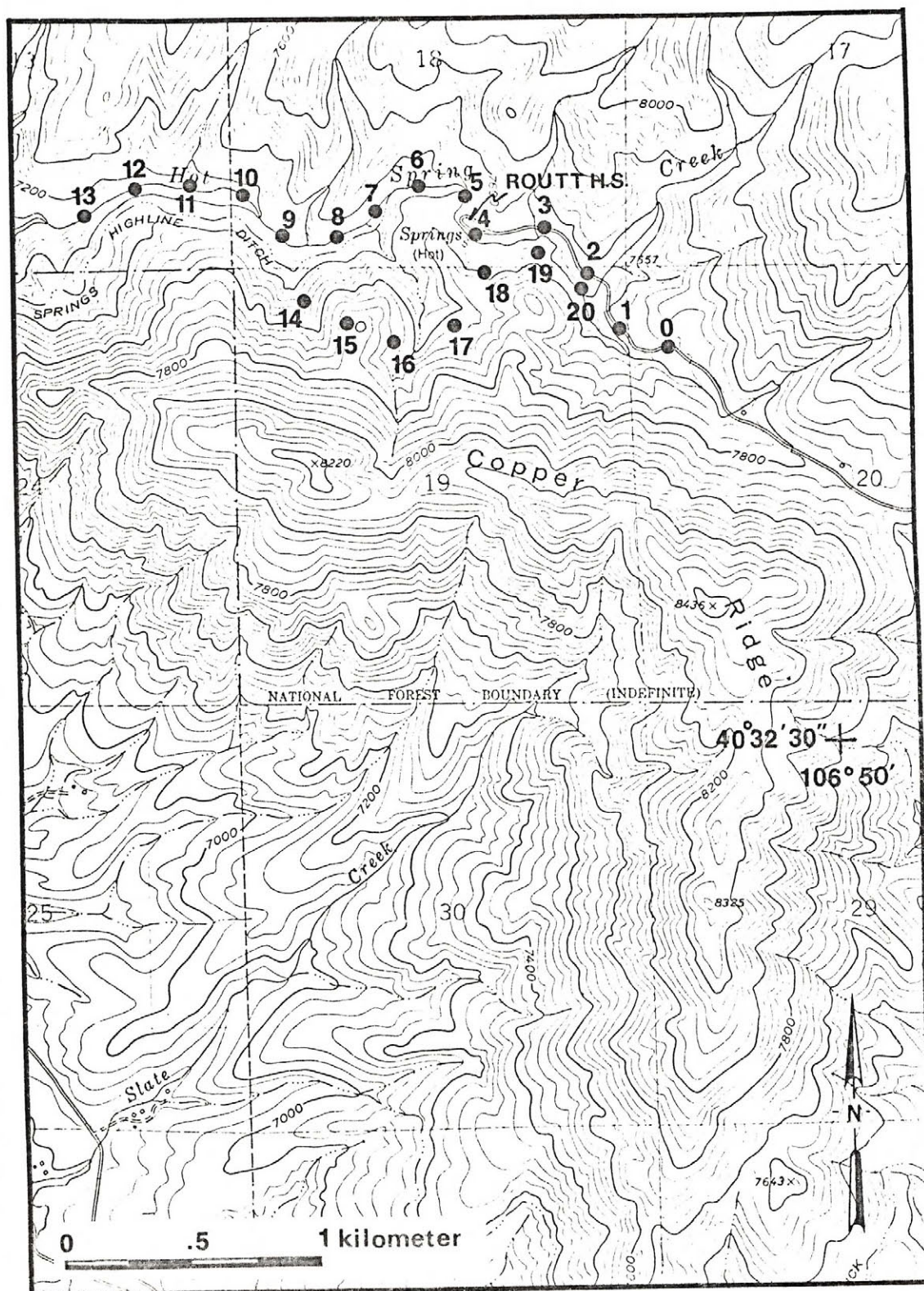


Figure 61. Self-potential station location map.



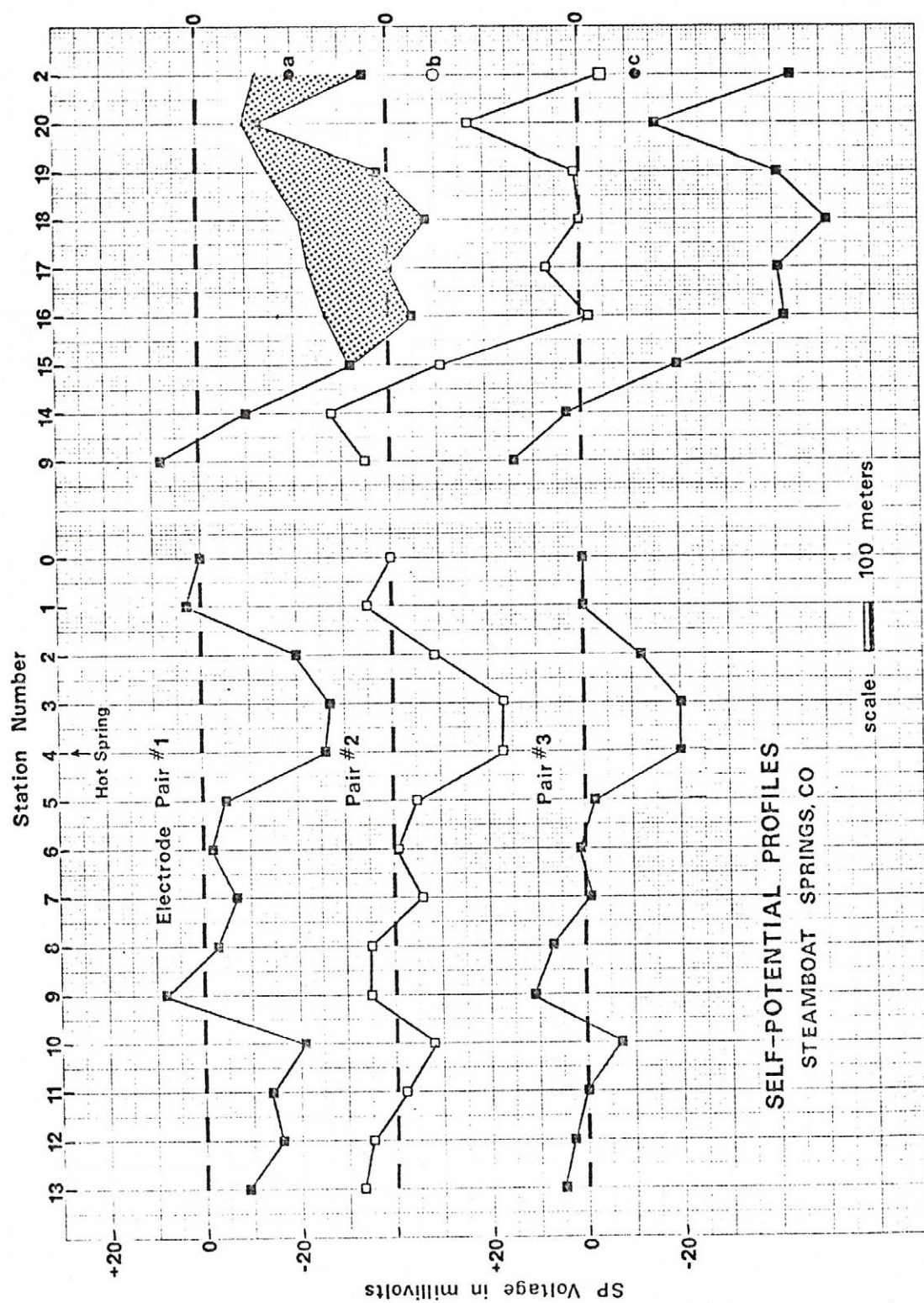


Figure 62. Self-potential profiles.

station 0 to have zero voltage. The letters a,b,c near the right hand margin of figure 62 denote the previous day's values for station 2 with the corresponding electrode pair.

In this survey, three lows were prominent on all electrode pairs. The low to the west (stations 10 to 12) is probably the result of increasing moisture in the ground (as the survey moved onto a small creek flood plain) and is not very large in amplitude. The low near the hot springs (stations 2 to 4) is about -20 millivolts in amplitude and is probably the result of geothermal activity and geologic changes.

The drop in voltage between stations 9, 14, and 15 of about 40 millivolts is probably largely the result of elevation increase. Streaming potential can cause a decrease in voltage with increase in elevation. The elevation decreases gradually from station 15 to 16, 17, 18, 19, and 20. If it is assumed that the voltage drop between 9 and 15 is just from elevation increase (at about -20 millivolts/80 meters elevation increase), this would result in a profile given by the upper line of electrode pair #1. Thus the stippled region designates a low of -20 to -30 millivolts at stations 16 through 19 not related to streaming. These stations all lie in or near the normal fault and gneiss-quartz monzonite contact creating a zone of more fracturing and greater permeability. The largest decrease in voltage occurs at station 18 which is closest to the hot springs, implying that part of the low comes from the presence of thermal waters.



The two profiles tie together fairly well using electrode pair #1 as evidenced by a 15 millivolt difference at station 2 (see letter "a" in figure 62) especially if the -10 millivolt nocturnal change between the two profiles is accounted for.

## CONCLUSION

The combination of mapped geology with geothermometry and data from the four geophysical surveys indicates two separate but similar hydrologic systems in the Steamboat and Routt Hot Springs areas.

Both systems appear to be fed by meteoric waters, mostly run-off from the Park Range, circulating along the many deep fault zones in the area where the water is heated and then returning to the surface. The surface discharge is mostly fault controlled -- the several Steamboat springs all lie on or near transverse faults except for Heart Spring which lies on the extension of a north-trending normal fault. Routt Hot Springs is situated between a north-trending normal fault (to the west), a pegmatite (to the south), and the gneiss-quartz monzonite contact (to the east). This provides a fractured and altered zone, perhaps 750 to 1000 meters wide, for the upflow of geothermal waters. Since the eastern side of the fault was upthrown and the quartz monzonite intruded into the gneiss, this zone probably dips steeply to the west.

The subsurface flow of water could be controlled by subhorizontal faults deep in the upper sheet of the reverse fault that runs the length of the study region. This fairly high angle (perhaps  $60^{\circ}$ ) fault should permit deep ground water flow in fractured zones several kilometers below the surface.

Historic seismicity locates 346 epicenters of earthquakes with magnitudes 1.0 to 4.5 (Richter scale) near Steamboat Springs



during the years 1966 through 1971 (Simon, 1969, 1972), which is far above the state average for any one area. Some of these quakes could be the result of mining, but the tensional strain suggested by these small quakes and the regional geology could provide the mechanisms to keep subsurface fractures open as permeable channels.

The heat source for the geothermal waters is probably the regional above-average heat flow in the northern Colorado mountains of perhaps 2.0 heat flow units (microcalories/cm<sup>2</sup>sec). This heat flow could be caused by the heat generation from granitic rocks and/or a higher mantle heat flux in the region. The youngest volcanics (intrusives) near Steamboat Springs are approximately 20 million years in age, too old to still be producing enough heat for geothermal activity. The only well data available gives a geothermal gradient of 47°C/km in shale (Apexo, 1978), which is high if taken as a regional gradient since shale has a less than average thermal conductivity. Even with a normal geothermal gradient of 30°C/km, waters would need to circulate to a depth of almost five kilometers to reach a temperature of 150°C, the average subsurface temperature denoted by geothermometry. With a higher than normal gradient or a surface temperature of more than 0°C, it is probable that waters are circulating to about four kilometers to reach predicted temperatures.

There is no indication that the two systems are connected laterally. The southern telluric traverse gave no indication of a subsurface low resistivity zone, and the chemical and dissolved solids contents of the two spring areas are quite different.

All four geophysical methods were useful in determining the subsurface conditions of the Steamboat Springs area. The gravity map confirms the mapped geology and provides some idea of basement depth and subsurface trends. The -232 mgal contour follows the reverse fault front from south to north close to both spring areas, and other contours delineate the metamorphic-igneous rock contact near Routt Hot Springs. The gravity also suggests that an upfaulted block of basement lies just south of Steamboat Springs, which is not obvious from surface geology alone.

The audio-magnetotelluric method doesn't provide deep information but does point out electrical conditions which may be related to structural and lithological changes, determines absolute resistivity values, and shows the geothermal source to be relatively deep. A low resistivity zone of 300 to 800 ohm-meters exists from the surface to about 1000 meters depth at Routt Hot Springs which is significant since it may indicate altered or fractured rock and a probable low volume of water flow. The AMT also gives an indication of basement depth at some stations. For example, the three stations southwest of town show a sharp increase in resistivity at 1000 to 2000 meters depth.

The telluric profiles are useful as a reconnaissance tool since they measure deep-seated resistivity changes. The southern traverse shows resistivity changes attributed to faults and lithologic changes. The northern profile suggests



an altered zone about 750 meters wide coupled with an eighty per cent drop in relative voltage near Routt Hot Springs. The self-potential survey also proved to be a quick method of spotting low near-surface resistivity, measuring a 20 millivolt drop near Routt Springs.

## REFERENCES

- Anderson, W. L., 1978, "Multics Documentation Program MARQPW", U.S.G.S. Unpublished Report.
- Barrett, J. K. and Pearl, R. H., 1978, An Appraisal of Colorado's Geothermal Resources, Colorado Geological Survey Bulletin 39.
- Beyer, J. H., 1977, "Telluric and D.C. Resistivity Techniques Applied to the Geophysical Investigation of Basin and Range Geothermal Systems, Part I: The E-Field Ratio Telluric Method", PhD Thesis, Lawrence Berkeley Laboratories, Univ. of California, Berkeley, Report LBL-6325 1/3.
- Bostick, F. X. Jr., 1977, "A Simple Almost Exact Method of MT Analysis", in "Workshop on Electrical Methods in Geothermal Exploration", Univ. of Utah, Dept. of Geology and Geophysics, U.S.G.S. Contract 14-08-0001-G-359.
- Corwin, R. F. and Hoover, D. B., 1979, "The Self-Potential Method in Geothermal Exploration", *Geophysics*, Vol. 44, no. 2, 226-245.
- Godson, R., Dansereau, D. and Sweeney, R., 1978, "USGS Gravity Reduction System", Unpublished documentation.
- Godson, R. H., 1978, "Program Bouguer", Unpublished U.S.G.S. documentation.
- Hoover, D. B., Frischknecht, F. C. and Tippens, C. L., 1976, "Audiomagnetotelluric Sounding as a Reconnaissance Exploration Technique in Long Valley, California", Journal of Geophysical Research, Vol. 81, no. 5, 801-809.
- Hoover, D. B. and Long, C. L., 1975, "Audio-Magnetotelluric Methods in Reconnaissance Geothermal Exploration", Proceedings, 2nd United Nations Symposium on the Development and Use of Geothermal Resources, Vol. 2, 1059-1064.
- Simon, R., 1969, "Seismicity of Colorado: Consistency of Recent Earthquakes with Those of Historical Record", *Science*, Vol. 165, 897-899.
- Simon, R., 1972, "Seismicity of Colorado, 1979-1970-1971", *Earthquake Notes*, Vol. 43, no. 2, 5-12.
- Snyder, G., 1977, "Geologic Map of the Central Part of the Northern Park Range, Jackson and Routt Counties, Colorado", U.S.G.S. Open File Report 77-189.



Snyder, G., 1977, "Geologic Map of the Northernmost Gore Range and Southernmost Northern Park Range, Grand, Jackson, and Routt Counties, Colorado", U.S.G.S. Open File Report 77-189.

\_\_\_\_\_, 1978, Personal communication.

Tweto, O., 1976, "Geologic Map of the Craig 1° x 2° Quadrangle, Northwestern Colorado", U.S.G.S. Misc. Investigations Map I-972.

Telford, W. M., Geldart, L. P., Sheriff, R. E. and Keys, D. A., 1977, Applied Geophysics, Cambridge, Ohio, Press Cambridge.

Apexo Inc., 1978, Personal communication.

---

## APPENDICES



APPENDIX A  
GRAVITY DATA

STATION IDENTIFICATION proj station	L U LATITUDE den min	C A T I LONGITUDE deg min	N N ELE (in ft)	G R A V I T Y OBSERVED	IN-EUCLIDICAL	TERRAIN BOUGUER CURV	C O R R E C T I O N S SPECIAL	FREE AIR	A N O M A L I E S COMPLET-ROUTIER dl=2.67 dl2=2.50
01/14:scr2	40 27.41	-106 49.16	6784.00	979568.10	960204.76	3.11	-231.58	-1.52	0.00
01/14:scr3	40 30.79	-106 49.30	6994.00	979562.11	960214.74	3.10	-230.55	-1.52	0.00
01/14:scr4	40 31.03	-106 49.32	7082.00	979556.66	960215.46	3.08	-241.55	-1.51	0.00
01/14:scr5	40 33.02	-106 50.62	7596.00	979525.41	960210.06	3.47	-259.08	-1.50	0.00
01/14:scr6	40 33.02	-106 49.77	7604.00	979511.52	960210.06	2.95	-269.04	-1.48	0.00
01/14:scr7	40 31.59	-106 47.03	8272.00	979462.45	960215.93	3.39	-282.13	-1.45	0.00
01/14:scr8	40 31.68	-106 48.08	7570.00	979527.09	960216.07	3.48	-280.19	-1.50	0.00
01/14:scr9	40 29.79	-106 46.31	7040.00	979538.29	960215.25	2.77	-240.39	-1.51	0.00
01/14:scr10	40 27.98	-106 40.53	6769.00	979511.31	960210.55	3.20	-280.07	-1.52	0.00
01/14:scr11	40 26.97	-106 48.42	6761.00	979507.94	960209.05	4.68	-280.00	-1.52	0.00
01/14:scr12	40 27.06	-106 48.40	6796.00	979506.51	960209.10	4.16	-281.79	-1.52	0.00
01/14:scr13	40 26.05	-106 48.07	6896.00	979500.99	960208.58	5.10	-283.20	-1.52	0.00
01/14:scr14	40 24.09	-106 46.81	6095.00	979516.59	960212.21	3.15	-280.35	-1.52	0.00
01/14:scr15	40 24.37	-106 50.40	6099.00	979518.26	960212.63	2.64	-280.48	-1.52	0.00
01/14:scr16	40 30.93	-106 51.84	6082.00	979509.40	960214.95	1.61	-284.72	-1.52	0.00
01/14:scr17	40 32.23	-106 53.03	6901.00	979510.20	960216.08	1.72	-285.37	-1.52	0.00
01/14:scr18	40 32.15	-106 54.51	6870.00	979505.00	960217.06	1.63	-287.77	-1.52	0.00
01/14:scr19	40 32.38	-106 56.32	6866.00	979504.63	960217.11	1.31	-287.15	-1.52	0.00
01/14:scr20	40 31.45	-106 57.15	6820.00	979506.50	960215.73	1.17	-287.79	-1.52	0.00
01/14:scr21	40 31.12	-106 58.87	6882.00	979502.59	960215.23	0.89	-287.90	-1.52	0.00
01/14:scr22	40 32.03	-106 59.20	6786.00	979517.11	960216.59	1.26	-281.45	-1.52	0.00
01/14:scr23	40 32.08	-106 59.84	6745.00	979519.76	960217.55	1.94	-280.05	-1.52	0.00
01/14:scr24	40 32.07	-106 58.60	6717.00	979500.60	960217.54	3.24	-289.10	-1.52	0.00
01/14:scr25	40 33.53	-106 59.79	6830.00	979513.40	960218.02	2.02	-282.95	-1.52	0.00
01/14:scr26	40 34.21	-106 59.73	6835.00	979510.87	960219.04	1.90	-281.76	-1.52	0.00
01/14:scr27	40 35.24	-106 59.74	7005.00	979504.07	960221.37	0.09	-280.92	-1.52	0.00
01/14:scr28	40 36.11	-106 59.17	6971.00	979505.79	960223.56	0.95	-287.97	-1.52	0.00
01/14:scr29	40 36.27	-106 58.35	6920.00	979510.01	960222.91	1.16	-280.07	-1.52	0.00
01/14:scr30	40 35.49	-106 57.32	6876.00	979513.28	960221.74	1.64	-284.59	-1.52	0.00
01/14:scr31	40 35.43	-106 55.91	6839.00	979516.94	960221.05	2.10	-283.22	-1.52	0.00
01/14:scr32	40 34.90	-106 55.60	6982.00	979507.87	960220.06	1.84	-280.14	-1.52	0.00
01/14:scr33	40 34.27	-106 55.94	6894.00	979512.24	960219.92	1.38	-282.13	-1.52	0.00
01/14:scr34	40 35.72	-106 55.03	6820.00	979518.76	960222.09	2.27	-282.01	-1.52	0.00
01/14:scr35	40 37.45	-106 57.03	6717.00	979511.61	960224.66	1.57	-280.92	-1.52	0.00
01/14:scr36	40 36.97	-106 56.29	6951.00	979510.22	960223.95	1.69	-287.08	-1.52	0.00
01/14:scr37	40 36.37	-106 55.59	6980.00	979509.31	960223.05	1.72	-280.07	-1.52	0.00
01/14:scr38	40 35.22	-106 56.00	6794.00	979502.12	960221.34	3.08	-281.72	-1.52	0.00
01/14:scr39	40 34.02	-106 53.20	6765.00	979501.10	960219.55	3.12	-280.07	-1.52	0.00
01/14:scr40	40 32.78	-106 53.08	6757.00	979518.51	960217.70	2.64	-280.46	-1.52	0.00
01/14:scr41	40 30.03	-106 53.82	6742.00	979510.75	960214.00	1.36	-280.95	-1.52	0.00

STATION IDENTIFICATION proj sta-10	L U C A T I O N S LATITUDE deg min	LONGITUDE deg min	ELE (in ft)	ST	GR A V I T Y OBSERVED	INFRA-RED TEMPERATURE	C O N D E C T I O N S CURV	SPECIAL	A I R FRE	A I R TEMPERATURE	A I R RELATIVE HUMIDITY	A I R WIND DIRECTION	A I R WIND SPEED
01/14:cccc26	40 31.07	-106 55.09	6872.0	cc	979572.81	960215.16	0.97	-234.58	-1.52	0.00	3.70	-231.24	-216.28
01/14:cccc27	40 31.76	-106 55.00	6840.0	cc	979573.15	960216.19	1.23	-233.29	-1.52	0.00	-0.00	-233.58	-216.71
01/14:cccc28	40 30.98	-106 56.05	6714.0	cc	979581.11	960215.02	0.97	-234.00	-1.52	0.00	-2.72	-232.51	-217.69
01/14:cccc29	40 30.88	-106 57.20	6593.0	cc	979587.32	960214.88	0.94	-234.67	-1.52	0.00	-7.73	-233.17	-218.02
01/14:cccc30	40 29.74	-106 58.43	6570.0	cc	979586.20	960215.23	1.26	-234.08	-1.52	0.00	-9.31	-233.71	-219.43
01/14:cccc31	40 30.26	-106 58.75	6597.0	cc	979588.36	960215.95	1.29	-235.01	-1.52	0.00	-5.31	-230.60	-216.28
01/14:cccc32	40 29.50	-106 51.65	6912.0	cc	979585.84	960215.52	1.91	-235.90	-1.52	0.00	3.82	-231.77	-216.71
01/14:cccc33	40 29.73	-106 52.09	6735.0	cc	979577.00	960215.16	1.91	-237.11	-1.52	0.00	-2.10	-231.42	-216.61
01/14:cccc34	40 29.73	-106 52.74	6690.0	cc	979581.66	960215.16	1.92	-233.18	-1.52	0.00	-2.55	-230.52	-215.62
01/14:cccc35	40 29.90	-106 53.46	6654.0	cc	979580.25	960215.41	1.40	-236.95	-1.52	0.00	-3.61	-230.67	-216.22
01/14:cccc36	40 29.02	-106 54.97	6650.0	cc	979588.34	960215.11	1.77	-236.81	-1.52	0.00	-2.50	-234.14	-214.71
01/14:cccc37	40 28.60	-106 55.02	6653.0	cc	979582.59	960211.98	2.06	-236.91	-1.52	0.00	-3.43	-234.00	-215.58
01/14:cccc38	40 28.08	-106 55.49	6717.0	cc	979577.07	960210.71	1.43	-237.10	-1.52	0.00	-2.14	-231.32	-216.73
01/14:cccc39	40 27.50	-106 55.10	6773.0	cc	979572.73	960209.68	2.16	-231.01	-1.52	0.00	-0.21	-230.57	-215.90
01/14:cccc40	40 26.56	-106 58.45	6919.0	cc	979581.90	960200.45	2.80	-235.99	-1.52	0.00	4.00	-230.71	-215.76
01/14:cccc41	40 26.10	-106 58.18	7030.0	cc	979584.63	960207.76	2.50	-239.77	-1.52	0.00	7.76	-231.14	-215.93
01/14:cccc42	40 25.19	-106 53.51	7200.0	cc	979584.76	960206.39	1.55	-243.57	-1.51	0.00	15.23	-230.30	-214.07
01/14:cccc43	40 24.16	-106 53.84	7545.0	cc	979520.02	960204.08	0.67	-257.50	-1.50	0.00	24.43	-233.54	-217.11
01/14:cccc44	40 23.53	-106 53.74	7140.0	cc	979540.13	960203.60	1.31	-243.52	-1.51	0.00	11.72	-232.01	-216.49
01/14:cccc45	40 23.06	-106 58.80	7349.0	cc	979526.73	960206.21	0.07	-242.02	-1.51	0.00	15.14	-237.71	-221.61
01/14:cccc46	40 23.50	-106 56.27	6944.0	cc	979550.74	960206.93	1.04	-236.88	-1.52	0.00	0.62	-236.60	-221.58
01/14:cccc47	40 23.56	-106 57.35	6950.0	cc	979553.83	960206.95	0.63	-237.04	-1.52	0.00	0.27	-237.06	-222.52
01/14:cccc48	40 20.56	-106 56.24	7219.0	cc	979540.53	960206.45	0.04	-240.22	-1.51	0.00	10.73	-236.52	-220.50
01/14:cccc49	40 24.08	-106 56.20	6658.0	cc	979581.71	960212.20	0.97	-237.09	-1.52	0.00	-4.55	-232.18	-217.69
01/14:cccc50	40 24.09	-106 56.77	6612.0	cc	979583.73	960212.21	0.99	-237.52	-1.52	0.00	-6.87	-232.71	-216.52
01/14:cccc51	40 24.24	-106 56.83	6553.0	cc	979587.93	960212.88	0.90	-235.50	-1.51	0.00	-8.84	-232.91	-216.65
01/14:cccc52	40 24.22	-106 58.00	6500.0	cc	979587.36	960212.41	1.03	-235.06	-1.51	0.00	-10.20	-233.75	-219.51
01/14:cccc53	40 24.17	-106 59.65	6512.0	cc	979587.16	960212.53	1.10	-232.11	-1.51	0.00	-11.95	-234.47	-220.30
01/14:cccc54	40 20.02	-106 50.39	7164.0	cc	979587.81	960211.01	4.53	-240.34	-1.51	0.00	9.54	-231.90	-216.01
01/14:cccc55	40 27.06	-106 50.52	7776.0	cc	979580.43	960210.38	5.05	-265.28	-1.49	0.00	30.72	-231.50	-214.64
01/14:cccc56	40 26.70	-106 49.61	6790.0	cc	979585.51	960208.66	2.19	-231.79	-1.52	0.00	-4.10	-234.70	-220.02
01/14:cccc57	40 25.93	-106 49.72	6812.0	cc	979580.43	960207.51	2.42	-232.50	-1.52	0.00	-2.67	-234.11	-219.37
01/14:cccc58	40 25.92	-106 50.88	7198.0	cc	979584.49	960207.49	1.96	-235.50	-1.51	0.00	17.67	-227.58	-211.78
01/14:cccc59	40 25.55	-106 51.41	7030.0	cc	979517.40	960206.94	2.50	-240.20	-1.49	0.00	27.72	-231.71	-215.19
01/14:cccc60	40 24.05	-106 56.73	6613.0	cc	979582.88	960207.00	2.50	-232.57	-1.52	0.00	-2.22	-233.61	-215.28
01/14:cccc61	40 23.93	-106 50.43	6610.0	cc	979581.43	960209.53	1.07	-232.27	-1.52	0.00	-2.80	-234.60	-220.03
01/14:cccc62	40 23.49	-106 51.20	6684.0	cc	979585.31	960205.68	1.47	-234.79	-1.52	0.00	-1.34	-236.18	-221.23
01/14:cccc63	40 23.03	-106 51.76	6661.0	cc	979586.17	960205.19	1.56	-234.01	-1.52	0.00	-2.01	-235.98	-221.04
01/14:cccc64	40 22.65	-106 50.27	6686.0	cc	979581.71	960202.59	1.60	-234.18	-1.52	0.00	-5.41	-239.50	-224.41
01/14:cccc65	40 23.65	-106 49.50	6630.0	cc	979586.60	960203.22	2.47	-232.95	-1.52	0.00	-4.40	-236.46	-221.69



STATION IDENTIFICATION	proj	station	L deg	C min	A deg	T min	I deg	O deg	N deg	S deg	G deg	P deg	A deg	V deg	T deg	C deg	O deg	R deg	E deg	C deg	T deg	O deg	N deg	S deg	S deg	A deg	N deg	O deg	M deg	A deg	L deg	I deg	E deg	S deg	
01714:00:00			40	24.54	-106	49.51	6834.0	00	00	00	00	00	00	00	00	00	00	00	00	00	00	00	00	00	00	00	00	00	00	00	00	00	00	00	00
01714:00:00			40	25.78	-106	48.10	6866.0	00	00	00	00	00	00	00	00	00	00	00	00	00	00	00	00	00	00	00	00	00	00	00	00	00	00	00	00
01714:00:00			40	25.75	-106	48.47	6803.0	00	00	00	00	00	00	00	00	00	00	00	00	00	00	00	00	00	00	00	00	00	00	00	00	00	00	00	00
01714:00:00			40	27.09	-106	47.16	7433.0	00	00	00	00	00	00	00	00	00	00	00	00	00	00	00	00	00	00	00	00	00	00	00	00	00	00	00	00
01714:00:00			40	25.69	-106	48.55	6931.0	00	00	00	00	00	00	00	00	00	00	00	00	00	00	00	00	00	00	00	00	00	00	00	00	00	00	00	00
01714:00:00			40	25.20	-106	48.85	6866.0	00	00	00	00	00	00	00	00	00	00	00	00	00	00	00	00	00	00	00	00	00	00	00	00	00	00	00	00
01714:00:00			40	26.94	-106	46.91	7406.0	00	00	00	00	00	00	00	00	00	00	00	00	00	00	00	00	00	00	00	00	00	00	00	00	00	00	00	00
01714:00:00			40	26.40	-106	47.93	7406.0	00	00	00	00	00	00	00	00	00	00	00	00	00	00	00	00	00	00	00	00	00	00	00	00	00	00	00	00
01714:00:00			40	26.68	-106	49.61	6125.0	00	00	00	00	00	00	00	00	00	00	00	00	00	00	00	00	00	00	00	00	00	00	00	00	00	00	00	00
01714:00:00			40	24.67	-106	48.39	7080.0	00	00	00	00	00	00	00	00	00	00	00	00	00	00	00	00	00	00	00	00	00	00	00	00	00	00	00	00
01714:00:00			40	32.18	-106	49.84	7231.0	00	00	00	00	00	00	00	00	00	00	00	00	00	00	00	00	00	00	00	00	00	00	00	00	00	00	00	00
01714:00:00			40	33.47	-106	50.69	6972.0	00	00	00	00	00	00	00	00	00	00	00	00	00	00	00	00	00	00	00	00	00	00	00	00	00	00	00	00
01714:00:00			40	24.57	-106	46.80	7114.0	00	00	00	00	00	00	00	00	00	00	00	00	00	00	00	00	00	00	00	00	00	00	00	00	00	00	00	00
01714:00:00			40	32.74	-106	50.54	8436.0	00	00	00	00	00	00	00	00	00	00	00	00	00	00	00	00	00	00	00	00	00	00	00	00	00	00	00	00
01714:00:00			40	32.52	-106	50.54	8325.0	00	00	00	00	00	00	00	00	00	00	00	00	00	00	00	00	00	00	00	00	00	00	00	00	00	00	00	00
01714:00:00			40	32.16	-106	50.57	8325.0	00	00	00	00	00	00	00	00	00	00	00	00	00	00	00	00	00	00	00	00	00	00	00	00	00	00	00	00
01714:00:00			40	31.41	-106	50.56	7642.0	00	00	00	00	00	00	00	00	00	00	00	00	00	00	00	00	00	00	00	00	00	00	00	00	00	00	00	00
01714:00:00			40	30.08	-106	50.50	7322.0	00	00	00	00	00	00	00	00	00	00	00	00	00	00	00	00	00	00	00	00	00	00	00	00	00	00	00	00
01714:00:00			40	30.50	-106	50.54	7500.0	00	00	00	00	00	00	00	00	00	00	00	00	00	00	00	00	00	00	00	00	00	00	00	00	00	00	00	00
01714:00:00			40	35.53	-106	52.79	7460.0	00	00	00	00	00	00	00	00	00	00	00	00	00	00	00	00	00	00	00	00	00	00	00	00	00	00	00	00
01714:00:00			40	35.75	-106	51.00	7500.0	00	00	00	00	00	00	00	00	00	00	00	00	00	00	00	00	00	00	00	00	00	00	00	00	00	00	00	00
01714:00:00			40	35.18	-106	52.01	7100.0	00	00	00	00	00	00	00	00	00	00	00	00	00	00	00	00	00	00	00	00	00	00	00	00	00	00	00	00
01714:00:00			40	27.22	-106	46.40	9076.0	00	00	00	00	00	00	00	00	00	00	00	00	00	00	00	00	00	00	00	00	00	00	00	00	00	00	00	00
01714:00:00			40	34.79	-106	57.51	7402.0	00	00	00	00	00	00	00	00	00	00	00	00	00	00	00	00	00	00	00	00	00	00	00	00	00	00	00	00
01714:00:00			40	34.98	-106	57.76	7285.0	00	00	00	00	00	00	00	00	00	00	00	00	00	00	00	00	00	00	00	00	00	00	00	00	00	00	00	00
01714:00:00			40	35.22	-106	57.71	6948.0	00	00	00	00	00	00	00	00	00	00	00	00	00	00	00	00	00	00	00	00	00	00	00	00	00	00	00	00
01714:00:00			40	34.78	-106	56.39	7036.0	00	00	00	00	00	00	00	00	00	00	00	00	00	00	00	00	00	00	00	00	00	00	00	00	00	00	00	00
01714:00:00			40	35.52	-106	55.99	6000.0	00	00	00	00	00	00	00	00	00	00	00	00	00															

STATION IDENTIFICATION proj sta-id	L U C A T I O N S LATITUDE deg min	LONGITUDE deg min	ELE (in ft)	ST	G P A V I T Y UPSERVED THEORETICAL	C O R R E C T I O N S TERRAIN BOUGUER CURV	SPECIAL	A N U M A L I E S FREE COMPLIF-ROUGHER AIR d1=2.07 d2=2.50
01714:0008	40 33.53	-106 50.96	7460.0	CO	979533.08	4.01 -254.44 -1.50	0.00	15.54 -230.50 -220.55
01714:0009	40 34.00	-106 48.95	8409.0	CO	979409.50	3.11 -280.83 -1.43	0.00	40.58 -244.58 -226.42
01714:0010	40 35.21	-106 45.74	10673.9	CO	979302.05	17.08 -364.06 -1.02	0.00	84.31 -263.09 -241.53
01714:0011	40 35.65	-106 40.30	8859.9	CO	979441.24	4.11 -302.19 -1.38	0.00	52.11 -247.54 -228.27
01714:0012	40 37.01	-106 53.98	7930.0	CO	979517.89	2.59 -270.74 -1.47	0.00	40.08 -229.55 -212.38
01714:0013	40 26.78	-106 45.74	9099.7	CO	979427.02	8.00 -310.37 -1.34	0.00	73.59 -230.12 -210.78
01714:0014	40 26.93	-106 44.80	10384.6	CO	979348.32	15.48 -354.20 -1.10	0.00	115.57 -224.45 -202.61

---

APPENDIX B

AUDIO-MAGNETOTELLURIC DATA SHEETS



## U.S. GEOLOGICAL SURVEY A.M.T. DATA LOG

pa = observed apparent resistivity in ohm-meters

N = number of observations

Er = standard error in ohm meters

- = no data

"NOTE" - Telluric line orientation indicated with station numbers.

Sta. No.	FREQUENCY												
		7.5	10	14	27	76	285	685	1.2K	3.3K	6.7K	10.2K	18.6K
1NS	pa	1891.	946.	980.	694.	629.	525.	1079.	88.9	561.	465.	374.	296.
	N	7	7	7	6	7	5	4	2	3	7	1	1
	Er	132.	57.7	99.6	84.8	46.2	37.5	143.	12.7	152.	28.9	-	-
1EW	pa	1795.	1296.	1280.	408.	720.	885.	746.	71.1	375.	217.	971.	120.
	N	5	7	5	7	6	6	4	3	3	7	1	1
	Er	170.	176.	157.	171.	49.7	198.	136.	5.04	109.	20.8	-	-
2NS	pa	638.	357.	372.	277.	232.	207.	243.	6.76	52.1	51.3	41.3	43.4
	N	6	7	10	11	7	6	3	3	4	6	6	1
	Er	34.3	28.4	47.6	12.0	13.8	3.46	5.77	0.26	6.06	1.08	2.20	-
2EW	pa	1685.	1930.	712.	455.	750.	2734.	563.	-	185.	373.	583.	139.
	N	5	5	8	5	5	3	1		2	5	1	1
	Er	108.	134.	150.	15.9	67.3	192.	-		23.6	45.7	-	-
3NS	pa	1632.	1674.	717.	468.	525.	874.	1079.	-	513.	351.	334.	219.
	N	6	5	6	6	6	7	7		4	8	6	1
	Er	382.	280.	18.2	47.8	69.3	82.6	92.6		66.9	14.8	31.9	-
3EW	pa	1238.	1782.	890.	680.	434	647.	257	-	199.	786.	169.	72.3
	N	6	5	5	6	6	7	5		3	6	5	1
	Er	149.	373.	92.2	125.	33.5	55.1	17.3		40.5	69.5	8.42	-
4NS	pa	252.	151.	117.	77.4	57.7	18.5	129.	14.3	45.2	27.1	32.3	18.4
	N	9	8	9	13	9	6	4	5	3	11	1	1
	Er	31.7	14.6	25.1	3.63	6.71	1.52	6.09	0.36	2.52	-	-	-
4EW	pa	393.	188.	181.	125.	63.1	26.4	61.3	11.8	72.0	26.1	35.5	27.0
	N	8	6	10	8	12	8	3	3	3	6	1	1
	Er	51.0	36.2	7.27	14.9	2.32	2.20	3.68	0.91	13.6	1.14	-	-

## U.S. GEOLOGICAL SURVEY A.M.T. DATA LOG

pa = observed apparent resistivity in ohm-meters

N = number of observations

Er = standard error in ohm meters

- = no data

"NOTE" - Telluric line orientation indicated with station numbers.

FREQUENCY													
Sta. No.		7.5	10	14	27	76	285	685	1.2K	3.3K	6.7K	10.2K	18.6K
5ns	pa	301.	622.	138.	240.	170.	-	-	-	-	10.4	54.6	10.9
	N	6	6	6	7	5					6	1	1
	Er	52.4	126.	17.3	38.8	11.2					0.70	-	-
5ew	pa	384.	592.	579.	915.	774.	-	-	-	-	12.6	39.4	13.1
	N	5	5	5	6	4					5	1	1
	Er	55.4	192.	44.9	91.4	110.					2.04	-	-
6ns	pa	8314.	1629.	1664.	121.	1182.	-	-	-	-	14.3	15.8	6.13
	N	3	3	2	5	3					6	1	1
	Er	774.	171.	287.	13.2	179.					1.93	-	-
6ew	pa	4014.	6888.	3599.	419.	243	-	-	-	-	52.8	22.0	9.17
	N	6	7	5	3	2					4	1	1
	Er	407.	843.	519.	56.6	24.0					4.79	-	-
7ns	pa	29.8	29.1	23.0	32.6	27.5	-	-	-	-	31.1	25.0	15.5
	N	6	6	6	6	7					6	1	1
	Er	4.51	1.07	1.88	1.93	1.45					2.07	-	-
7ew	pa	42.5	23.6	23.5	24.1	28.2	-	-	-	-	38.2	36.7	10.9
	N	6	6	6	5	7					6	1	1
	Er	5.82	3.18	1.94	5.24	3.26					0.91	-	-
8ns	pa	22.0	40.1	32.8	29.3	25.3	-	-	-	-	35.4	46.9	20.7
	N	7	12	10	9	9					9	1	1
	Er	3.51	1.87	1.98	1.31	1.48					1.31	-	-
8ew	pa	68.4	31.4	26.5	22.3	20.5	12.8	-	-	-	38.9	74.5	41.7
	N	5	7	10	5	9	3				10	1	1
	Er	8.73	4.56	2.12	2.66	2.74	2.18				2.75	-	-

## U.S. GEOLOGICAL SURVEY A.M.T. DATA LOG

pa = observed apparent resistivity in ohm-meters

N = number of observations

Er = standard error in ohm meters

- = no data

"NOTE" - Telluric line orientation indicated with station numbers.

Sta. No.		FREQUENCY											
		7.5	10	14	27	76	285	685	1.2K	3.3K	6.7K	10.2K	18.6K
9WS	pa	1398.	1399.	598.	421.	947.	-	-	-	-	16.1	41.5	41.5
	N	5	6	6	5	5					6	1	1
	Er	291.	126	132.	34.9	92.9					1.01	-	-
9EW	pa	1888.	1792.	458.	379.	173.	-	-	-	-	6.74	39.9	20.8
	N	6	6	5	5	5					5	1	1
	Er	206.	283.	73.3	73.3	899					1.50	-	-
10WS	pa	200.	208.	109.	26.9	214.	-	719.	487.	160.	11.9	16.8	8.68
	N	4	3	5	4	5		3	9	10	10	-	-
	Er	27.4	36.0	23.3	4.31	26.4		115.	41.8	6.43	0.32	-	-
10EW	pa	244.	243.	272.	403.	1208.	796.	-	270.	192.	28.0	20.7	11.3
	N	8	5	3	5	6	4		9	9	6	1	1
	Er	22.1	17.3	64.8	45.3	196.	58.9		13.0	6.52	2.48	-	-
11WS	pa	867.	570.	693.	550.	290.	-	-	-	-	33.5	22.9	17.7
	N	7	6	6	6	6					7	1	1
	Er	63.2	60.0	73.4	48.8	32.9					1.48	-	-
11EW	pa	-- NO DATA --											
	N												
	Er												
12WS	pa	330.	756.	366.	1336	1370.	666.	-	-	-	51.1	-	4.93
	N	7	6	9	6	9	1				5		1
	Er	53.0	61.2	47.9	107.	63.3	-				3.07		-
12EW	pa	414.	729.	321.	903.	2336.	-	-	-	-	25.6	6.91	6.31
	N	6	5	8	6	4					5	1	1
	Er	41.9	107.	70.3	96.6	168.					2.19	-	-







